Enabling Brain-Computer Interface Co-Adaptation with Performance-Related Signals

Nile R. Wilson

A dissertation

Submitted in partial fulfillment of the

Requirements for the degree of

Doctor of Philosophy

University of Washington

2019

Reading Committee:

Rajesh Rao, Co-chair

Jeffrey Ojemann, Co-chair

Eric Chudler

Program Authorized to Offer Degree:

Department of Bioengineering

University of Washington

Abstract

Enabling Brain-Computer Interface Co-Adaptation with Performance-Related Signals

Nile R. Wilson

Co-chairs of the Supervisory Committee:
Rajesh P. N. Rao
Paul G. Allen School of Computer Science & Engineering
Jeffrey G. Ojemann
Department of Neurological Surgery

Brain-Computer Interfaces (BCIs) have the potential to positively impact the lives of many people with sensorimotor disabilities due to neurological conditions, such as spinal cord injury and stroke. Through BCIs, individuals are able to interact with their surroundings and perform simple daily tasks independently, which once proved difficult or impossible without assistance. However, most BCIs are restricted to research settings due to cost, extensive setup, or need for researchers to monitor and modify the system. Many factors, such as difficulty of use and cost, prevent current BCIs from being integrated into regular daily use for health applications outside the lab or hospital. One direction of research hoping to push BCI out of the research setting focuses on enabling co-adaptation between the BCI and the user to increase BCI longevity and encourage better performance over time. This dissertation work focuses on investigating two performance related neural signals at the cortical level, namely error-related potentials and attention, and developing a co-adaptive BCI using these performance related signals to estimate subject performance during BCI use.

We reveal the topography of cortical error-related potentials during a continuous control one-dimensional BCI task where subjects utilize motor imagery and rest to control the vertical velocity of a cursor to reach and dwell within a target. In this investigation, we found increased local activity in

various cortical areas, including the somatosensory, motor, premotor, and parietal areas. We also investigate the effects of Default Mode Network (DMN) disruption on reaction time and on cortical activity and connectivity in a modified Stroop Task. In this work, we find that subject reaction time following auditory disruption of the DMN tends to be shorter than without disruption, and we find that connectivity between regions within the DMN tends to decrease with both auditory disruption and direct cortical stimulation disruption of the DMN. Lastly, we build and test a co-adaptive BCI using both error-related potentials and DMN activity to create "confidence scores" which estimate BCI performance. Our novel "confidence score" based co-adaptation was able to improve overall BCI performance across subjects and led to better performance than with no decoder adaptation. Using the same data, we use simulation to study the feasibility of applying transfer learning to allow first time users to attempt BCI control without training.

Our findings not only contribute to a greater understanding of the presentation of two performance related signals at the cortical level and their roles in task contexts, but also contribute to the growing field of co-adaptive BCIs. Future BCIs may benefit from this co-adaptive design which relies on non-control neural signals already being recorded during BCI operation. Understanding various signals related to our internal performance monitoring system and how to utilize them to estimate BCI performance in a co-adaptive BCI system will enable future systems to adapt automatically over time without manual intervention from researchers. This should improve BCI longevity and use and bring these systems one step closer to being useful in at-home settings for potential users.

1. Contents

1.1 Table of contents

1.2 List of figures

1.3 List of tables

2. Acknowledgments

It is with the invaluable support of many peers, mentors, family, and friends that I have been able to successfully complete this work.

First, I would like to thank my co-advisors Rajesh Rao and Jeffrey Ojemann and mentor Kurt Weaver for their patience, support, and guidance throughout the program. I would also like to thank my supervisory committee – Eric Chudler, Chet Moritz, Azadeh Yazdan-Shahmorad, and Wendy Thomas.

I also want to thank the members of the GRIDlab for their incredible and continuous support throughout my time in the lab – James Wu, Devapratim Sarma, Nancy Wang, David Caldwell, Jenny Cronin, and Kaitlyn Casimo. In particular, I want to thank James, Dev, and Kurt for the significant time and effort they put into mentoring me. I also want to thank Preston Jiang for helping me mentor summer and undergraduate students, and for assisting in EEG experiments.

Outside of the lab, I received a great deal of support from peers and faculty from the Center for Neurotechnology (CNT, formerly known as the Center for Sensorimotor Neural Engineering). In particular, I would like to thank Eric Chudler for acting as a mentor for all manners of CNT business including education/outreach activities and the hackathon and also thank Tim Brown and Katherine Pratt for their mutual peer support.

Finally, I would like to thank my family and friends, both online and present in the greater Seattle area, for believing in me and supporting me in all my endeavors.

3. Introduction

This introduction provides an overview of the key concepts and work in the field which are fundamental to this dissertation work.

3.1 Motivation

Over the past five decades, the concept of controlling devices and interacting with your surroundings through just brain signals has developed from science fiction to reality. Since Fetz first developed a Brain-Computer Interface, where a monkey was able to control a meter with their brain activity to deliver rewards (Fetz, 1969), these systems have become more robust and commercially available.

Brain-Computer Interfaces (BCIs) have the potential to positively impact the lives of many people with sensorimotor disabilities due to neurological conditions, such as spinal cord injury and stroke. Through BCIs, individuals are able to interact with their surroundings and perform simple daily tasks independently, which once proved difficult or impossible without assistance.

However, most BCIs are restricted to research settings due to cost, extensive setup, or need for researchers to monitor and modify the system. For instance, one individual enrolled in a BrainGate clinical trial has demonstrated the ability to control a robotic arm well enough to perform simple daily tasks such as bringing a bottle to her mouth to drink coffee through a straw (Hochberg et al., 2012), but the BCI usage was restricted to the highly-controlled lab setting. In addition, it took many months of training with the implanted recording device, with the assistance of an entire research team, for the user to ultimately achieve stable control of the robotic arm.

Many factors, such as difficulty of use and cost, prevent current BCIs from being integrated into regular daily use for health applications outside the lab or hospital. One major barrier preventing these systems from having a greater impact is the lack of individualized adaptation of the BCI to the user. Such individualized adaptation would allow for the BCI to continue to work well with the user over time.

Through investigating methods regarding individualized adaptation, we could increase BCI longevity by allowing the decoder to compensate for changes in either the recording hardware or the neural activity. This co-adaptation should also lead to decreased learning time, which can increase user motivation when first adopting the BCI. Of particular interest are neural signals related to performance that are collected alongside the control signal used. These performance related signals provide information which can be used as automatic feedback to the BCI decoder. Automatic feedback eliminates the need for a researcher to manually adjust the system for a user over time. The presence of these performance related signals is task-agnostic, meaning the use of these signals as feedback can be generalized to multiple tasks, and is not restricted to specific, well-controlled, experimental settings. In particular, we investigate the presence of cortical error-related potentials and the effects of disrupting the Default Mode Network (DMN) on subject attention and response timing.

When performing tasks, we constantly monitor our own performance and consciously take note of unexpected actions and responses. Error-related potentials are elicited when there is a mismatch between expected sensory feedback and actual feedback (Holroyd and Coles, 2002). These signals exist in various contexts and already serve as a powerful feedback mechanism in adjusting our own behavior. If we implement this feedback system with the BCI decoder, then we could also enable the BCI to learn and improve over time, similar to how we learn naturally.

Activity in the Default Mode Network (DMN) has been shown to increase during mind wandering and decrease with task engagement (Mittner et al., 2014). Some research suggests reward signals, and potentially other performance-monitoring signals, are modulated by attention (Diez et al., 2015; Lakey et al., 2011; Ordikhani-Seyedlar et al., 2014). If we are able to monitor DMN activity, we can provide weights to the error-related potentials we detect and use in our co-adaptive system. If we transiently disrupt DMN activity during BCI usage, we may be able to keep users focused and improve BCI performance.

While we have the unique opportunity to study these cortical potentials through electrocorticography (ECoG), the vast majority of individuals who would benefit from the co-adaptive BCI we are proposing would find a non-invasive system more accessible. In recent years, the number of consumer-grade

electroencephalography (EEG) products has greatly increased. These systems are orders of magnitude less expensive than their research-grade counterparts (hundreds versus tens of thousands of dollars) and often require less extensive setup. Such EEG systems are more easily adoptable for use in at-home settings.

Our ultimate goal is to increase the efficacy and accessibility of such systems through improving their function while reducing the need for researcher intervention, allowing for lower-cost systems to work effectively in at-home settings. Specifically, we are interested in creating a BCI which automatically updates and adapts to the individual user, using only data already present in their brain signals.

In this dissertation work, we focus on investigating two types of non-control, performance-related neural signals present during BCI use. We then develop a co-adaptive BCI which utilizes these two performance monitoring signals to adapt to the user over time without explicit task information. In this introduction, we provide an overview of two such signals – error-related potentials and Default Mode Network activity – and of BCI decoder adaptation.

3.2 Recording neural signals

In investigating error-related potentials and Default Mode Network activity, and in BCI development, we record neural signals either invasively or non-invasively using ECoG or EEG, respectively. Although ECoG (also referred to as intracranial EEG) electrodes rest on the surface of the brain and EEG electrodes rest on the scalp, they both record the same basic phenomenon. Although significantly attenuated and dispersed in EEG, Local Field Potentials (LFPs) are generated by transmembrane current in neurons and are measured through both recording methods (Buzsáki et al., 2012; Lopes da Silva, 2013). Although these currents primarily emerge from synaptic activity, contributions from calcium ion spikes and action potentials, among other events, impact extracellular current (Buzsáki et al., 2012). In terms of measuring LFPs, the cytoarchitecture of cortex and source synchrony have the most significant effect on the signals recorded through ECoG and EEG.

Of particular interest throughout this dissertation work are the strengths of oscillations in different frequency bands. In EEG, we are limited to recording reliably from lower frequency bands due to the

exponential decrease in power inherent in LFPs in combination with signal attenuation from traveling out to the scalp (Buzsáki et al., 2012). However, in ECoG we have access to and primarily focus on high frequency power, which is more spatially localized and indicative of local neuronal population activity than low frequency oscillations (Buzsáki et al., 2012; Miller et al., 2010).

3.2.1 Error-related potentials

Error-related potentials (ErrPs) are event-locked, electrophysiological responses generated during task rule violations. They are changes in voltage we see when mistakes are made, whether we make those mistakes ourselves or observe others making mistakes. The vast majority of our understanding to date of the ErrP originates from EEG studies (Ferrez and del R Millan, 2008; Iturrate et al., 2013; Kreilinger et al., 2016; Spüler and Niethammer, 2015; Zhang et al., 2015). However, there has also been work done to investigate ErrPs at the cortical level using ECoG (Bechtereva et al., 2005; Milekovic et al., 2012, 2013). Investigations at these scales have provided insight into the possible physiology behind the generation of these signals.

Error-related potentials are generally separated into two categories, each of which are believed to have their own distinct pathways. These categories have various names in the literature, but will be referred to in this dissertation as high-level and low-level error (Krigolson and Holroyd, 2007; Milekovic et al., 2012; Spüler and Niethammer, 2015). High-level error, also known as outcome or target error, occurs when the individual/observer fails to achieve the goal of a task; this type of error is not immediately correctable. Low-level error, also known as execution error, occurs when the individual/observer makes a mistake in their control in the process of achieving a goal; this type of error is immediately correctable and does not necessarily prevent the person from achieving the task goal. For example, a reactionary turn of the steering wheel to adjust for an unseen bump in the road would be considered a low-level error, whereas failing to reach your destination would be considered a high-level error.

3.2.1.1 Physiology of error-related potentials

A well-studied high-level error is the error-related negativity (ERN) (Gehring et al., 1993), also known as error negativity (Ne) (Falkenstein et al., 1991), which is often localized to the medial-frontal cortex (Krigolson and Holroyd, 2007; Wessel, 2012) and is believed to be essential to reinforcement learning (Nieuwenhuis et al., 2004). The reinforcement learning (RL) theory of the ERN suggests the error signals are generated in the basal ganglia and propagate to the cortex through the anterior cingulate cortex (ACC) (Frank et al., 2005; Nieuwenhuis et al., 2004). Specifically, it is believed the basal ganglia monitor performance in real-time and predict whether the current action will result in a success or a failure. The basal ganglia relay to the midbrain whether a prediction was correct or not once it receives feedback from the cortex. If the prediction was not correct (error occurred), then the midbrain decreases phasic dopaminergic neuron activity, decreasing the amount of dopamine sent to the ACC, which lessens the inhibition of the apical dendrites of the motor neurons there, leading to measurable ERN (Nieuwenhuis et al., 2004). Involvement of the ACC in cortical error-related potentials has been suggested in EEG (Krigolson and Holroyd, 2007; O'Connell et al., 2007) and confirmed through ECoG (Bechtereva et al., 2005). Low-level error, however, is believed to evoke activity primarily in the posterior parietal cortex.

Unlike in the RL theory of the ERN, the generation of the low-level error is not dependent on trial/task outcome. Rather, work by (Chavarriaga and Millan, 2010; Ferrez and del R Millan, 2008; Kim and Kirchner, 2013; Krigolson and Holroyd, 2007; Spüler and Niethammer, 2015; Völker et al., 2018) suggest low-level error, presented as a positive deflection detected in the parietal cortex (Pe; error positivity), is produced when there is a conflict between the sensory feedback estimated by the internal forward model and the actual received feedback (Holroyd and Coles, 2002; Nieuwenhuis et al., 2004; Wolpert et al., 1998).

The vast majority of the neurophysiological studies on error detection have relied on scalp-based measurements. EEG studies have typically reported on high-level and low-level errors as a function of event-locked voltage responses in the time domain, or as changes in theta (4-7 Hz) frequency band power (Cavanagh and Frank, 2014; Zhang et al., 2015). One previous ECoG study by Milekovic and

colleagues demonstrated the presence of ErrPs across multiple cortical regions in a continuous, overt-movement task in human ECoG (Milekovic et al., 2012, 2013). The researchers observed low-level and high-level ErrPs, described as execution and outcome errors, respectively, in the motor, somatosensory, parietal, temporal, and pre-frontal areas.

In Chapter 5, we utilize ECoG to investigate whether errors induced during a motor-imagery BCI task also result in ErrPs. We focus exclusively on high gamma (70-100 Hz) activity, where this high frequency broadband power (HBP) is thought to best reflect local activity (Manning et al., 2009; Miller et al., 2009a; Ray et al., 2008) and is reliably recorded through ECoG. We were particularly interested in examining local response activity for error-processing across the surface of the human brain. Much attention has been given to the anterior cingulate cortex and other frontal areas, but in Chapter 5 we examine all cortical areas available in our subjects.

3.2.2 The Default Mode Network and attention

The Default Mode Network (DMN) is a network of brain regions shown to have increased activity during rest and decreased activity during attention-demanding task engagement (Shulman et al., 1997; Raichle et al., 2001; Raichle, 2015). This task-negative network consists of the medial and lateral parietal, medial prefrontal, and medial and lateral temporal cortices bilaterally and symmetrically in humans (Raichle, 2015). The DMN is also shown to have increased activity during self-referential mental activity, such as reflection and self-reference in emotional processing (Raichle, 2015). However, for the purposes of this dissertation, we are most interested in the DMN's role in mind-wandering and rest during task execution as a measure of attention, as it may modulate task performance (Diez et al., 2015; Lakey et al., 2011; Ordikhani-Seyedlar et al., 2014).

Blood oxygen levels in this network have been studied extensively in functional Magnetic Resonance Imaging (fMRI) (Raichle, 2015), but previous work in the lab by Miller et al. (2009b) confirmed these fMRI findings were indeed related to local neuronal activity through measuring the electrical activity directly via ECoG. Further work by Ossandón et al. (2011) has shown that DMN activity is measurable in ECoG in various Brodmann Areas, including the posterior cingulate cortex (PCC, BA31), ventrolateral

prefrontal cortex (VLPC, BA45/47), medial prefrontal cortex (MPFC, BA32/10), temporal parietal junction (TPJ, BA40), lateral temporal cortex (LTC, BA21), and middle frontal gyrus (MFG, BA9). In both ECoG studies, high gamma band (ranging from 60-200 Hz) activity was used to measure local activity.

The Default Mode Network has also received some interest in the EEG community. Work by Knyazev et al. (2011) demonstrates that estimates of DMN activity are measurable in the alpha band of a specific independent component in non-invasive EEG, using a voltage source estimation technique (sLORETA) coupled with Independent Component Analysis (ICA). Earlier work by Jann et al. (2010) suggests increases in DMN activity can be detected in EEG through simultaneous increases in alpha band activity in occipital electrodes and increases in beta band amplitude in parietal channels.

3.3 Disrupting cortical activity through direct cortical stimulation

In Chapter 6, we utilize direct cortical stimulation to disrupt Default Mode Network activity. Intraoperative cortical stimulation is a standard procedure performed in the subjects in our ECoG studies (Formaggio et al., 2013), as they are patients undergoing clinical seizure monitoring at the hospital. The stimulation delivered in the Chapter 6 investigation was not intraoperative, but instead took place after subjects were back on anti-epileptic drugs during their week of clinical monitoring.

Although stimulation is commonly used for functional mapping in ECoG, stimulation parameters may be changed to create transient disruptions in local activity, also known as virtual lesions. The term "virtual lesion" comes from Transcranial Magnetic Stimulation (TMS) literature, where it has been applied non-invasively to study function since 1999 (Pascual-Leone et al., 1999, 2000; Siebner et al., 2009). TMS affects neuronal populations in superficial cortex, similar to in ECoG. The TMS literature suggests that the underlying cause of these virtual lesions is either, or a combination of, (1) GABAergic inhibition resulting from synchronized high frequency bursts of discharge from neuronal populations (Siebner et al., 2009) or (2) the addition of "noise" to the local network activity.

3.4 Brain-Computer Interfaces (BCIs)

Brain-Computer Interfaces (BCIs) consist of three major components: (1) the neural signals of the BCI user, (2) the decoder which is responsible for processing the neural signals to affect control, and (3) the end effector (e.g., robotic arm) which performs some action.

Neural signals can be recorded either invasively or non-invasively using a variety of recording methods. Invasive recording methods, such as penetrating electrodes and surface electrodes (ECoG), provide greater signal quality and spatial specificity but require surgery and are less common in humans due to the risks associated with implantation (Normann and Fernandez, 2016; Parvizi and Kastner, 2018). Non-invasive recording methods, such as electroencephalography (EEG) and magnetoencephalography (MEG), are commonly employed for BCI investigations as they allow for data collection with minimal risk. However, due to attenuation as the signals travels through the skull and the scalp, computationally heavy source localization techniques are often applied to estimate where signals of interest originate in the cortex (Lopes da Silva, 2013).

Once the neural signal is acquired, specific features of the signal are extracted using one or more signal processing techniques. In EEG and ECoG, signals are often filtered into frequency bands of interest prior to calculating signal power. In the case of motor imagery BCI, event-related desynchronization or synchronization (ERD/ERS) due to the imagination of movement is often measured by changes in spectral power in the alpha/mu (8-12 Hz), beta (13-30 Hz), or high gamma (70-200 Hz) band in electrodes over the primary motor cortex (Jeon et al., 2011; Miller et al., 2010). While changes in spectral power may be observed in centrally located channels C3 and C4 in EEG, techniques such as Common Spatial Pattern (CSP) filtering may be applied to extract spatial features that may better reflect the ERD/ERS (Ang et al., 2008; Fukunaga, 1990; Ramoser et al., 2000; Xygonakis et al., 2018). Similar to in motor imagery BCI, EEG signals recorded in Steady-State Visually Evoked Potential (SSVEP) BCI are filtered into the frequency bands of interest and the power of the filtered signals are used to inform control (Kuś et al., 2013). Signal features may also be extracted primarily in the time domain,

as is the case in P300 BCIs which rely on time-locked positive deflections in voltage signal based on the response to oddball stimuli (Donchin et al., 2000; Farwell and Donchin, 1988).

Lastly, once signal features have been extracted, they are used for end effector control. The features are either mapped to influence control, such as with cursor velocity (Wolpaw and McFarland, 2004), or are fed into a classifier to output one of two or more distinct outcomes.

3.4.1 Classification of BCI features

Classifiers used as BCI decoders are often simple machine learning models which learn to differentiate between data belonging to one of two, or one of many, classes. Common models used in BCI classification include Linear Discriminant Analysis (LDA), Support Vector Machines (SVM), and variants of these two models (Lotte et al., 2007, 2018).

Recent advances in processing power and efficiency have led to a boom in machine learning applications in the past decade. Many fields have greatly benefited from the power of computationally heavy machine learning methods, such as computer vision with deep convolutional neural networks (Krizhevsky et al., 2012). In the BCI field, we typically use simple thresholding methods or basic machine learning techniques such as Linear Discriminant Analysis (LDA), Support Vector Machines (SVM), or Filter Bank Common Spatial Pattern (FBCSP) to classify pre-selected signal features with the decoder (Ang et al., 2008; Lotte et al., 2007). However, there has also been interest in applying convolutional neural networks to raw EEG data without preselecting features (Schirrmeister et al., 2017). Through testing different network architectures, Schirrmeister et al. (2017) were able to demonstrate classification performance in their deep convolutional neural network using raw EEG that was comparable to classification performance of FBCSP using pre-selected features.

Although deep convolutional networks show promise for classifying raw EEG, we utilize shallow Multilayer Perceptron models for signal classification using preprocessed signal features, as described in Chapter 7, due to the relatively low computational power and time required to run.

3.5 BCI adaptation

BCIs rely on closed-loop feedback (typically visual) to inform the user of their control and overall performance. This feedback is hypothesized to be key to the BCI learning process and performance improvement (Green and Kalaska, 2011), similar to how sensory feedback is needed for typical motor skill learning (Newell, 1991). BCI decoders have traditionally been static, in the sense that initial parameters in the algorithm would be set and only changed by manual updates performed by the BCI technician. Recently, however, there has been a push to develop dynamic feedback systems that automatically update over time (DiGiovanna et al., 2009; Merel et al., 2015; Orsborn et al., 2014; Pohlmeyer et al., 2014). This adaptation of the decoder overtime as the user learns to control or perfect control of a BCI is called co-adaptation.

One example of such a co-adaptive BCI is the closed-loop decoder adaptation (CLDA) algorithm developed by Orsborn et al. (2014). CLDA uses knowledge of actuator position and velocity, in addition to knowledge of task goals, to update decoder weights. This algorithm yielded increased BCI performance relative to the standard static model in a group of macaque monkeys (Orsborn et al., 2014). Other work by (Faller et al., 2014; Myrden and Chau, 2016) have also demonstrated BCI co-adaptation using task metrics in humans. However, these and other co-adaptive BCIs (Margaux et al., 2012; Mondini et al., 2016; Rozado et al., 2015) rely on knowledge of behavioral data as recorded in the task paradigm or from external sensors, limiting co-adaptation to the research setting.

To circumvent this limitation, there has also been work done on developing unsupervised co-adaptive BCIs using neural signals indicative of performance. For example, error-related potentials in a Steady-State Visually Evoked Potential (SSVEP) BCI task (Spüler et al., 2012a) and short-term psychological state changes in motor imagery, mental arithmetic, music imagery, and word generation BCI tasks (Myrden and Chau, 2016) have been used to enable co-adaptation based on neural estimates of performance. In this dissertation, we build upon this work by creating a novel co-adaptation method using “confidence scores” generated from both error-related potentials and Default Mode Network activity, as further described in Chapter 7.

4. Common methods

Throughout the following chapters, neural signals are recorded during task performance by research subjects who have consented to participate in our studies. In this chapter, we briefly summarize common methods used in the following chapters.

4.1 Institutional approval

Prior to data collection for any experiment, subjects provided written informed consent to participate in the relevant study in accordance with the University of Washington Institutional Review Board. All subject data were de-identified in compliance with the Health Insurance Portability and Accountability Act (HIPAA). Subjects for the ECoG studies were intractable epilepsy patients at either Harborview Medical Center or Seattle Children's Hospital, and subjects for the EEG study were healthy individuals associated with the University of Washington.

4.2 Task presentation

In all tasks detailed in this dissertation work, subjects observe stimuli on a screen and are instructed to perform certain actions based on the stimuli presented. While the subjects perform the task, their neural signals are recorded using either ECoG (Chapters 5 and 6) or EEG (Chapters 7 and 8). Simultaneously, behavioral data relevant to the task, such as key press value and speed, are recorded. All tasks in this dissertation work followed a trial based format, where subjects performed the instructed actions within trials of predetermined length and had rest periods between each trial.

4.3 Neural recording

For the ECoG subjects, experimental neural signals were recorded alongside their clinical recordings without disrupting their clinical monitoring. This was achieved by recording a duplicate of the neural signals through our recording equipment, either with g.USBamps (GugerTec, Graz, Austria) or the Tucker Davis Technologies (TDT) (Alachua, FL) recording system at our own sampling rate of choice

(often 1200 Hz). The recording hardware would interface with the BCI2000 software suite (Schalk et al., 2004) or with TDT OpenEx and MATLAB to record the signals to our system. The ECoG electrodes would vary in shape and size, with electrode grids providing the most coverage. Grids consisted of 8x8 platinum electrodes of 4 mm diameter (2.3 mm exposed) embedded in Silastic, with 10 mm inter-electrode distance (Ad-Tech). Electrode strips consisted of 1x12, 1x8, 1x6, or 1x4 electrodes of the same size and spacing as the grid electrodes. Placement of the electrodes would vary by subject depending on their clinical needs.

For the EEG subjects, neural signals were recorded using the Neuroelectrics Enobio 8 channel cap (using dry electrodes) through the Neuroelectrics NIC2 recording software and custom Python code written to control the stimuli displayed on the screen and communicate with NIC2 using Lab Streaming Layer.

4.4 Cortical reconstructions for ECoG

Voltage recordings from the cortex do not inherently contain information regarding their spatial location on the cortex. To have a better understanding of where the electrodes are located than just by observing clinical montage sheets, we perform cortical reconstruction of each subject's brain and localize the electrodes based on the subject's pre-operative MRI and post-operative CT scans. In more detail, we reconstruct the surface using recon-all in FreeSurfer (Fischl, 2012) while simultaneously acquiring electrode location via the CT which has been co-registered to the MRI using SPM8 (Wellcome Trust Centre for Neuroimaging, University College London). Electrode locations are hand labeled using the electrode editor in BioImage Suite (Papademetris et al., 2006). Once the surface reconstruction is complete, grid and strip electrodes are projected down to the nearest pial surface. After obtaining the estimated locations of each individual electrode on the individual's cortical surface, we transform the electrode coordinates to Talairach or MNI space to estimate Brodmann Area labels for each electrode. This allows us to gain a better understanding of which functional area each electrode may be located and is relevant for grouping and isolating channels of interest in Chapters 5 and 6.

5. Error-related potentials in a cortical BCI

Error-related potentials have been investigated extensively in EEG (Cavanagh and Frank, 2014; Chavarriaga and Millan, 2010; Ferrez and del R Millan, 2008; Iturrate et al., 2013; Spüler and Niethammer, 2015; Zhang et al., 2015) and in ECoG (Bechtereva et al., 2005; Milekovic et al., 2012, 2013). However, the studies that employ BCI to study error typically do so with discrete-control systems. Continuous control BCI for error analysis has been performed with non-invasive EEG, but not with ECoG. In this chapter, we investigate error-related potentials in a one-dimensional center-out BCI task in ECoG to study the involvement of local activity during continuous control. At the end of the chapter, we also discuss a short-term collaborative project where we investigated error-related potentials in a naturalistic, task-free setting. Exploring error-related potentials at the cortical level during continuous control BCI will allow us to better understand cortical error presentation in the context of continuous control systems such as with neuroprostheses and co-adaptive BCIs.

This investigation on error-related potentials in ECoG BCI has been accepted for publication and reviewed in Frontiers Neuroscience - Neuroprosthetics as “Cortical topography of error-related high-frequency potentials during erroneous control in a continuous control Brain-Computer Interface” (Wilson et al., 2019). Note that Jeremiah Wander, alumnus of the lab, designed the task and collected the data prior to my joining the lab. The unique analysis approach in this chapter was conceived and performed by me. In the following chapters, I designed the tasks and collected the data in addition to analyzing and reporting the data/results.

5.1 Abstract

Brain-Computer Interfaces (BCIs) benefit greatly from performance feedback, but current systems lack automatic, task-independent feedback. Cortical responses elicited from user error have the potential to serve as state-based feedback to BCI decoders. To gain a better understanding of local error potentials, we investigated responsive cortical power underlying error-related potentials (ErrPs) from the human cortex during a one-dimensional center-out BCI task, tracking the topography of high

gamma (70-100 Hz) band power (HBP) specific to BCI error. We measured electrocorticography (ECoG) in three human subjects during dynamic, continuous control over BCI cursor velocity. Subjects used motor imagery and rest to move the cursor towards and subsequently dwell within a target region. We then identified and labeled epochs where the BCI decoder incorrectly moved the cursor in the direction opposite of the subject's expectations (i.e., BCI error). We found increased HBP in various cortical areas 100-500 ms following BCI error with respect to epochs of correct, intended control. Significant responses were noted in primary somatosensory, motor, premotor, and parietal areas and generally regardless of whether the subject was using motor imagery or rest to move the cursor towards the target. Parts of somatosensory, temporal, and parietal areas exclusively had increased HBP when subjects were using motor imagery. In contrast, only part of the parietal cortex near the angular gyrus exclusively had an increase in HBP during rest. This investigation is, to our knowledge, the first to explore cortical field changes in the context of continuous control in ECoG BCI. We present topographical changes in HBP characteristic specific to the generation of error. By focusing on continuous control, instead of on discrete control for simple selection, we investigate a more naturalistic setting and provide high ecological validity for characterizing error potentials. Such potentials could be considered as design elements for co-adaptive BCIs in the future as task-independent feedback to the decoder, allowing for more robust and individualized BCIs.

5.2 Introduction

Everyone makes mistakes and can learn from them. But the neurophysiological mechanisms behind how we recognize and use these mistakes to learn is still not completely understood. Prior studies have focused on the error-related potential (ErrP), an event-locked electrophysiological response generated during task rule violations. The vast majority of our understanding to date of the ErrP originates from electroencephalography (EEG) studies (Ferrez and Millan, 2008; Iturrate et al., 2013; Kreilinger et al., 2016; Spüler and Niethammer, 2015; Zhang et al., 2015). The typical coverage and high temporal resolution of EEG, relative to fMRI, allow for the identification of wide-spread voltage changes in response to error. However, because EEG is non-invasive, electrical signals from the cortex attenuate and diffuse as they travel up through the skull, leading to lower signal-to-noise ratio (SNR) and

challenges in source localization (Jatoi et al., 2014; Olson et al., 2016). To circumvent some of these limitations, we investigate error-related potentials in a one-dimensional brain-computer interface (BCI) task using subdural electrocorticography (ECoG) in human subjects.

BCIs represent a particularly useful opportunity to characterize error-related brain responses. BCIs rely on closed-loop (typically) visual feedback to inform the user of their control and on-going performance. This feedback is hypothesized to be key to the BCI learning process and performance improvement (Green and Kalaska, 2011), analogous to the utility of somatosensory feedback during the acquisition of new motor skills (Newell, 1991). BCI decoders have traditionally been static, in the sense that initial parameters in the algorithm would be set and only changed by manual updates performed by the BCI technician. Recently, however, there has been a push to develop dynamic feedback systems that automatically update over time based on pre-task parameters (DiGiovanna et al., 2009; Merel et al., 2015; Orsborn et al., 2014; Pohlmeyer et al., 2014). However, most efforts so far rely on knowledge of the task and of actuator kinematics, thus limiting BCI co-adaptation to the research setting and do not allow for automatic updating based on signals generated by the user. A co-adaptive BCI may improve the user experience by promoting faster mastery of the BCI and by allowing longer term use through accounting for changes in the brain due to plasticity.

Our motivation in this report was to gain a better understanding of the electrophysiological signatures of error potentials in BCI and whether this will serve to better inform unsupervised co-adaptive BCIs. Specifically, relying on ErrPs as a feedback source to inform adaptive BCI decoders, rather than on specific task data, will allow for BCI use in less constrained environments.

Previous work suggests there are different types of error-related potentials which manifest in different contexts (Milekovic et al., 2012; Spüler and Niethammer, 2015). Such potentials are generally categorized into two classes, high-level error and low-level error (Krigolson and Holroyd, 2007). Krigolson and Holroyd distinguish the two on temporal disparities. Specifically, low-level errors are those immediately correctable in control, and high-level errors as not immediately correctable, which prevent the achievement of a desired goal (Krigolson and Holroyd, 2007). For example, a reactionary turn of the steering wheel to adjust for an unseen bump in the road would be considered low-level

error, and failing to reach your destination would be considered high-level error. High-level error, also called outcome error, is thought to be represented by the error-related negativity (ERN), which is often localized to the medial-frontal cortex (Krigolson and Holroyd, 2007; Wessel, 2012) and is believed to be essential to reinforcement learning (Nieuwenhuis et al., 2004). The reinforcement learning theory of the ERN suggests the error signals are generated in the basal ganglia and propagate to the cortex through the anterior cingulate cortex (ACC). Localization of the cortical error-related potentials to the ACC has been suggested in EEG (Krigolson and Holroyd, 2007; O'Connell et al., 2007) and confirmed through ECoG (Bechtereva et al., 2005).

Low-level error, known as target error (Krigolson and Holroyd, 2007; Krigolson et al., 2008) or execution error (Milekovic et al., 2012, 2013), is believed to be represented by positive deflections originating from the posterior parietal cortex (PPC) following commitment of a behaviorally-defined error (Krigolson and Holroyd, 2007; Krigolson et al., 2008; Ladouceur et al., 2007). Although the exact role of this positive activity over PPC is not completely agreed upon, the extent literature converges on a general hypothesis that the PPC is involved with action conflict monitoring, including movement correction (Falkenstein et al., 2000; Krigolson and Holroyd, 2007; Nieuwenhuis et al., 2001; Van Veen and Carter, 2002).

Various EEG studies have identified and investigated ErrPs in the form of ERN (Iannaccone et al., 2015; Krigolson et al., 2008; Ladouceur et al., 2007; Nieuwenhuis et al., 2001; Ullsperger and von Cramon, 2006), P_E (Ladouceur et al., 2007; Navarro-Cebrian et al., 2016; Nieuwenhuis et al., 2001), P300 (Krigolson et al., 2008; MacLean et al., 2015), and other signals (Chavarriaga and Millan, 2010; Ferrez and Millan, 2008; Kim and Kirchner, 2013; Krigolson and Holroyd, 2007; Spüler and Niethammer, 2015).

Here we aimed to expand upon our understanding of ErrPs by bridging EEG efforts and characterizing time-frequency responses through ECoG, cross-referencing evoked power effects to the common cortical-localized sites of evoked response ErrPs. We focus on low-level error and its presentation in the parietal cortex, as clinical requirements of electrode placement often constrain consistent frontal coverage. In addition, low-level error is ultimately more relevant in influencing real-time BCI control

on a finer time scale than high-level error, which can only be used to provide feedback on longer time-scales (e.g., once per trial).

A previous ECoG study by Milekovic and colleagues demonstrated the presence of ErrPs across multiple cortical regions in a continuous, overt-movement task in human ECoG (Milekovic et al., 2012, 2013). The researchers observed low-level and high-level ErrPs, described as execution and outcome errors, respectively, in the motor, somatosensory, parietal, temporal, and pre-frontal areas. Here, we utilize ECoG to investigate whether errors induced during a motor-imagery BCI task would also result in the typical ErrP profile. We focused exclusively on high gamma (70-100 Hz) activity. High frequency broadband power (HBP) is thought to best reflect local activity (Manning et al., 2009; Miller et al., 2009a; Ray et al., 2008) and is reliably recorded through ECoG. We are particularly interested in examining local response activity for error-processing across the surface of the human brain. Rather than examining errors resultant from (1) failed trial outcomes, (2) induced error, or (3) unexpected stimuli beyond the user's control, we took a novel approach by examining naturally occurring errors in the BCI decoder's performance in a continuous control one-dimensional center-out task.

We hypothesize significant HBP changes in error-related detection cortex. This is built on literature and computational models describing ErrPs as a mismatch between sensory expectation from an efference copy and from actual sensory input (in this case, visual) (Holroyd and Coles, 2002; Nieuwenhuis et al., 2004). This mismatch can be thought of as the sensory discrepancy described in Miall and Wolpert's forward model, which is the difference between actual sensory feedback and expected sensory feedback from an efference copy (Miall and Wolpert, 1996). By gaining a better understanding of the contribution of HBP to ErrPs, we eventually hope to enable unsupervised reinforcement learning in the BCI decoder allowing for robust co-adaptation and improvement of BCI usability.

5.3 Methods

5.3.1 Participants

Three patients with medically intractable epilepsy (mean age 19.67 yrs, 1 male), undergoing clinical seizure monitoring at either Harborview Medical Center or Seattle Children's Hospital, consented and

volunteered to participate in research in accordance with the University of Washington Institutional Review Board (see Table 1 for demographics).

5.3.2 Data recording and electrode localization

The electrocorticogram was acquired from subdural macro-scale grid electrodes (Ad-Tech 8x8 platinum, 10mm contact spacing). Cortical potentials were recorded at 1200 Hz using g.USBamps (GugerTec, Graz, Austria) through the BCI2000 software suite (Schalk et al., 2004). Pre-operative T1 MRI scans were co-registered with post-operative CT scans (SPM8) to allow for individualized electrode localization through BioImageSuite software imaging package (Papademetris et al., 2006) in accordance with previously published reports (Casimo et al., 2016). Each subjects' electrodes were then normalized to the 1 mm MNI 251 brain coordinate system (Evans et al., 1993) using Freesurfer's ReconAll for multi-subject analysis (Fischl, 2012) and a secondary transform through FSL FLIRT (part of the FMRIB Software Library - FSL, www.fmrib.ox.ac.uk/fsl) algorithms. Center value MNI coordinates for each electrode were transformed to Talairach space using the MNI anatomical labeling atlas, and Brodmann Area (BA) labels were estimated using the Talairach Daemon Client (Talairach and Tournoux, 1988).

5.3.3 BCI task

Subjects were instructed to control the vertical velocity of a cursor in a one-dimensional center-out BCI task, to reach and dwell within a trial target for one second using motor imagery (Figure 1a). Although trial success was determined by whether the cursor dwelled within the target for one second, our investigation focused on correct and erroneous movements made towards or away from the target (specific details provided below). The control electrode was selected through a prior motor screening task, which was used to identify the channel exhibiting the strongest HBP response to a cued imagined movement task of the contralateral hand or tongue (depending on electrode coverage) as previously described (Wander, 2015; Table 1). Consequently the control electrode was always localized to the primary motor cortex.

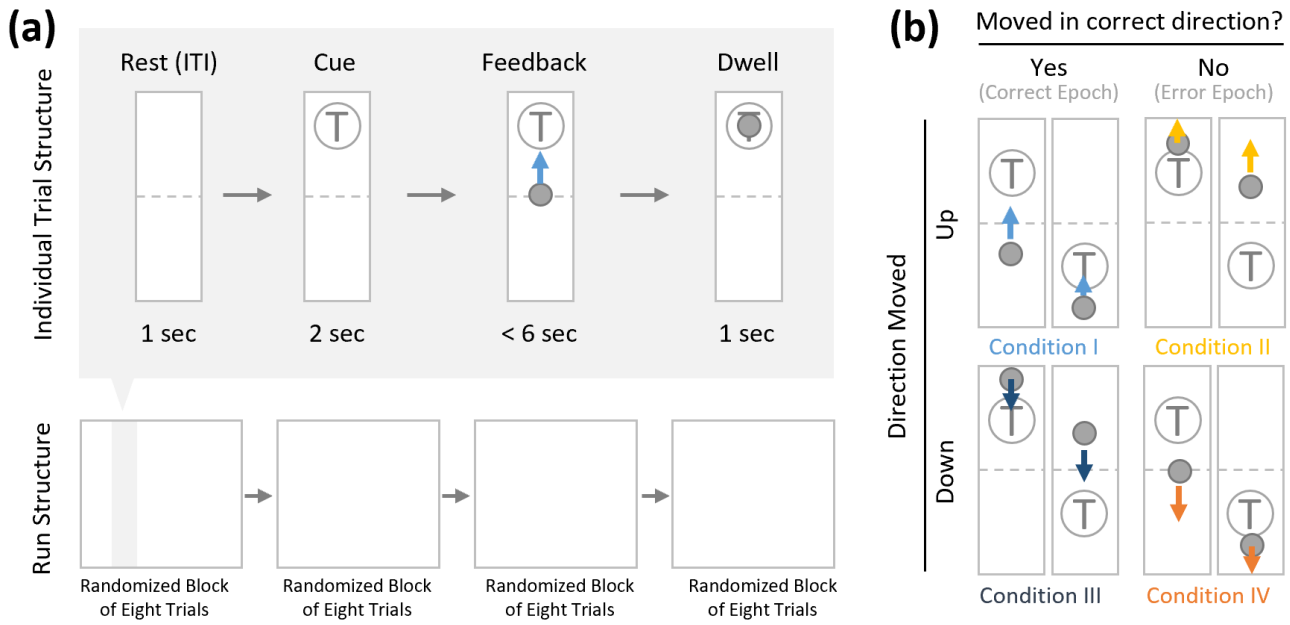

Figure 1. Task structure and epoch conditions. (a) Subjects modulated cursor velocity in a one-dimensional center-out BCI task using imagined hand or tongue movement (Table 1) in order to reach and dwell within a target. Cursor was re-centered prior to each trial and was not displayed during the inter-trial interval (ITI) and cue period. Trials were randomized to have the target located above or below the start position, near or far, and small or large. Trials were organized into four blocks, each containing eight randomized trials. (b) Within trials, data was binned into epochs based on four movement conditions: cursor moved up correctly (I, light blue), moved up erroneously (II, yellow), moved down correctly (III, navy blue), or moved down erroneously (IV, orange).

Each BCI run consisted of four blocks of eight randomly ordered trials. Targets were placed either above or below the starting center point, either large or small (35% or 20% of screen height, respectively) and placed either near or far from the starting center point (20% or 16% of screen height, respectively). This resulted in eight unique trial configurations per block. Each trial was structured to include a one second rest period where neither the cursor nor target were displayed (inter-trial interval; ITI), followed by a two second cue period where the target was visible, followed by a feedback period of up to six seconds where subjects would attempt to reach and dwell within the trial target for one second. Each trial would terminate either when dwell time was reached or the trial timed out, whichever came first.

For the purposes of these analyses, we grouped trial configurations to only distinguish between trials where the target was placed above or below the starting point, reflecting differences in behavioral task demands.

To drive the cursor up, subjects were required to increase HBP in their control electrode using motor imagery. HBP was estimated using BCI2000's auto-regressive filter on the preceding 500 ms of data. HBP was normalized to 6 seconds of pre-trial data using the BCI2000 built-in normalizer, and were linearly mapped to cursor velocity as described in (Wolpaw and McFarland, 2004). To drive the cursor down, they were instructed to rest. The cursor velocity was updated every 40 ms.

5.3.4 Offline analysis for error-related potentials

All signal processing and statistical analyses were conducted in MATLAB (MathWorks, Natick, MA) computing environment. For each subject, we performed common average referencing to account for common noise across all channels in the grid. We then removed 60 Hz noise and isolated the high gamma frequency band activity (HG, 70-100 Hz) using 4^{th} order Butterworth filters (non-causal), and estimated the amplitude envelope of the signals using a Hilbert transform. Power was calculated by taking the absolute square of the analytical amplitude across the full time series. Then the power for each trial was normalized with respect to the preceding inter-trial interval (baseline) by calculating the z-score specifically for HBP. The full normalized power time series was smoothed using a sliding Gaussian window with a window width of 40 samples to match the update rate of the task ran in BCI2000.

5.3.4.1 Error and correct window extraction

We were specifically interested in the topography of the responsive HBP during periods of BCI error. To accomplish this, we first grouped subject's electrodes by identified Brodmann Areas. Second, we defined decoder error as a mismatch between the decoder assessment of HBP and the subject's goal-directed intention. This was defined operationally as when the slope of the cursor movement (at any junction across the 6000 ms duration of a trial) was in the direction opposite of the target position for a continuous period of 400 ms. This definition allowed for the identification of improper decoding under the assumption that subjects intend to move the cursor towards a target during trial feedback (for clarification, see Figure 1b). We reasoned 400 ms duration is sufficient time for the subjects to realize error during real-time continuous feedback (Gerson et al., 2005). We then identified the

beginning of this period as t = 0 in error identification. Likewise, correct performance windows were extracted where the cursor movement was in the direction towards the target for a 400 ms period, with t = 0 at the start of this period. We then extracted error and correct epochs from these error and correct windows, respectively.

To prevent overlap between epochs, we extracted only one epoch per window, where we defined windows of 1000 ms starting from 200 ms prior to our t = 0 time points to 800 ms after, based on previously published reports investigating error-related potentials in an overt-movement ECoG task (Milekovic et al., 2012). Figure 2 shows data of one full length trial from an example electrode with example windows and example epochs. Note that there are often multiple error and/or correct epochs within any given trial, based on our pre-defined states described below.

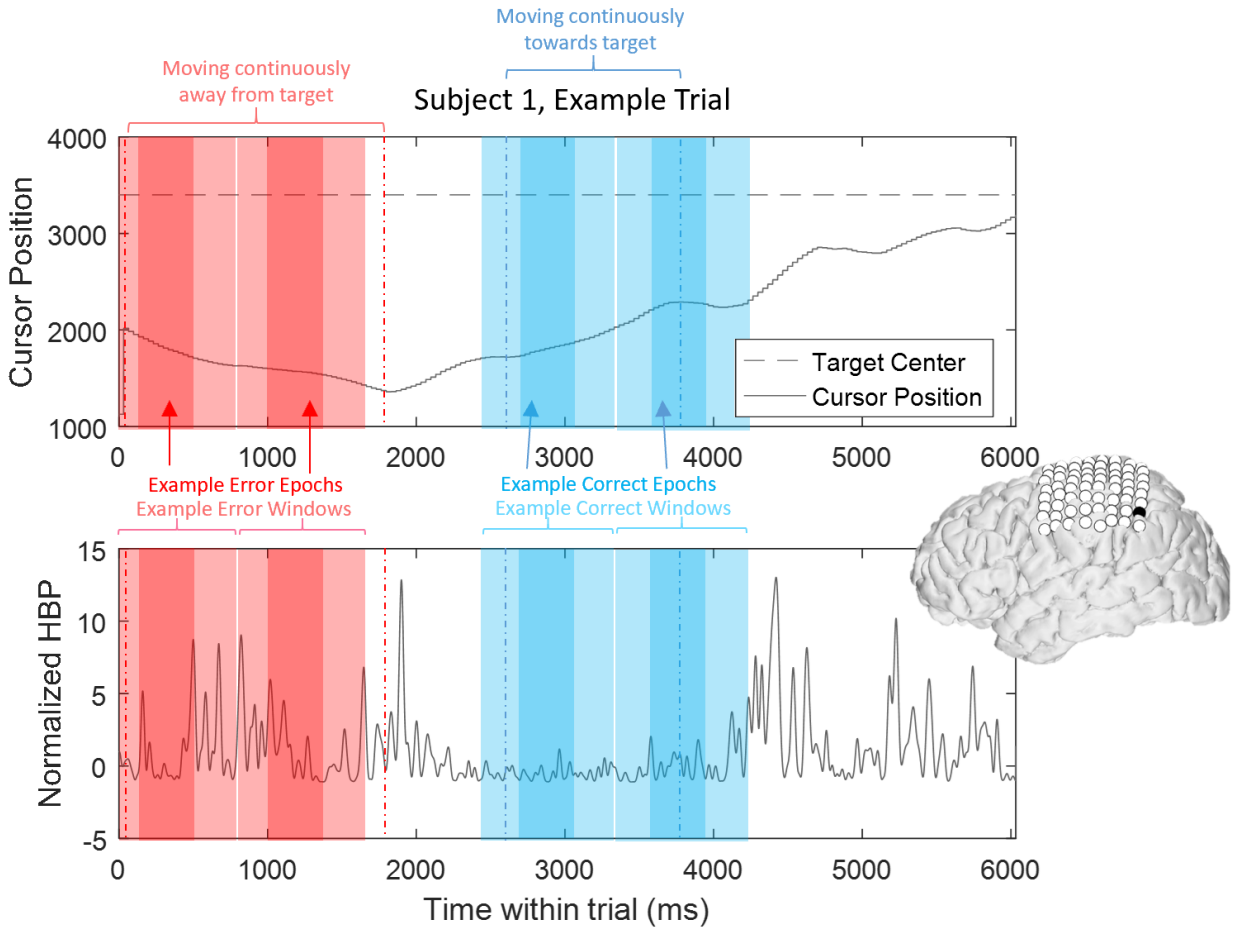

Figure 2. HBP throughout one trial. In this parietal channel in one subject (shown in black), we see a decrease in HBP as the cursor moves correctly towards the target and increase when the cursor is no longer moving as intended. The highlighted light red sections shows example error windows, where their t = 0 time points are defined by 400 ms of continuous movement away from the target. The darker red areas represent example error epochs. Likewise, the highlighted light blue sections show example correct windows, and the dark blue sections show example correct epochs, as detailed in Section 2.4.

From these defined windows, we classify epochs into the four conditions presented in Figure 1b. Specifically, error epochs were classified as when the cursor moves incorrectly upwards when located above a target (Condition II) and when the cursor moves incorrectly downwards when located below a target (Condition IV). Finally, correct epochs were defined as when the cursor moves correctly upwards when located below a target (Condition I) and when the cursor moves correctly downwards when located above a target (Condition III).

5.3.4.2 Statistical analysis epochs from windows

To contrast HBP behavior across the cortical sampling space during real-time continuous error detection, we generated statistical analysis epochs from error and correct windows. These epochs were

defined as the samples from t = 100-500 ms in their respective 1000 ms windows (where t = 0 corresponds to the start of 400 ms consecutive movement in one direction, as described above). Previous ErrP work by (Milekovic et al., 2012) observed that the window from 100-800 ms after error onset engendered ECoG, error-related components during an overt motor control task. We used the length and range of t = 100-500 ms after error onset to characterize responsive HBP behavior based on (1) a relatively short, continuous trial period (6000 ms) and (2) previous EEG observations of typical higher-order processing time of visual cues ranging from 150-500 ms, depending on the cortical area being examined (Gerson et al., 2005).

5.3.5 Statistical analysis

At the group analysis level, we conducted a two-way ANOVA by extracting mean HBP from our defined statistical analysis epochs and estimating main effects of trial type (whether the target was located above or below the center starting position, requiring motor imagery or rest, respectively) and performance (whether the epoch was a correct epoch (Conditions I and III) or an error epoch (Conditions II and IV)) on HBP for each Brodmann Area available.

We utilized post hoc two-sample t-tests (FDR corrected) to identify significant interactions of correct and erroneous decoder behavior epochs by subject action type (active motor imagery or rest). We present our findings through exploring error-related potentials as changes in HBP across cortical areas. That is, our post hoc approach compares (1) HBP of all error epochs and (2) HBP of all correct epochs from all channels falling within each Brodmann Area of interest. Finally, at the individual level, we utilized these two-sample t-tests.

5.4 Results

5.4.1 Task performance

As common with motor imagery controlled BCIs, the users experienced difficulty in achieving high task performance without an extensive calibration period (Blankertz et al., 2007, 2008a, 2010; Wolpaw and McFarland, 2004). The low overall trial success of the subjects (average trial success 30.67%, Table 1)

may be due to the difficulty of the task requirement to dwell within the target, and the limited amount of time we had with each subject for training (Table 1). Overall, all three subjects had greater trial success when the target was below the cursor starting position (average trial success 37.93%, Table 1). The effects of task performance on error potentials is discussed in the discussion section.

ID	Sex	Age	Hemisphere	Control Channel	# of Trials	Successful Up Trials Per Run	Successful Down Trials Per Run	Overall Trial Success	# of Up error epochs	# of Up correct epochs	# of Down error epochs	# of Down correct epochs
S1	F	11	Left	Hand	49	20.8%	40.0%	30.6%	6	40	39	13
S2	M	13	Left	Tongue	141	28.6%	39.4%	34.0%	31	59	43	32
S3	F	35	Left	Hand	62	20.0%	34.4%	27.4%	21	27	17	22

Table 1. Subject information and task performance separated by trial type.

5.4.2 Effect of trial type and performance on group HBP responses

To determine the HBP response topography of error performance (whether the cursor moved accurately towards or away from the target) we conducted a two-way ANOVA on HBP across BA regions. Results from all available BA regions are presented in Table 2. Here we focus on specific BA regions of interest related to ErrPs. Table 3 denotes the number of contributing electrodes from each subject within each BA investigated.

Brodmann Area	Subjects Included	ANOVA results (interaction)	ANOVA results (trial type)	ANOVA results (performance)
1	Subjects 1, 3	F(1, 649) = 1.65, p = 0.1999	F(1, 649) = 2.44, p = 0.1187	F(1, 649) = 2.31, p = 0.1288
2	All	F(1, 1037) = 2.69, p = 0.1011	F(1, 1037) = 2.59, p = 0.1078	F(1, 1037) = 2.3, p = 0.1296
3	All	F(1, 912) = 3.97, p = 0.0466	F(1, 912) = 3.76, p = 0.0529	F(1, 912) = 5.92, p = 0.0152
4	All	F(1, 999) = 8.46, p = 0.0037	F(1, 999) = 4.49, p = 0.0343	F(1, 999) = 2.49, p = 0.115
5	Subjects 1, 3	F(1, 573) = 2.48, p = 0.1157	F(1, 573) = 3, p = 0.0836	F(1, 573) = 9.61, p = 0.002
6	All	F(1, 4258) = 0.08, p = 0.775	F(1, 4258) = 14.01, p = 0.0002	F(1, 4258) = 1.93, p = 0.1648
7	Subjects 1, 3	F(1, 845) = 2.73, p = 0.0987	F(1, 845) = 0.28, p = 0.5981	F(1, 845) = 3.42, p = 0.0649
9	Subjects 2, 3	F(1, 413) = 0.24, p = 0.6209	F(1, 413) = 3.01, p = 0.0833	F(1, 413) = 3.92, p = 0.0485
21	Subjects 2, 3	F(1, 2246) = 0.12, p = 0.7312	F(1, 2246) = 0.26,p = 0.6104	F(1, 2246) = 2.54, p = 0.1112
22	Subjects 2, 3	F(1, 2099) = 0.76, p = 0.3833	F(1, 2099) = 2.86, p = 0.0909	F(1, 2099) = 18.69, p = 0
37	Subject 2	F(1, 656) = 1.62, p = 0.203	F(1, 656) = 0.82, p = 0.3642	F(1, 656) = 1.82, p = 0.1777
39	Subjects 2, 3	F(1, 335) = 0.76, p = 0.3845	F(1, 335) = 1.31, p = 0.2509	F(1, 335) = 0.04, p = 0.8385
40	All	F(1, 4918) = 6.09, p = 0.0136	F(1, 4918) = 4.48, p = 0.0342	F(1, 4918) = 7.21, p = 0.0073
42	Subjects 2, 3	F(1, 500) = 0.08, p = 0.7749	F(1, 500) = 0.01, p = 0.9105	F(1, 500) = 0.66, p = 0.4158
43	Subject 2	F(1, 161) = 9.45, p = 0.0025	F(1, 161) = 9.41, p = 0.0025	F(1, 161) = 7.59, p = 0.0065
44	Subject 3	F(1, 257) = 1.53, p = 0.2176	F(1, 257) = 0.09, p = 0.7683	F(1, 257) = 0.0967
45	Subject 3	F(1, 170) = 0, p = 0.9737	F(1, 170) = 0.23, p = 0.6301	F(1, 170) = 3.78, p = 0.0536

Table 2. Resultant p-values for the two-way ANOVA estimating the main effects of trial type (whether the target was located above or below the center starting position, requiring motor imagery or rest, respectively) and performance (whether the epoch was a correct epoch (Conditions I and III) or an error epoch (Conditions II and IV)) on HBP for each Brodmann Area available. Values below alpha of 0.05 are highlighted in green.

A significant main effect of trial type was observed in BA4 (primary motor cortex - F(1, 999) = 4.49, p = 0.0343), BA6 (premotor cortex - F(1, 4258) = 14.01, p = 0.0002), BA40 (inferior parietal lobule - F(1, 4918) = 7.21, p = 0.0073), and BA43 (F(1, 161) = 7.59, p = 0.0065). A significant main effect of performance was observed in BA3 (primary somatosensory cortex, F(1, 912) = 5.92, p = 0.00152), BA40 (F(1, 4918) = 4.48, p = 0.0342), and BA4 (F(1, 999) = 4.49, p = 0.0343). Importantly, we noted a statistically significant interaction between the trial type, control requirement and performance in primary somatosensory cortex (BA3; F(1, 912) = 3.97, p = 0.0466), in primary motor cortex (BA4; F(1, 999) = 8.46, p = 0.0037) as well in the inferior parietal cortex (BA40; F(1, 4918) = 6.09, p = 0.0136). For all ANOVA results, please refer to Table 2.

	Brodmann Area	1	2	3	4	5	6	7	9	21	22	37	39	40	42	43	44	45
Number of Electrodes	Subject 1	4	3	5	5	5	16	6	0	0	0	0	0	16	0	0	0	0
	Subject 2	0	4	1	1	0	10	0	2	11	8	4	1	14	2	1	0	0
	Subject 3	3	1	3	4	1	12	3	1	5	9	0	2	12	2	0	3	2
	Total	7	8	9	10	6	38	9	3	16	17	4	3	42	4	1	3	2

Table 3. Number of electrodes per Brodmann Area.

5.4.3 Error-related HBP time series by Brodmann Areas

To illustrate our overall HBP response profiles, we plotted the mean time-series for all four epoch conditions generated by averaging the responses of all constituent electrodes from all subjects for significant BA regions. Figure 3 shows the mean time-series during the correct and error windows used to extract our Condition I and IV epochs in all electrodes placed over the inferior parietal lobule (BA40). We observed increased HBP after error onset at t = 0 ms (red) when the decoder failed to recognize the subject's motor imagery as intent to move the cursor upwards towards the target (Condition IV). Contrarily, we did not see a general increase in HBP when the decoder was correctly decoding the subject's motor imagery (Condition I). During rest, we did not see a change in HBP relative to error onset (Figure 4). We generated similar plots for all available BAs during both motor imagery and during rest. Note, that t = 0 ms is a window-unique classification based on our behavioral mismatch between cursor trajectory and decoder output. Our t = 0 is not a phase-resetting, evoked boundary event in the classic sense of evoked potentials. Importantly, because there were typically multiple error and correct epochs within any given trial, t < 0 reflects behaviorally heterogeneous conditions.

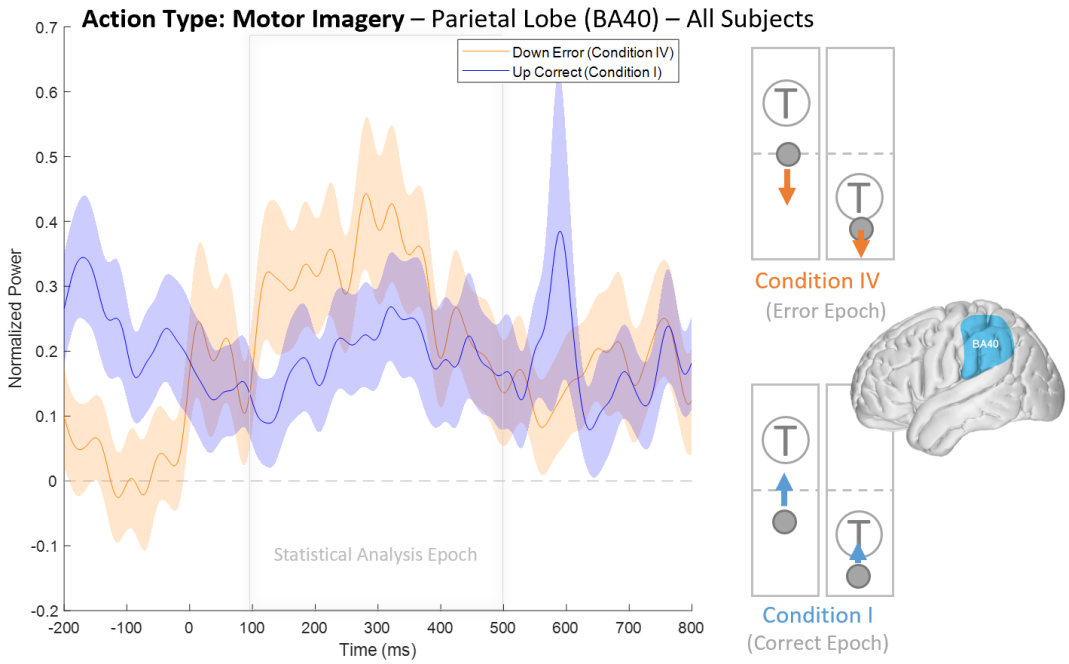

Figure 3. Time series of mean HBP during motor imagery in the decoder error and correct conditions in the parietal lobe (BA40, highlighted in the brain inset). In these conditions, the subjects were attempting to move the cursor towards the target through eliciting motor imagery. In the erroneous condition, the BCI mistakenly decoded the subject's intention as wanting to move downwards with rest. Error onset begins at time t = 0 ms for the Condition IV plot. Statistical analyses were performed using the time window of t = 100-500 ms (i.e. the statistical analysis window), as indicated by the window on the figure. Shaded region shows standard error of the mean. Dashed gray line represents baseline.

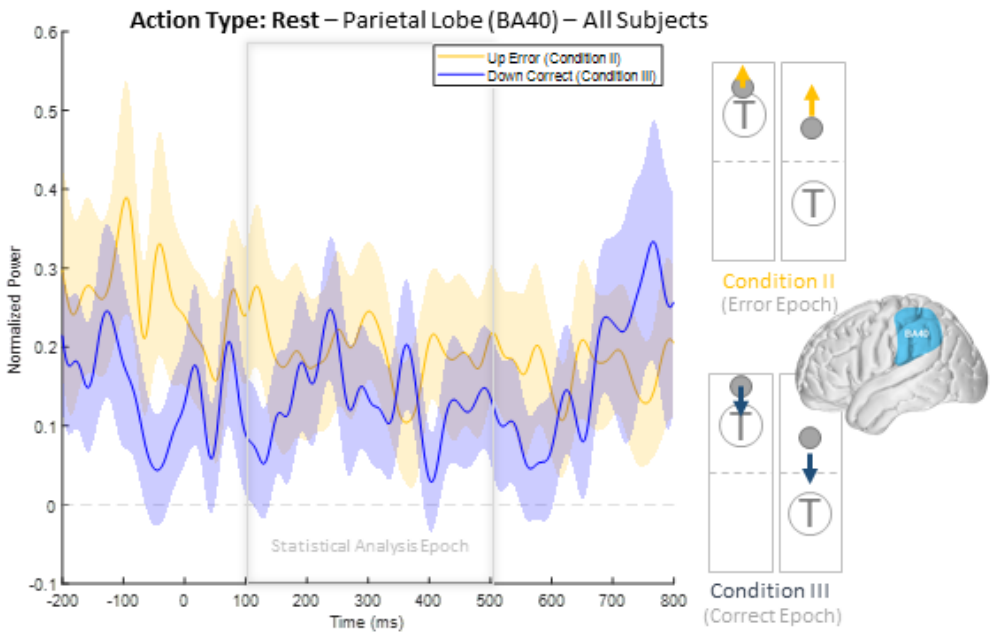

Figure 4. Time series of mean HBP during rest in the decoder error and correct conditions in the parietal lobe (BA40, highlighted in the brain inset). In these conditions, the subjects were attempting to move the cursor towards the target through rest. In the erroneous condition, the BCI mistakenly decoded the subject's intention as wanting to move upwards with motor imagery. Error onset begins at time t = 0 ms for the Condition II plot. Statistical analyses were performed using the time window of t = 100-500 ms, as indicated by the window on the figure. Shaded region shows standard error of the mean. Dashed gray line represents baseline.

Collectively, this approach provides a useful description of the overall responsive cortical regions generating ErrPs. We next used post hoc tests to determine the specific nature of HBP activity as a function of error and correct condition type. We contrasted two different populations for a given action type, motor imagery or rest for significantly responsive regions: (1) the mean value for each error epoch 100-500 ms following error onset from all electrodes within the specified BA, and (2) the mean value for each epoch during correct decoder performance 100-500 ms following the start of recognized correct performance, from all electrodes within the specified BA. We applied a one-sided t-test to test the specific hypothesis that HBP is greater in error than in correct epochs.

When comparing average responses following error onset (100-500 ms) during motor imagery (Condition IV – Condition I), we found motor, somatosensory, temporal, and parietal areas as having greater HBP in error epochs than in correct epochs (Figure 5). Specifically, HBP in Condition IV (motor imagery error) were significantly greater than in Condition I (motor imagery correct) in BAs 4 and 40 (one-sided student t-test, FDR-adjusted $p < 0.05$). During rest error (Condition II – Condition III), BA4 was statistically significant (Figure 6).

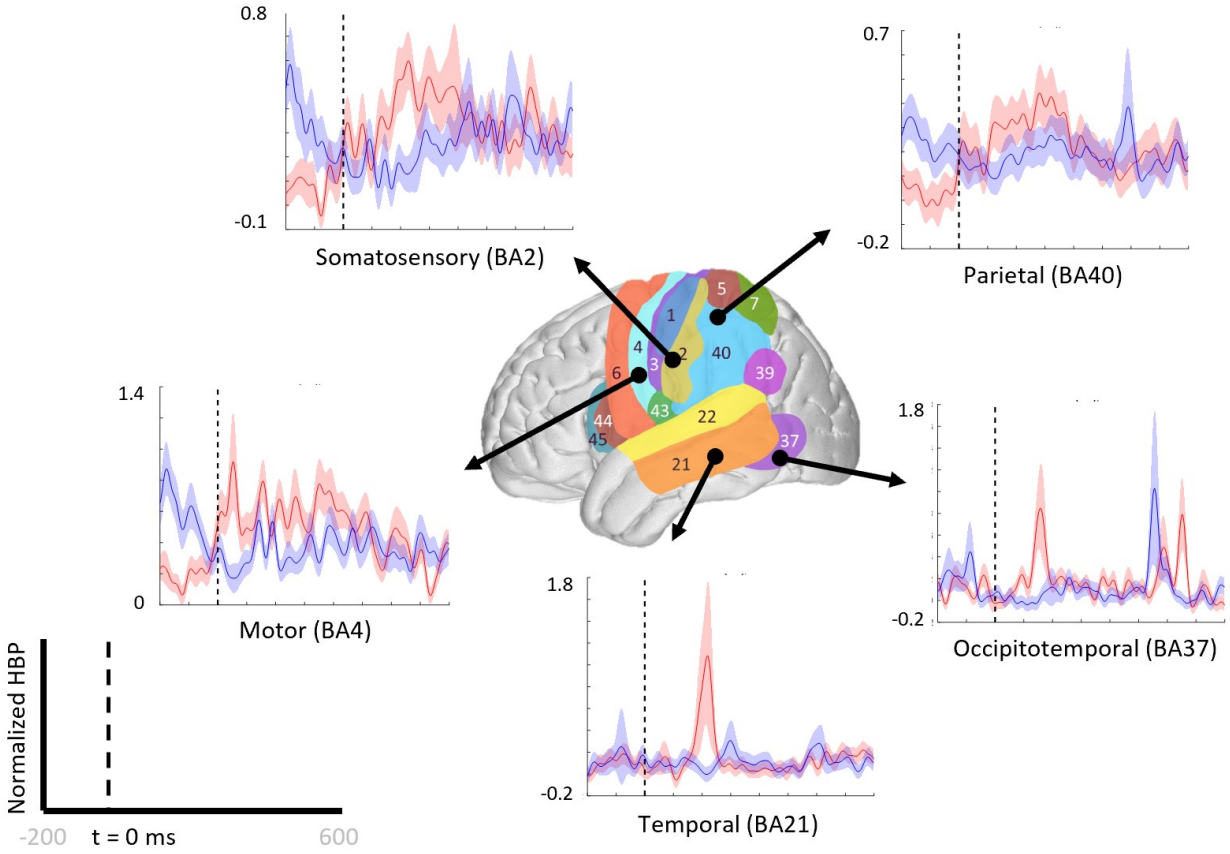

Figure 5. Increased HBP in multiple cortical areas during motor imagery error. The brain in the center shows the spatial range for each Brodmann Area available in our subject population, with each area labeled by their corresponding number. Each plot shows the average response within the specified Brodmann Area during erroneous decoding (red) and during correct decoding (blue), 100 ms to 500 ms after error onset (indicated by the vertical dashed line).

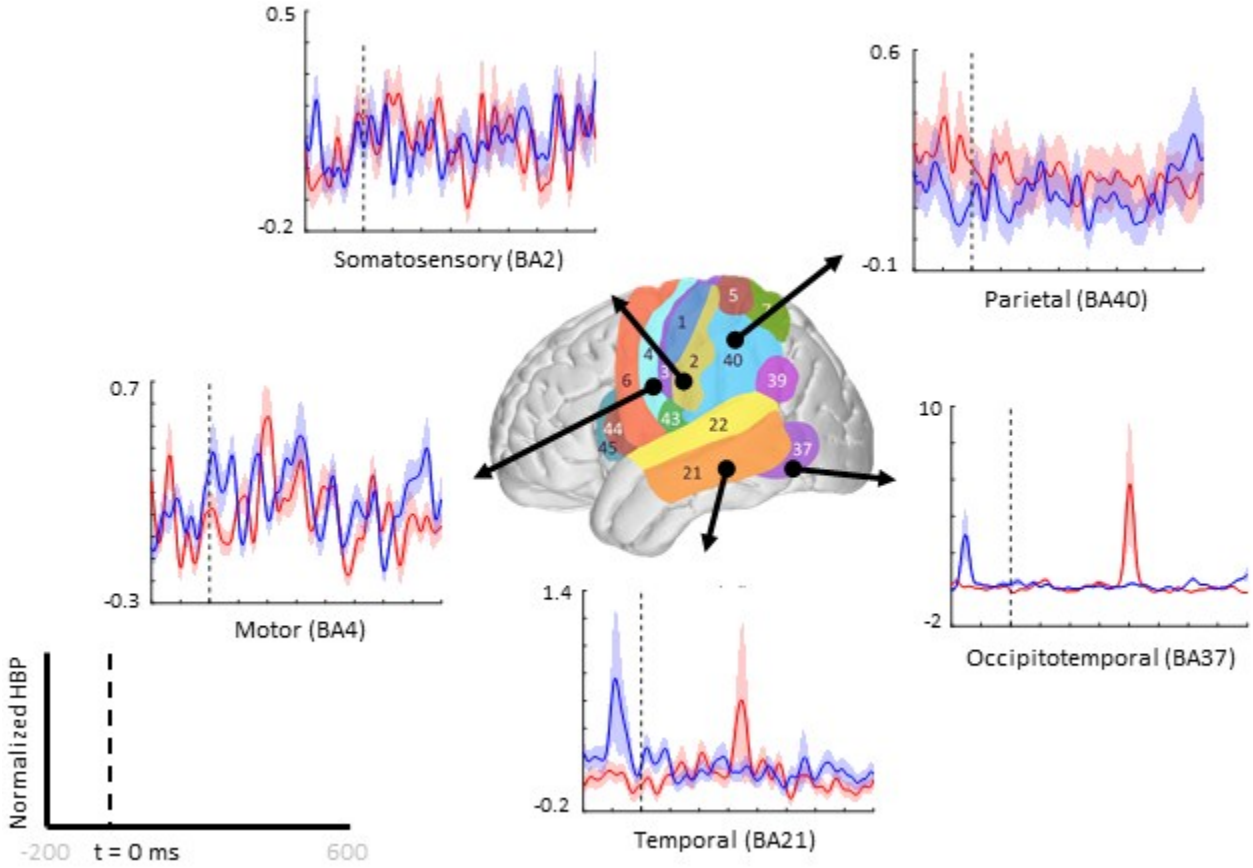

Figure 6. Increased HBP in multiple cortical areas during rest error. The brain in the center shows the spatial range for each Brodmann Area available in our subject population, with each area labeled by their corresponding number. Each plot shows the average response within the specified Brodmann Area during erroneous decoding (red) and during correct decoding (blue), 100 ms to 500 ms after error onset (indicated by the vertical dashed line).

5.4.4 Low frequency error-related potentials by Brodmann Areas

In addition to investigating increases in HBP in error epochs as compared to correct epochs, we also observed increases in spectral power in lower frequency bands in these same conditions. Although lower frequency activity is not as localized as high gamma activity, some lower frequency bands have played an important role in ErrP investigations in EEG work (Atchley et al., 2017; Glazer et al., 2018; Trujillo and Allen, 2007).

Like with HBP, we compared the band power between 100-500 ms after error onset and correct performance using one-sided student t-tests (alpha = 0.05) and correcting for multiple comparisons using FDR-adjusted p-values. For the delta band (< 4 Hz), we observed significantly greater power in error epochs compared to correct epochs, regardless of movement direction, posterior to the

temporoparietal junction (BA39). For the theta band (4-8 Hz), we observed significantly greater power in error epochs compared to correct epochs, regardless of movement direction, in Brodmann Area 9 (frontal) and in the temporal lobe (BAs 21, 22, and 37). For the alpha band (8-13 Hz), we observed significantly greater power in error epochs compared to correct epochs, regardless of movement direction, posterior to the temporoparietal junction (BA39) and in the temporal lobe (BAs 21 and 22). Lastly, for the beta band (13-30 Hz), we observed significantly greater power in error epochs compared to correct epochs, regardless of movement direction, only in the temporal lobe (BA21). For a full table of t-test results for all available Brodmann Areas and bands, see Table 4.

			Brodmann Area	1	2	3	4	5	6	7	9	21	22	37	39	40	42	43	44	45
FDR-corrected p-values	HG (70-100 Hz)	MI		<0.001	<0.001	<0.001	<0.001	<0.001	0.5939	<0.001	0.5939	<0.001	0.5939	<0.001	0.5939	<0.001	0.5939	0.5939	0.5939	0.5939
		Rest		<0.001	0.5939	0.5939	<0.001	<0.001	0.5939	<0.001	0.5939	0.5939	0.5939	0.5939	<0.001	0.5939	0.5939	0.5939	0.5939	0.5939
	Beta (13-30 Hz)	MI		0.8312	0.8312	0.8312	0.8312	0.8312	0.8312	0.8312	0.8312	<0.001	<0.001	0.8312	<0.001	0.8312	0.8312	0.8312	0.8312	0.4655
		Rest		<0.001	<0.001	<0.001	<0.001	<0.001	0.3559	<0.001	0.3559	<0.001	0.3559	<0.001	0.3559	<0.001	<0.001	0.3559	<0.001	0.3559
	Alpha (8-13 Hz)	MI		0.7283	0.7283	0.7283	0.7283	0.7283	0.7283	0.7283	0.7283	<0.001	<0.001	0.7283	<0.001	0.7283	0.7283	0.7283	0.0027	0.0326
		Rest		<0.001	0.0778	<0.001	<0.001	0.2947	<0.001	0.2947	<0.001	<0.001	<0.001	<0.001	<0.001	<0.001	<0.001	<0.001	0.2947	0.2947
	Theta (4-8 Hz)	MI		0.6532	0.6532	0.6532	0.6532	<0.001	0.6532	0.6532	<0.001	<0.001	<0.001	<0.001	0.6532	0.6532	0.6532	0.6532	<0.001	0.6532
		Rest		0.4747	<0.001	0.4747	<0.001	0.4747	<0.001	0.4747	<0.001	<0.001	<0.001	<0.001	<0.001	<0.001	0.4747	0.4747	0.4747	0.4747
	Delta (<4 Hz)	MI		<0.001	0.7124	0.7124	<0.001	<0.001	0.7124	<0.001	0.7124	0.7124	0.7124	0.7124	<0.001	0.7124	0.7124	0.7124	0.7124	0.7124
		Rest		0.4153	<0.001	0.4153	0.4153	0.4153	<0.001	0.4153	<0.001	<0.001	<0.001	<0.001	<0.001	<0.001	<0.001	<0.001	0.4153	0.4153

Table 4. Resultant p-values for testing if band power in error epochs (100-500 ms after error onset) was greater than band power in correct epochs using a one-sided paired student t-test (p-values FDR-adjusted for multiple comparisons, alpha = 0.05) across all subjects. Values below alpha of 0.05 are highlighted in green.

5.4.5 Error-related potentials in individual subjects

Beyond region of interest event-related error analysis, we also explored individual electrode response topography for each subject. Contributions from each electrode are presented in Figure 7 as the difference in mean HBP 100-500 ms following error onset in erroneous and correct decoding, during motor imagery. To visualize this topography, we used a Gaussian spatial smoothing kernel across electrodes allowing for the visualization of cortical-response 'heat maps' at the individual level. Warm

colors indicate a positive difference where HBP during error is greater than HBP during correct decoding.

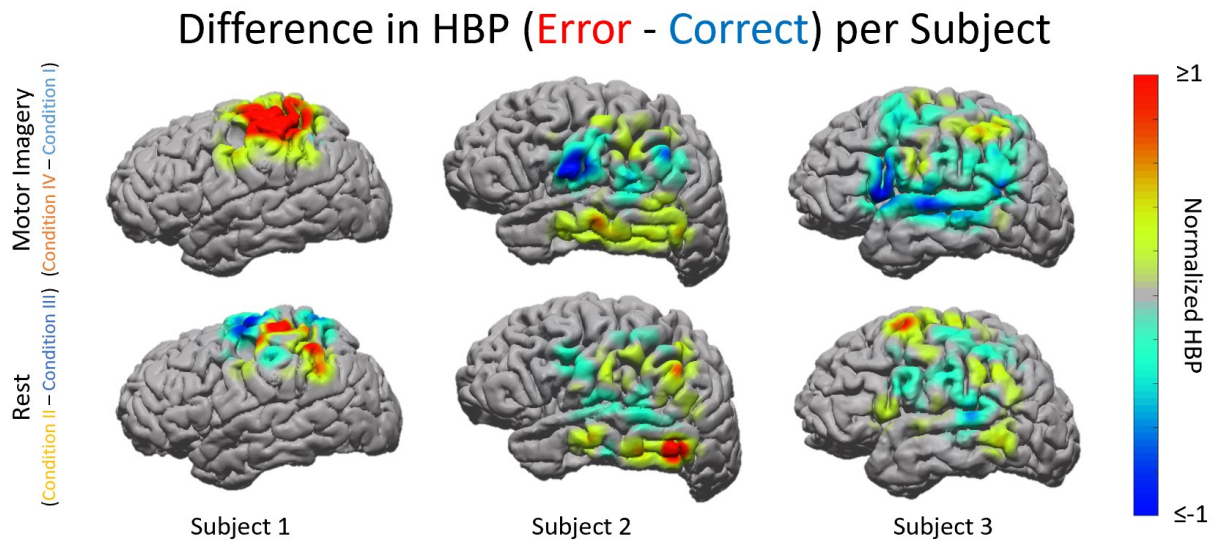

Figure 7. HBP during correct and erroneous BCI decoder performance per individual subject. Difference in high gamma power during correct and error epochs 100-500 ms after error onset for each subject. Top row shows power of Condition IV - Condition I, bottom row shows power of Condition II - Condition III. Heat maps were scaled to visualize the most robust effects.

As seen in Figures 7 and 8a, electrode coverage per subject varies thus yielding variable number of electrodes per Brodmann Area (Table 3). Similar to the group-wide analysis, we also determined significance of BAs within individual subjects by comparing the respective error and correct epochs applying one-sided student t-tests (alpha = 0.05) and correcting for multiple comparisons using FDR-adjusted p-values.

For Subject 1 (11 years old), the majority of electrodes present within the following areas had statistically significant greater HBP during error than during correct in the motor imagery case (Condition IV – Condition I): BAs 1, 3, 5-7, and 40 (one-sided student t-test, FDR-adjusted $p < 0.05$). Brodmann Areas 2 and 4 had a few significant electrodes. There was at least one significant electrode for all observable areas in this subject during motor imagery. During rest (Condition II – Condition III), the number of significant electrodes per respective area was lower than during motor imagery, except for in BA4. Like during motor imagery, there was always at least one electrode per area that was significant.

For Subject 2 (13 years old), 50% or more of electrodes present within the following areas had statistically significant greater HBP during error than during correct in the motor imagery case: BAs 2-4, 9, 21, 37, 40, and 42 (one-sided student t-test, FDR-adjusted $p < 0.05$). Brodmann Area 6 had one significant electrode, BA22 had three significant electrodes, and BAs 39 and 43 did not have any. During rest, the number of significant electrodes per respective area was typically lower than during motor imagery. Some areas, which had most of their electrodes significant during motor imagery, do not have any significant differences during rest (BAs 3-4, 9, 42).

For Subject 3 (35 years old), 50% or more of electrodes present within the following areas had statistically significant greater HBP during error than during correct in the motor imagery case: BAs 4 and 5 (one-sided student t-test, FDR-adjusted $p < 0.05$). Brodmann Areas 1, 6, 21, and 40 had at least one significant electrode each, and areas 2, 3, 7, 9, 22, 39, 42, 44, and 45 had no significant differences. During rest, the number of significant electrodes per respective area was typically higher than during motor imagery. With the exception of BA7, all the areas which had no significant electrodes during motor imagery had at least one significant electrode during rest.

5.4.6 Group analysis: Cortical topography of error-related HBP responses

Using the data from each electrode of all subjects (Figure 8), we generated cortical heat maps to observe the overall activity of the group. Figure 8 serves to show the contributions by electrodes instead of presenting the mean response of any given Brodmann Area. As seen when we project each subject's electrodes onto the MNI brain, each subject has different coverage and therefore contributes a different number of electrodes to each area of interest.

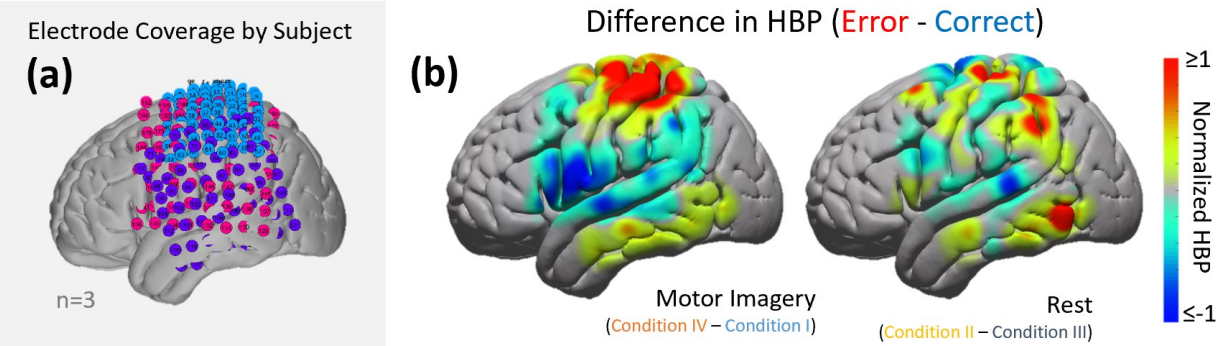

Figure 8. HBP during correct and erroneous BCI decoder performance. (a) Electrode coverage by subjects in the left (n=3), separated by color (Subject 1 in blue, Subject 2 in purple, Subject 3 in pink). (b) Difference in high gamma power during correct and error epochs 100-500 ms after error onset. Left shows power of Condition IV - Condition I, right shows power of Condition II - Condition III. Heat maps were scaled to visualize the most robust effects.

The areas with the most common coverage were BA40 (part of the parietal cortex) and BA6 (posterior-most part of the frontal cortex), with 42 and 38 total electrodes per area, respectively. Areas 2-4 also had common coverage but had 10 electrodes or less per area.

We zoom-in to a portion of the parietal lobe in Figure 9 to show examples of individual electrode contributions from all subjects in BA40, one of the few areas with multiple electrodes from each subject.

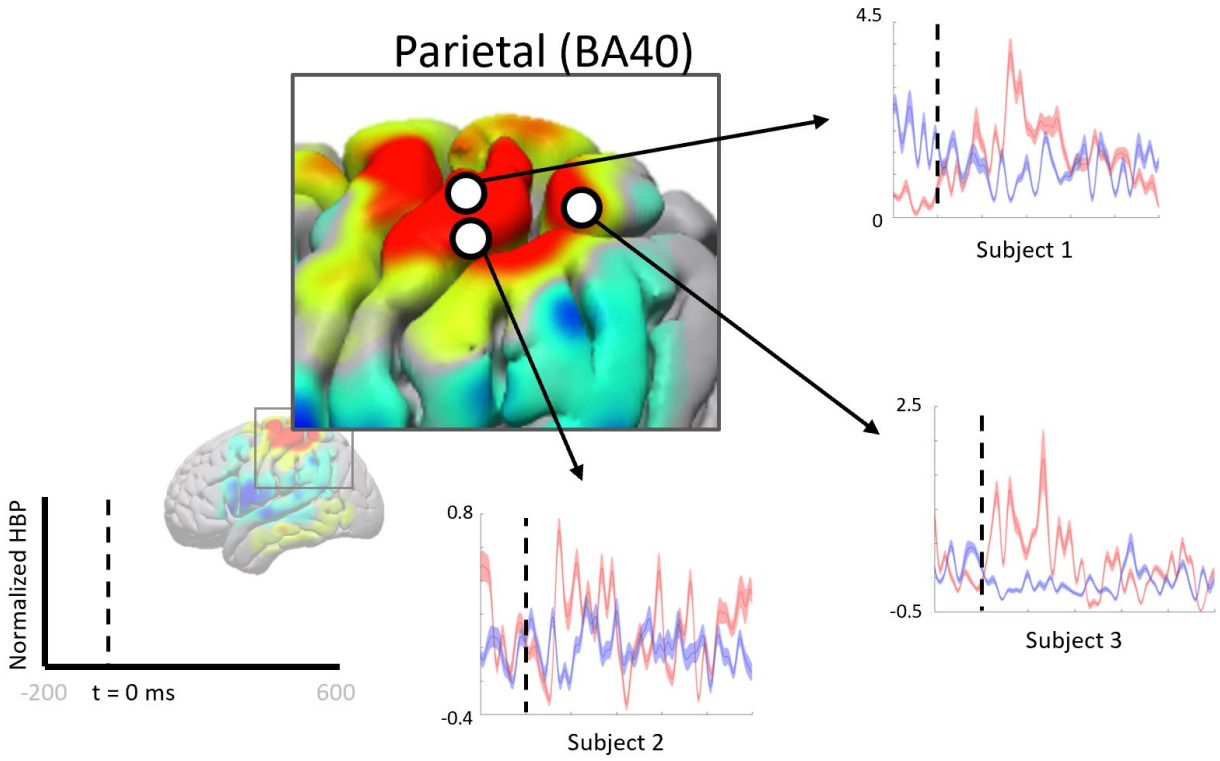

Figure 9. Increased HBP in multiple cortical areas during motor imagery error (parietal). Each plot shows the average response of a single electrode (from one subject, each) within Brodmann Area 40 during erroneous decoding (red) and during correct decoding (blue).

5.5 Discussion

We present the brain topography of HBP changes associated with error processing in the context of visual feedback, closed-loop, motor-imagery BCI. Our novel approach to extracting epochs of behaviorally defined error within a free-running BCI context is likely to be more reflective of naturalistic error processing, provides high ecological validity and is specifically relevant to contemporary co-adaptive BCI design. That is, our post hoc identification of error epochs, based on violations of intention, circumvent limitations of artificially-induced error events which do not take subject intention into account. To this end, our results are in agreement with a previous study investigating error-related potentials in ECoG in an overt movement task (Milekovic et al., 2012).

Our BCI task involved using both active motor imagery and rest to control the vertical velocity of a cursor to reach and dwell within a target. We investigated the involvement of different Brodmann

Areas and individual electrodes across subjects for these two different control paradigms when the decoder incorrectly decodes the subject's intention and moves the cursor away from the target.

5.5.1 Interpreting effects of trial type and performance on HBP

The interaction of trial control requirement (whether the subject needed to bring the cursor up to a target placed above the center starting position using motor imagery) and performance (whether the cursor moved correctly towards or erroneously away from the target) had a statistically significant interaction on HBP in Brodmann Areas 3, 4, 40, and 43. In other words, the difference in HBP between correct performance and erroneous performance were affected by whether motor imagery or rest was required as the initial action to reach the target in the trial. The specificity of this significant interaction was clarified by post hoc t-test results for the motor imagery conditions and the rest conditions.

Importantly, we noted a statistically significant effect of trial control requirement on HBP in the primary motor cortex (BA4) and premotor cortex (BA6), providing internal validity for our statistical approach. Specifically, the control electrode, located in primary motor cortex, moved the cursor up or down through increasing or decreasing HBP.

5.5.2 Broader response observed for motor imagery error than for rest error

Overall, more areas of the cortex exhibited significantly greater HBP during error in motor imagery cursor control rather than in rest cursor control. BA regions which showed more significant HBP changes in both the motor imagery and rest cases, when including all subjects, were the somatosensory (BAs 1 and 5), motor (BA4), and parietal (BA7) cortices. Areas which were exclusively significant during motor imagery include part of somatosensory (BAs 2 and 3), temporal (BAs 21 and 37), and parietal (BA40) cortices. The only area which was significant during rest but not motor imagery was near the angular gyrus in the parietal lobe (BA39). Note that we did not have much frontal coverage from any of the subjects, preventing investigation of common areas of interest associated with outcome (not execution) error, such as the anterior cingulate cortex (Figure 8a). In Milekovic et al.'s overt movement ECoG study (Milekovic et al., 2012, 2013), ErrPs in the motor, somatosensory, parietal,

temporal, and pre-frontal areas were observed when an execution error was induced in the subject's joystick control.

ErrPs in the motor and somatosensory areas are not unexpected considering they are directly involved in the control and immediate feedback associated with the control. Involvement of other areas may not be as obvious. Previous work has suggested that the parietal lobe is involved with low-level error processing, which cursor control error can be considered (Krigolson and Holroyd, 2007). Although not traditionally explored for error analyses, as there is typically a focus on the anterior cingulate cortex and other frontal areas, previous fMRI work suggests the temporal lobe is also involved in error processing (Stevens et al., 2009).

5.5.3 Corrective movement

The extent literature also suggests the parietal lobe may be involved in the execution of corrective movements in response to error or low-level error (Calhoun et al., 2006; Krigolson et al., 2008; Navarro-Cebrian et al., 2016). It is of note that the temporoparietal junction (TPJ; BA40) only had significant HBP during motor imagery error, but the more posterior and superior area of the parietal lobe (BA7) had significant HBP during both motor imagery and rest error conditions. Krigolson et al. suggest that low-level errors are mediated in the posterior parietal cortex (Krigolson et al., 2008), which may be reflected by the increased HBP in BA7 for both error conditions. Interestingly, the same group showed that a P300 response from the TPJ would immediately precede corrective movements in response to error in an earlier study (Krigolson and Holroyd, 2007). Instead of being directly responsible for the corrective movement, Krigolson et al. postulate that the P300 indicates the updating of an internal model of the task at hand (Krigolson et al., 2008). Navarro-Cebrain et al. (2016) instead suggest the P_E from the parietal lobe indicates that enough error information has been gathered to make a decision to change motor output in order to correct for the error. In our current work, the TPJ had significant increases in HBP during motor imagery error, but not during rest error. This may imply that the parietal lobe elicits a greater response when the corrective action to take requires an increase or change in motor output, in this case, increased motor imagery. Rest error may not have resulted in

increased local activity in the TPJ because the corrective action to take would be to suppress motor imagery.

5.5.4 Low performance and error elicitation

Error-related potentials are typically investigated in settings where instances of correct performance greatly outnumber the instances of error. However, recent work by Pezzetta et al. (2018) reverses the correct/error ratio by inducing error events for 70% of the task. In their study, Pezzetta et al. (2018) find that error-related potentials are still elicited even when error occurs during the majority of the task, confirming that the performance-monitoring system engages in the presence of error and not just in the presence of uncommon stimuli.

The subjects of this present investigation had relatively low task performance, with an average trial success rate of 30.67% (Table 1). This low trial success rate can be partially explained by task difficulty and / or BCI task novelty, as the targets would be placed at varying distances from the center and would also vary in size. In particular, the success condition of having to dwell within the target made the task more difficult than similar one dimensional cursor control tasks, such as the Right-Justified Box task. Note that our behavioral definition of low-level error is not dependent on trial success, but instead on successful cursor movements within each trial. Overall, subjects performed marginally better on trials where the target was placed below the cursor starting position (Table 1). Even with this generally poor performance, we believe our investigation to still be valid as error-related potentials are still elicited in tasks where the majority of actions are erroneous (Pezzetta et al., 2018).

5.5.5 Impact of age on error potentials

Two of the subjects in this investigation were early adolescents of the ages 11 and 13 years old (Subjects 1 and 2, respectively), and the other subject was 35 years old (Subject 3) (Table 1). Human brain maturation from childhood to adulthood is characterized by changes in the structure of and activation of various brain structures, including in the ACC in the prefrontal cortex (Adleman et al., 2002; Casey et al., 1997), a structure essential to conflict monitoring.

Previous work by (Ladouceur et al., 2007) found that with a more developed ACC, adults (19+ years old) and late adolescents (14-18 years old) had stronger ERN responses than early adolescents (9-13 years old), however, the P_E responses did not differ significantly between any of the groups.

Although most subjects exhibited greater HBP in more areas during motor imagery error, Subject 3 had more electrodes with significantly greater HBP differences between error and correct in rest rather than in motor imagery. While this does not seem to be directly related to the aforementioned developmental changes, it is still possible that error presentation in Subject 3 differed from the younger subjects due to processes related to cortical maturation.

5.5.6 Error presentation in the time domain

Unlike with well-established error potentials in EEG, which are often measured as particular phase-locked negative and positive deflections in the time domain, we explored ErrPs related to specific changes in the band-limited time-frequency domain due to the high temporal/spatial resolution inherent to ECoG. Our use of a post hoc defined behavioral marker for detecting error-onset instead of a controlled, elicited error in control may have also led to less distinct, non-event locked ErrP waveforms. As discussed, analyses in the frequency domain do not provide a clean time-stamped waveform present in multiple electrodes in or across any of the subjects. The higher spatial resolution of ECoG, in addition to our unique epoch boundary markers were determined, contributed to the difficulty of relying on time-domain data for ErrP identification in this study.

Regardless, we attempted to compare topographical results more directly with EEG literature by investigating changes in the raw voltage potentials recorded per channel per subject in all conditions. Due to the nature of our task not having an experimentally controlled induced onset of error, we did not expect, nor did we see, as robust a response as in EEG. We only saw significantly greater voltage amplitude during error than during correct in a few select electrodes in two subjects.

5.5.7 Implications for BCIs

Although this investigation focused on identifying cortical error-related potentials post hoc, online classification of error-related potentials have been demonstrated in a few EEG studies (Cruz et al.,

2018; Iturrate et al., 2015; Zander et al., 2016). With online ErrP monitoring, future cortical BCI can infer BCI performance without explicit task information, allowing for automatic adaptation of the system based on estimated performance. The task-independent nature of this method could allow for robust adaptive systems that allow for long-term use of BCI that account for changes in recorded brain signals over time.

As this was a preliminary investigation into error-related potentials in cortical BCI, we did not employ online classification methods. The methods presented here could be adapted to work for online classification by continually calculating HBP via a sliding window, and setting a threshold for channels located on particular regions of interest, such as over BA7. The baseline may be set as the data prior to the start of the sliding window, of a length longer than the sliding window itself. Alternatively, a machine learning model could be developed and trained to classify error and non-error signals and fed the necessary sliding window information for continual classification.

5.6 Conclusion

In this study, we examined the cortical activity of human subjects during a one-dimensional center-out BCI task and investigated how different areas of the cortex behaved during erroneous BCI decoding versus during correct performance. Of all the cortical areas available for analysis, the somatosensory (BAs 1 and 5), motor (BA4), and the parietal lobe (BA7) showed significantly greater HBP 100-500 ms after error onset than during correct behavior, regardless of whether the subject was actively imagining movement or resting to achieve their goal. During motor imagery, parts of the somatosensory (BAs 2 and 3), the temporal lobe (BAs 21 and 37), and part of the parietal cortex (BA40) were exclusively significant. During rest, only part of the parietal cortex near the angular gyrus (BA39) was exclusively significant. Overall, more areas were involved in error processing during the motor imagery error cases rather than during rest error, although there were differences between subjects, with one subject having more significant electrodes during rest. The observed activity of these areas agrees with previous work suggesting the involvement of the parietal and temporal areas in error processing.

Although our results generally agree with previous work performed with overt movement in ECoG (Milekovic et al., 2012), our error-related potentials (ErrPs) do not present themselves as the well-defined waveforms discussed in the EEG literature, likely due to the diffuse timing of our error events. The presence of ErrPs in both overt- and imagined-movement controlled ECoG tasks suggests error processing is impartial to the method of control in a task.

Our investigation is the first to explore ErrPs in the context of continuous control in a cortical BCI. As the BCI field delves further into understanding error and reinforcement learning, it is critical that we understand error processing at various spatial and temporal levels in a multitude of conditions. This study contributes to the field by focusing on continuous control (instead of discrete control for simple selection) representing a more naturalistic setting for characterizing error potentials in the brain. Additionally, we report the first description of the responsive local high-frequency activity using high gamma band power in a BCI, instead of more global signals such as theta band activity in EEG.

In addition to exploring error processing in the context of motor BCI, we are also interested in the effects of different forms of feedback during continuous control, not just visual (as is typical with most current BCIs). In the future of BCIs and their adoption into neuroprostheses, we will need to understand the effect of other forms of feedback, which inform volitional control, on BCI learning. Ultimately, the use of ErrPs as an automatic feedback signal to future BCIs will allow for co-adaptation, leading to better and longer-lasting control. Greater performance and longer ability of use will allow these co-adaptive BCIs to break out of the confines of the research setting and make their way into clinics and home settings.

We would like to explore the long-term effects of learning on the error-related potentials, but our limited time with research subjects renders this nearly impossible. A better understanding of ErrPs and their usability over time is crucial for implementing co-adaptive BCI systems which rely on ErrPs for feedback. Longer use in the experimental setting may allow for the development of robust classification techniques which can assist in real-time error detection in the future.

5.7 Additional work exploring spontaneous error

Error-related potentials are typically investigated in the context of controlled experiments, where investigators either present pre-determined stimuli or have subjects perform specific tasks. However, if we are interested in using error as a feedback signal to BCI decoders in the future, where BCIs may be used outside of controlled settings, it is important to also investigate spontaneous error in a naturalistic context.

In this project, we began to investigate errors made by subjects in both controlled, experimental settings, and in spontaneous behavior. This work was accepted as an abstract into and presented at the Society for Neuroscience meeting in November 2017 (Wilson et al., 2017). However, due to difficulty in reliably labeling spontaneous error in an efficient manner, this project was discontinued.

This project was mainly a collaborative effort with Nancy Wang. Nancy and her team focused on processing the audio, generating the speech labels, and time-syncing the clinical ECoG recordings to the simultaneous audio and video recordings. I focused on analyzing the cortical signals in the experimental data collected by the lab, and also on analyzing the clinical ECoG corresponding to the spontaneous mistakes.

Objective. We investigated cortical potentials associated with both naturalistic and in-task error in the same human subjects, providing a first look into how error-related potentials in controlled experimental settings may differ from those during free behavior.

Approach. Utilizing long-term simultaneous ECoG, audio, and video recordings (approximately one week of data per subject), we applied automated approaches, an extension of our previous study (Wang et al., 2016), to detect when spontaneous errors were committed within hundreds of hours of patient monitoring. Using these labels, we defined timestamps of verbal admission of error and extracted large epochs of 10 second length to then further analyze. In the controlled tasks, we stored epochs of 1 second length. The controlled task epochs are much shorter than the spontaneous (non-task) epochs due to the fast timing of the task being performed.

Main Results. We found increased high gamma (70-100 Hz) power in the ventrolateral prefrontal cortex in both conditions (task and spontaneous error); in addition, we found activation in Brodmann Area 8 (BA8) only in the natural condition (Figure 10). As activation in BA8 is thought to be associated with uncertainty estimation, this increased high gamma power implies the subjects may be more uncertain of mistakes made in the natural context. These results suggest there may be important differences between error-related potentials for mistakes made inside and outside of strictly controlled experiments; further, they motivate further investigation of error and reward in spontaneous behavior, an analysis enabled by automated algorithms for extracting features from long-term monitoring.

Significance. In everyday life, we continuously evaluate our interactions with our surroundings; we feel, see, and hear information telling us how well we are able to perform a desired action, thus allowing us to adjust our behavior, learn, and improve. There are multiple theories on how our brain uses this feedback for performance monitoring (Ullsperger et al., 2014) based on knowledge gathered through controlled, non-invasive (West and Travers, 2008) and invasive (Phillips et al., 2016) electrophysiology studies. However, this is the first, to our knowledge, exploration of error-related potentials in a naturalistic setting. Understanding how error-related potentials present in uncontrolled settings could greatly improve future systems that rely on error-related potentials for optimizing BCI function.

5.7.1 Methods

In this project, we use audio recordings in conjunction with ECoG data to investigate error-related potentials. The data consists of three subjects monitored continuously over at least one week after electrode array implantation; each subject had approximately 100 intracranial ECoG electrodes with wide coverage of cortical areas (Figure 10). Importantly, each subject was asked to perform a word and picture association task (in-task context) (Figure 11), and also monitored for the remainder of their clinical monitoring (naturalistic context). During this naturalist context for the duration of their pre-surgical epilepsy monitoring, they received no instructions to perform specific tasks, and they behaved freely inside their hospital room.

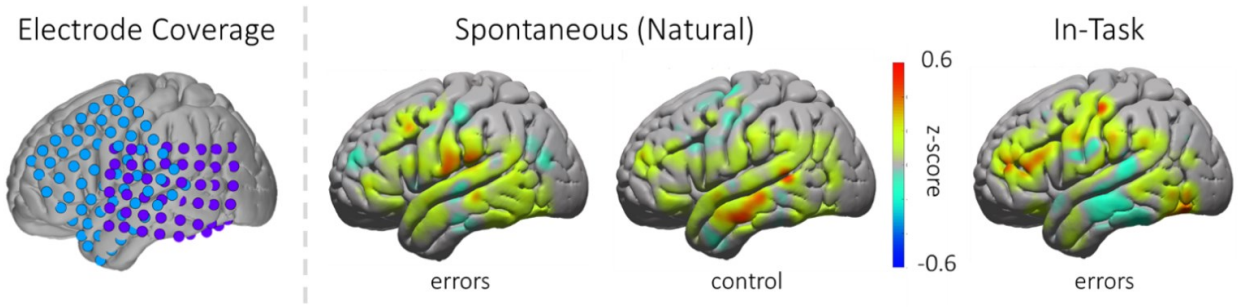

Figure 10. Differences in high gamma activation between errors committed in the naturalistic vs in-task contexts. Mean high gamma power (normalized to baseline) from two subjects were plotted on a standard MNI brain. A third subject was analyzed with electrode coverage on the right hemisphere (results not shown). Error-related potentials were computed for in-task errors, spontaneous errors, and also compared to a spontaneous control condition.

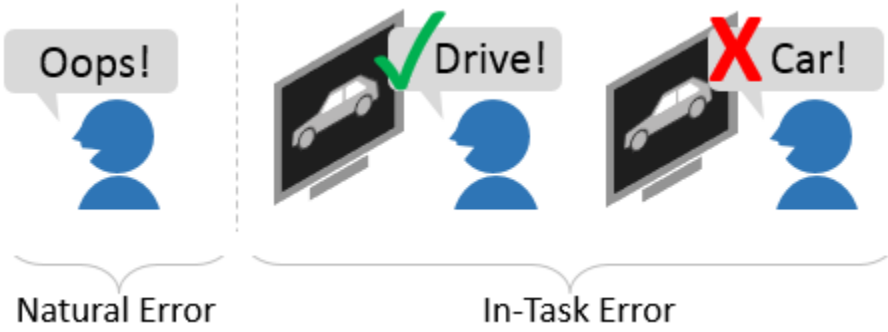

Figure 11. Natural error and in-task error. Natural error is made spontaneously outside of the controlled task setting. In-task error occurs while performing a controlled task administered by the researchers.

Instead of relying on manual annotations, we use speech processing and machine learning techniques to automatically determine key points when subjects may have made spontaneous mistakes. For naturalistic error detection, automatic speech recognition selected candidate timestamps when the subjects said error-related keywords (e.g., “oops,” “sorry,” and various expletives). All audio recorded for the subject's hospital stay was searched for error-related keywords using keyphrase spotting as implemented in the Sphinx toolkit (Huggins-Daines et al., 2006). These timestamps were verified by manual annotators for accuracy; on average, we confirmed approximately 10 candidate timestamps per day. The manual annotators also sorted the timestamps based on if the keywords were said in an error or non-error context. The non-error (control) condition included when the error-related keywords were used as sarcasm or expletive infixation (e.g., “Abso-f***ing-lutely”).

Once we had error timestamps for all three subjects, we extracted the ECoG data from grid electrodes at the corresponding timestamps. We stored data from 500 ms before to 500 ms after labeled error for

task data, and from 5000 ms before to 5000 ms after for natural data (the epochs for task data are smaller to prevent overlap from neighboring trials). Raw voltage values were common average referenced and notch filtered for 60 Hz noise. We then calculated power for the high gamma (70-100 Hz) frequency band and normalized to baseline. After error epochs were stored for each channel, we collectively sorted all subject electrodes into functional Brodmann Areas. With the epochs sorted by Brodmann Area across all subjects, we then investigated normalized high gamma power before error onset (t=0) by functional cortical areas. Epochs were stored as either in-task error, natural error, or natural control for analysis.

5.7.2 Results

Preliminary analysis suggests increased activation in the ventrolateral prefrontal cortex (VLPFC) and inferior parietal cortex during error, and dissimilar activation in BA8, which is associated with uncertainty (Volz et al., 2005). The increased activity in the VLPFC may imply involvement of cognitive control of memory (Badre and Wagner, 2007) during error realization and verbalization. Increased activity in BA8 may imply there is greater uncertainty during error in the natural setting than in the controlled task setting.

5.7.3 Conclusion

In order to progress with this study, we would need to collect experimental error data from more subjects and also improve the automated speech recognition to obtain more candidate labels. The major limiting factor of this study was the low label count in both in-task and spontaneous recording.

6. DMN disruption and reaction timing in a modified Stroop task

6.1 Motivation

In the previous chapter, we explored the presentation of error-related potentials across the cortex in a continuous movement one-dimensional Brain-Computer Interface as one of the performance monitoring signals of interest. In this chapter, we investigate the other performance monitoring signal of interest for this dissertation, attention via Default Mode Network (DMN) activity. Through testing the effects of DMN disruption on subject performance and on cortical activity, we gain a better understanding of how attention affects task performance, local DMN activity, and communication between DMN regions.

Preliminary work from this chapter was accepted as an abstract in and presented at the Society for Neuroscience meeting in 2018 under the title "The effect of Default Mode Network disruption on reaction-timing and cortical activity in a modified Stroop task" (Wilson et al., 2018).

6.2 Introduction

When engaged and focused on a task that requires processing of external stimuli (e.g., visual), activation in particular regions of the brain decrease (Raichle et al., 2001; Shulman et al., 1997). This network of task-negative regions is commonly referred to as the Default Mode Network (DMN) (Raichle, 2015). As the term "task-negative" implies, the DMN recruitment is negatively related to task involvement and can subsequently be used as an estimated measure of attention via increased activation due to mind-wandering (Scheibner et al., 2017). This measure of attention through neural signals is of particular interest for Brain-Computer Interface (BCI) development, as decreased attention has been linked to worsening BCI performance in various studies (Diez et al., 2015; Lakey et al., 2011; Ordikhani-Seyedlar et al., 2014). To prevent this decrease in BCI performance due to reduced attention, we propose a BCI which monitors attention and uses attention and error-based estimations of performance to adapt the decoder in Chapter 7. In this chapter, we focus on exploring the effect of

disrupting the DMN on subject performance, as measured through reaction time, and on DMN activity at the cortical level.

Transient suppressions of DMN activity, on the scale of milliseconds, can naturally occur through increases in task complexity (Ossandón et al., 2011), but can we exhibit controlled suppression of DMN activity using perceptible or below perceptual threshold stimulation? In this study, we employ perceptible audio stimulation in the form of an audible beep and deliver sub perceptual threshold direct cortical stimulation to the DMN and to a control area. While the audio beep does not directly disrupt DMN activity, the automatic auditory processing of this external stimuli should engage other brain regions (Nourski, 2017) and naturally suppress DMN activity. Conversely, direct cortical stimulation can be used to directly disrupt normal cortical function (Haglund et al., 1994; Keles et al., 2004; Miller et al., 2007a). Recent work by Foster and Parvizi (2017) demonstrated that direct cortical stimulation to non-somatosensory areas can be delivered below the perceptual threshold of the individual receiving stimulation. Through direct cortical stimulation of the DMN, we hope to observe an effect on subject performance without the subject consciously feeling their performance being affected.

To test the effects of DMN disruption on DMN activity and on task performance, we collected behavioral and electrocorticography (ECoG) data from subjects performing a Stroop reaction timing task. Through the ECoG data, we were able to use spectral power as a measure of DMN activity. Specifically, local activity at various DMN sites was measured via high gamma band power (Miller et al., 2007b). In addition to spectral power, we also investigated changes in functional connectivity between DMN areas using coherence and Phase-Amplitude Coupling, where functional connectivity is defined as how similar frequency, phase, and/or amplitude is for correlated activity between multiple brain regions (Bowyer, 2016). Coherence is a common measure for determining how significantly correlated signal from different areas are and may imply communication between areas (Bowyer, 2016). Phase-Amplitude Coupling examines how statistically dependent high frequency amplitude is to the low frequency phase and, like coherence, may imply communication between areas (Canolty and Knight, 2010; Canolty et al., 2006; Florin and Baillet, 2015; Jensen and Colgin, 2007). By introducing DMN

disruption in the experiment, we investigate if disruption lessons communication between the various sub-regions within the DMN.

In terms of studying the Default Mode Network and attention, the work presented in this chapter is novel in that it explores the effect of DMN disruption not only on behavior and local DMN activity, but also on communication within the DMN as measured through coherence and Phase-Amplitude Coupling.

6.3 Methods

6.3.1 Participants

Patients with medically intractable epilepsy (n = 5), undergoing clinical seizure monitoring at Harborview Medical Center consented and volunteered to participate in research in accordance with the University of Washington Institutional Review Board.

6.3.2 Data recording and electrode localization

The electrocorticogram (ECoG) for each subject was recorded through subdural macro-scale grid electrodes (Ad-Tech 8x8 platinum, 10mm contact spacing) and electrode strips of varying size and varying placement. Cortical potentials were recorded at 1525.88 Hz or at 12.207 kHz using the Tucker-Davis Technologies (TDT) recording system (Alachua, FL), depending on if cortical stimulation was delivered or not. The higher sampling rate was used for the subject who received cortical stimulation as part of the task. Pre-operative T1 MRI scans were co-registered with post-operative CT scans (SPM8) to allow for individualized electrode localization through BioImageSuite software imaging package (Papademetris et al., 2006). These localized electrode coordinates were also transformed to fit the Montreal Neurological Institute (MNI) standard brain space to allow for Brodmann Area identification and comparison across multiple subjects.

6.3.3 Default Mode Area identification

For analysis purposes, we labelled individual channels as recording from Default Mode Network (DMN) areas if their MNI coordinates fall within designated Brodmann Areas, as defined by the MNI brain atlas.

Specifically, channels labelled as falling in Brodmann Areas 9, 10, 21, 31, 32, 40, 45, and 47 were identified as DMN channels (Table 5). Although most electrodes were located laterally across subjects, some electrodes were located medially, leading to DMN coverage along the medial parietal wall, the lateral temporal regions, and temporal frontal regions.

BA Number	Anatomical Location	Sources
9	Dorsolateral prefrontal cortex	(Fink et al., 1999)
10	Anterior prefrontal cortex	(Rogers et al., 1999)
21	Middle temporal gyrus	(Vorobyev et al., 2004)
31	Posterior cingulate gyrus	(Fiddick et al., 2005)
32	Anterior cingulate gyrus	(Goel et al., 1998)
40	Inferior parietal lobule	(Hirsch et al., 2001)
45	Inferior prefrontal cortex	(Gold et al., 2005)
47	Orbitofrontal cortex	(Völlm et al., 2006)

Table 5. Brodmann Areas in the Default Mode Network summary table.

Because this method relies on having the MNI coordinates of the subjects' electrodes calculated, we did not have the information necessary to identify channels as being in the DMN through this method during data collection. For the stimulation subject, we identified the DMN stimulation and control stimulation electrodes anatomically.

6.3.4 Task design

Subjects performed a modified Stroop Task, where they were instructed to press the left arrow key when presented congruent stimuli (i.e., word color matched meaning of the word), and the right arrow key when presented incongruent stimuli (i.e., mismatch between the word color and the meaning of the word) as fast as they can (Figure 12). For example, seeing the word "green" written in green text warrants a left arrow key press (congruent), and seeing the word "red" written in blue text warrants a right arrow key press (incongruent). The word stayed displayed on the screen for two seconds, or until the subject responded if they responded within two seconds. After two seconds, the screen would remain blank until the subject responded with a key press.

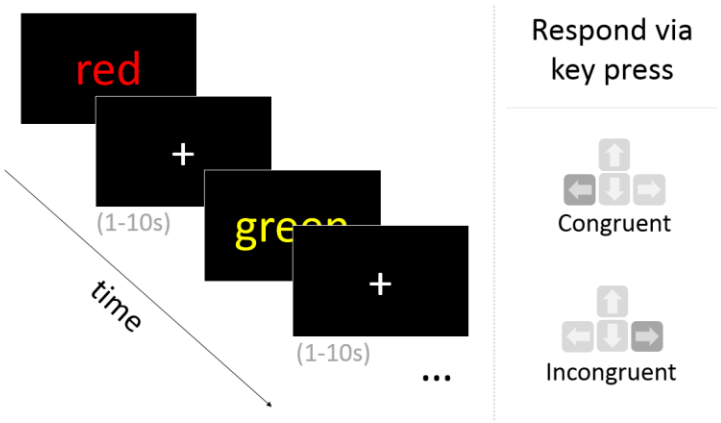

Figure 12. Task trial examples. Subjects respond with either a left or right arrow key press when the stimulus shown is congruent or incongruent, respectively. Individual trials (word presentations) are separated by inter-stimulus intervals ranging from 1 to 10 seconds in length.

The task begins with a primer block to allow subjects to learn the task. In the primer block, subjects respond to congruent and incongruent stimuli with Inter-stimulus Intervals (ISI) ranging randomly and uniformly from 2-4 seconds. During ISIs, a fixation dot is displayed in the center of the screen. The primer is followed by randomized blocks containing standard trials with no disruption prior to word presentation, trials with an audio beep presented one second prior to word presentation, trials with cortical stimulation delivered to the DMN at the time of word presentation, trials with cortical stimulation delivered to a control area at the time of word presentation, or any combination of the above. For all blocks, stimuli (words) are presented following ISIs of varying length until 20 trials have been completed, where 50% of these trials have congruent stimuli. The task then moves onto the next randomly selected block (Figure 13).

There is a 1 second delay between audio stimulus onset and word stimulus presentation to allow for the subject to reorient their attention (Dastjerdi et al., 2011). We initially planned to introduce the same delay with the cortical stimulation but forgot to account for a built-in delay in the code which the stimulation circuit was based off of. As a result, cortical stimulation was delivered at the time of trial start when the word was presented. The stimulation was designed to be below the perceptual threshold, so subjects should not be aware of when the cortical stimulation is occurring within the block (see Stimulation Parameters).

This task was developed with Psychtoolbox-3 (Brainard, 1997; Kleiner et al., 2007) in MATLAB 2016a and interfaced with the TDT OpenEx suite.

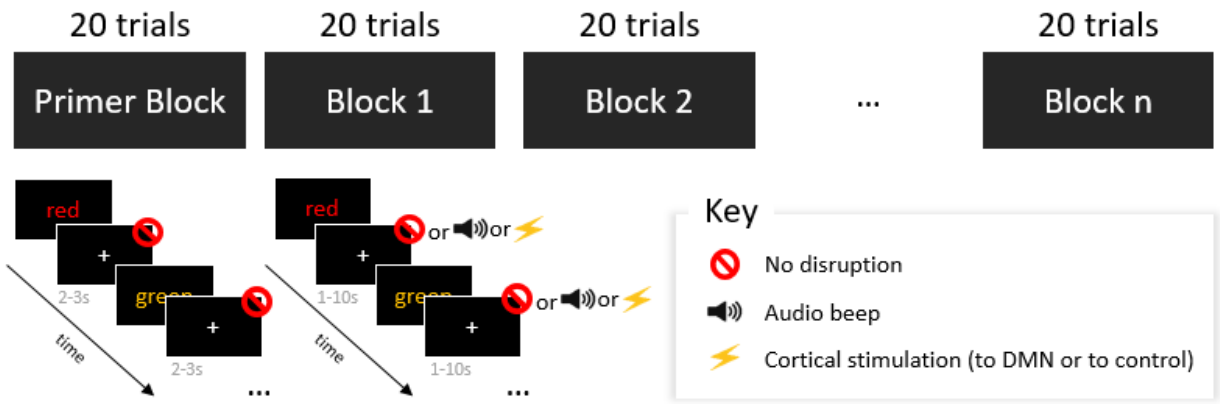

Figure 13. Task Structure. Subjects first complete a Primer Block to get acquainted with the task. The Primer Block is then followed by n number of blocks, with each block containing a balanced number of congruent and incongruent trials. Trial disruption type (no disruption, audio disruption, DMN stimulation, control stimulation) is randomized within each block.

6.3.5 Stimulation parameters

We determined stimulation parameters based on previous work performed in the lab for eliciting sensations (Collins et al., 2017; Cronin et al., 2016) and on published accounts utilizing transcranial magnetic stimulation (TMS) (Siebner et al., 2009; Sliwinska et al., 2014).

Stimulation of non-sensory areas can be perceived by subjects given high enough pulse amplitude and frequency (Pascual-Leone et al., 2000). However, our broad goal here was to disrupt non-sensory cortical network function (i.e., of the Default Mode Network). Consequently, we aimed to present sub-threshold stimulation. To this end, we delivered repeated single 1 mA biphasic pulses of 200 μs phase widths at 200 Hz for 150 ms, similar to short pulse duration virtual lesions in TMS (Siebner et al., 2009; Sliwinska et al., 2014). The exact parameters were determined prior to starting the task by tailoring stimulation for each subject based on subjective perception.

Traditionally, stimulation through cortical electrodes for clinical mapping is performed in a bipolar fashion using two neighboring electrodes, spaced 6-10 mm apart, over the target area (Formaggio et al., 2013). Due to the setup of the TDT recording system, we could not simultaneously record and stimulate within any given electrode. Stimulation electrodes must directly interface with the

stimulator, meaning they are not connected to the recording setup. As a result, we selected two adjacent electrodes anatomically located in the DMN for DMN stimulation, and two adjacent frontal electrodes not believed to be in DMN for control stimulation.

6.3.6 Spectral analysis

6.3.6.1 Pre-processing

Prior to analyzing the ECoG data, we removed DC offset between channels and eliminated channels containing at least one voltage value with an absolute value greater than or equal to three times the average standard deviation of voltage of all channels. Common Average Referencing (CAR) was performed by grid or by strip for all subjects except for 822e26. We did not perform CAR for 822e26 to prevent the spread of residual stimulation artifacts from channels near the stimulation sites. Stimulation artifact removal is detailed in the following section. In addition, to reduce computational load, we downsampled the ECoG data from the stimulation subject by a factor of 10, reducing the sampling rate from 12.207 kHz to 1220.7 Hz. Next, we removed 60 Hz noise by applying non-causal 4^{th} order Butterworth notch filters centered around 60 Hz, and its harmonics at 120 Hz and at 180 Hz.

6.3.6.2 Stimulation artifact removal

To recover the underlying ECoG data during delivery of high amplitude direct electrical stimulation, we used the cortical stimulation artifact removal package in MATLAB, made available online by colleagues Caldwell et al. (2019). Implementation of this package requires our data be organized into two sets of epochs: (1) epochs centered around stimulation to the DMN electrodes, and (2) epochs centered around stimulation to the control electrodes. Each set is then fed separately into the template_subtract function to return two sets of processed signals with the stimulation artifacts removed. The function parameters shown in Table 6 were set for the epochs used in the template_subtract function. Default values from the example code in the package were used for most parameters with the exception of minPts and minClustSize, which were adjusted by epoch set to ensure stimulation templates fit the raw data well, as verified through visual inspection (Table 6).

Parameter	Value for DMN stim epochs	Value for control stim epochs
pre	0.8	0.8
post	1	1
useFixedEnd	0	0
fixedDistance	4	4
distanceMetricDbscan	'eucl'	'eucl'
distanceMetricSigMatch	'corr'	'corr'
recoverExp	0	0
normalize	'preAverage'	'preAverage'
amntPreAverage	3	3
minDuration	0.5	0.5
bracketRange	[-6:6]	[-6:6]
threshVoltageCut	75	75
threshDiffCut	75	75
expThreshVoltageCut	95	95
expThreshDiffCut	95	95
onsetThreshold	1.5	1.5
minPts	5	5
minClustSize	15	10
outlierThresh	n/a	0.95

Table 6. Stimulation artifact removal function parameters. Values which were not manually entered but were instead left for the function defaults are indicated by n/a.

6.3.6.3 Power calculation

Although we were primarily interested in changes in band-limited high gamma (HG) power behavior during task performance, we also investigated changes in lower frequency bands, as they are often the focus in the extent EEG literature (Aoki et al., 2015; Chen et al., 2008; Imperatori et al., 2016; Knyazev et al., 2011). To circumvent the issue of $1/f^2$ power law inherent to the power spectrum, we used the flat band-limited power calculation method detailed in Ramot et al. (2012). This method accounts for the power loss by scaling the power calculations per band at logarithmically spaced subranges.

Instead of bandpass filtering for each frequency band and calculating power by taking the absolute value of the Hilbert transform, we divided each band into subranges of exponentially growing width and calculated power within each subrange. For each subrange, we calculated power by squaring the absolute value of the Hilbert transform, smoothing with a 50 ms sliding window, and then normalizing by dividing by within-band baseline power, which was estimated by taking the mean value of all power

in this subrange 500 to 0 ms prior to all trial starts (when the word was presented). The final power of the whole frequency band was calculated by taking the mean of all the scaled subrange power.

We calculated flat band-limited power using 6 subranges each for alpha (8-13 Hz), beta (15-30 Hz), gamma (32-70 Hz), and high gamma (72-200 Hz).

6.3.6.4 Epoch definition

After we calculated power in each band of interest, we extracted epochs of 4 second lengths, specifically from 2 seconds before each word presentation (trial start) to 2 seconds after. These epochs were of sufficient length to capture a period prior to potential DMN disruption at t = -1 seconds and to capture data up to and after reaction time for most trials. These epochs were organized by disruption type (no disruption, audio beep, DMN stimulation, or control stimulation) and by channel.

We then generated average response spectrograms for each channel for each disruption condition using short-time Fourier transform (400 point symmetric Hamming window, 300 overlapped samples).

6.3.7 Coherence

Coherence is a measure of how synchronous the frequency and amplitude content of two oscillating brain signals are, and is used to quantify synchronicity between spatially separated recording channels (Bowyer, 2016). The magnitude-squared coherence between Brodmann Areas was estimated using the mscohere function in MATLAB. Coherence during each trial was measured between two channels using the preprocessed voltage values from t=0-500 ms, where t=0 is the start of the trial where the Stroop stimulus is presented. The electrode pairing from two different Brodmann Areas, defined as belonging to the DMN (BAs 9, 10, 21, 31, 32, 40, 45, 47), remained consistent throughout our analysis.

The output of the magnitude-squared coherence function detailed coherence values for varying frequencies. Through visual inspection of the coherence across all bands, we observed a fairly large and consistent change in coherence around 20 Hz. In our analysis, we take the mean of the coherence

values below 20 Hz, and take the mean of the coherence values above 20 Hz, to return two values for coherence in each channel pair for each trial.

6.3.8 Phase-Amplitude Coupling

Phase-Amplitude Coupling (PAC) is a measure of how well the amplitude of the signal within a particular frequency range is modulated by the phase of the signal within another frequency range (Tort et al., 2010). The strength of PAC within and between DMN channels were calculated following the methods detailed in Tort et al. (2010). We calculated the Modulation Index for the normalized amplitude of signal bandpass filtered from 70-200 Hz (high gamma) and the phase of the signal bandpass filtered either from 7-12 Hz (alpha) or from 13-30 Hz (beta), where the signal was the preprocessed voltage data in each DMN channel 0-500 ms after word presentation (t=0). This resulted in one Modulation Index value per trial per channel combination.

6.3.9 Statistics

6.3.9.1 Behavior

To investigate the effect of the various disruption types and inter-stimulus interval (ISI) length on reaction time, we fit Linear Mixed Effects (LME) models to our reaction times and conducted ANOVAs on these models. LME models were employed on the reaction time (RT) data directly to control for the random effect introduced by individual subjects.

We performed two LME model fittings and ANOVAs. For both models, ISI lengths were split into the following categories: short (≤3 seconds), medium (3≤7 seconds), and long (>7 seconds). For the first model and consequent ANOVA, we limited the disruption types to just “no disruption” and “audio disruption”, as the stimulation disruption types were only present in one out of all five subjects.

$$RT \sim DisruptionType + ISILength + (1|Subject) \quad (1)$$

For the second model and ANOVA, we focused on investigating the effects of cortical stimulation by limiting the RT data to just subject 822e26, who was the only subject to receive cortical stimulation during data collection.

$$RT \sim DisruptionType + ISILength \quad (2)$$

To further investigate effects observed from these ANOVAs, we followed up with unpaired, two-sample t-tests comparing the RTs of the conditions of interest.

6.3.9.2 Power changes

As with our behavioral data, we wanted to control for the random effect introduced by including multiple subject's data in our comparison of change in power due to the varying disruption types.

To investigate whether audio disruption had an effect on mean power in DMN channels prior to RT, we initially fit a Linear Mixed Effects model to the mean power within each band from t=0-500 ms in each epoch for all subjects together.

$$Mean\ Power \sim DisruptionType + (1|Subject) + (1|FrequencyBand) + (1|Channel) \quad (3)$$

We then ran an ANOVA on this model to see if there was a significant main effect from disruption type. We then followed up with unpaired t-tests to better understand the specific effects. Specific pairing is discussed in the results.

To investigate whether cortical stimulation, as well as audio disruption, had an effect on mean power in DMN channels prior to RT, we fit a Linear Mixed Effects model to the mean power within each band from t=0-500 ms in each epoch for subject 822e26, who was the only subject to received cortical stimulation.

$$Mean\ Power \sim DisruptionType + (1|FrequencyBand) + (1|Channel) \quad (4)$$

Like with the first model, we then ran an ANOVA on this model to see if there was a significant main effect from disruption type. We then followed up with unpaired post hoc t-tests to better understand the specific effects.

Lastly, to investigate whether power in DMN channels changed over different ISI lengths (short: ≤3 seconds, medium: 3≤7 seconds, long: >7 seconds), we fit a Linear Mixed Effects model to the mean

power within each band from the final second in the ISI preceding any possible disruption (t=-2000 ms to t=-1000 ms), for all subjects.

$$Mean\ Power \sim ISIlength + (1|Subject) + (1|FrequencyBand) + (1|Channel) \qquad (5)$$

An ANOVA was applied to this model to see if there was a significant main effect from ISI length. We then followed up with unpaired post hoc t-tests to better understand the specific effects.

6.3.9.3 Coherence

Prior to investigating the relation of coherence between various Brodmann Areas, we first had to decide which electrodes we would use. Electrode pairs were selected such that only one representative electrode from each Brodmann Area was present in each pair. Electrode pairs were determined by cycling through all possible combinations of channel pairs between two Brodmann Areas and seeing which pair resulted in the lowest p-value when comparing the mean coherence between conditions. Specifically, one-sided t-tests were conducted to test if the coherence during trials with no preceding disruption was greater than during trials that were preceded with some form of disruption (audio or cortical stimulation). Regardless of if the difference was statistically significant or not, the pair that resulted in the lowest p-value for that specific Brodmann Area pair was stored for further analysis.

When observing the statistical significance of the difference in coherence between conditions across all Brodmann Areas, we accounted for multiple comparisons by applying False Discovery Rate (FDR) correction to the p-values.

6.3.9.4 Phase-Amplitude Coupling

In addition to coherence, we investigated Phase-Amplitude Coupling as another measure for connectivity. Specifically, for each epoch, we used the Modulation Index as a single value to represent the Phase-Amplitude Coupling within and between the channels identified in the coherence analysis.

We calculated the Modulation Index for the alpha phase (7-12 Hz) to high gamma amplitude (70-200 Hz) coupling and for the beta phase (13-30 Hz) to high gamma amplitude (70-200 Hz) coupling for each individual channel – where both phase and amplitude were taken from the channel of interest – and for

each pair of channels. Prior to running Phase-Amplitude Coupling on the data from t=0 to t=500 ms for each trial, we removed linear trends in the data using the detrend function in MATLAB, and preprocessed as described in the pre-processing section.

Following the methods as described in Tort et al. (2010), we calculate the Modulation Indices using two phase ranges (7-12, and 13-30 Hz) and one broad amplitude range (70-200 Hz). To account for our relatively short time window of 500 ms, we normalize the amplitude modulation to the mean and standard deviation of 200 surrogate signals which were generated through running phase randomization (Gias, 2011; Prichard and Theiler, 1994) on the amplitude signal.

6.4 Results

6.4.1 DMN coverage

Subjects had varying coverage of Default Mode Network areas (Figure 14, Table 7). Between all five subjects, there was a total of 127 DMN channels for investigation, with most DMN channels in BA21 (middle temporal area) (Table 7).

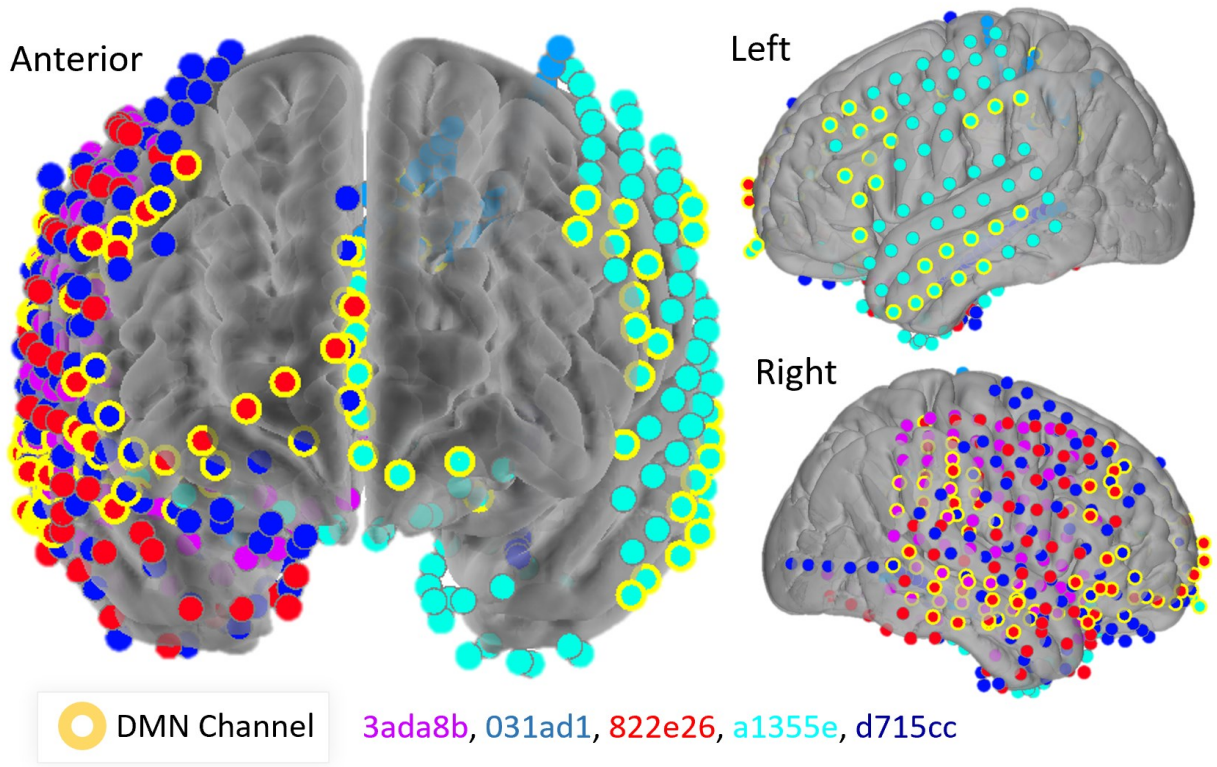

Figure 14. Cortical coverage of all subjects separated by color. Electrodes outlined in yellow represent channels within Brodmann Areas associated with the Default Mode Network. Subjects by color: 3ada8b (magenta), 031ad1 (medium blue), 822e26 (red), a1355e (cyan), d715cc (navy).

	Number of Channels per Subject					
Brodmann Area	**3ada8b**	**031ad1**	**822e26**	**a1355e**	**d715cc**	Total
9	1	0	5	5	3	14
10	0	0	7	4	3	14
21	13	0	11	10	5	39
31	0	8	0	0	0	8
32	0	0	0	4	2	6
40	8	2	9	3	3	25
45	0	0	2	4	3	9
47	2	0	4	2	4	12
Total Count	24	10	38	32	23	127

Table 7. Default Mode Network channels per subject. Each subject had a varying amount of electrodes present within the various Brodmann Areas constituting the Default Mode Network.

6.4.2 Reaction time and task performance

Our initial aim was to examine interactions between disruption type, ISI length, and behavioral performance metrics.

Overall, subjects performed well on the Stroop task with an average response accuracy of 92.07% and with an average reaction time (RT) of 1.28 seconds (Table 8). Note that subject 822e26's relatively low response accuracy was due to confusion regarding the color yellow. The subject recognized text in yellow as being in orange and thus responded with incongruent whenever a congruent yellow stimulus was presented.

Subject ID	Hemisphere	Age	Sex	Handedness	Response Accuracy	Mean RT (congruent)	Mean RT (incongruent)	Total Number of Trials
a1355e	L	28	M	R	91.6667%	2.3146	1.6260	60
031ad1	L	30	M	R	95%	0.9062	1.3739	60
d715cc	R	19	M	R	90%	1.6530	1.0113	60
3ada8b	R	31	F	R	100%	0.8556	0.9633	100
822e26*	R	32	F	R	83.6842%	0.9467	1.1364	190

Table 8. Subject performance. Subjects with stimulation trials are noted with an asterisk (*) by their subject ID.

In subject 031ad1, there was a positive association for RT as a function of ISI (Figure 15, left), an effect which was ameliorated when applying the audio beep disruption cue type (Figure 15, right).

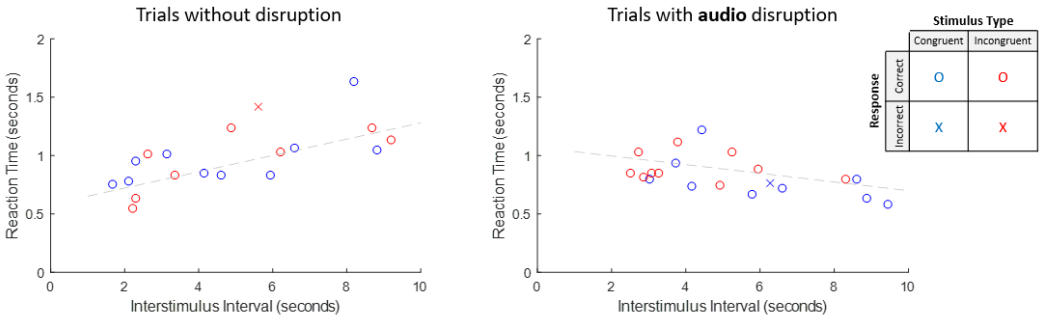

Figure 15. Effect of disruption on reaction time in subject 031ad1. (Left) Subject reaction time increasing over increasing inter-stimulus interval length. (Right) Subject reaction time decreasing over increasing inter-stimulus interval length.

Across subjects, reaction time was slower for trials following long ISIs than for trials following medium length ISIs. Although reaction time is generally faster for trials following shorter ISIs than for trials following longer ISIs, there is a great degree of variation between subjects (Figure 16).

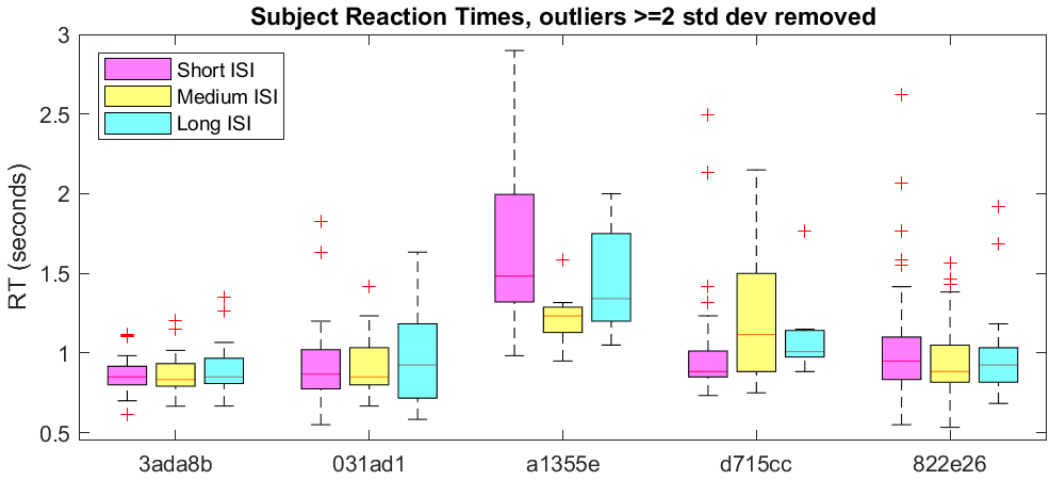

Figure 16. Reaction time by ISI length. Subject reaction times for trials with varying preceding ISI lengths, excluding reaction times greater than or equal to two times the standard deviation of reaction time for the individual subject.

If we observe the average reaction time per condition on a subject by subject basis, we see that RT appears to be lower with DMN disruption via audio beep as compared to RT for trials with no disruption for subjects 031ad1, 3ada8b, a1355e, and 822e26 (Figure 17). However, the one exception was subject d715cc, who took longer to respond when a word was presented following an audio beep.

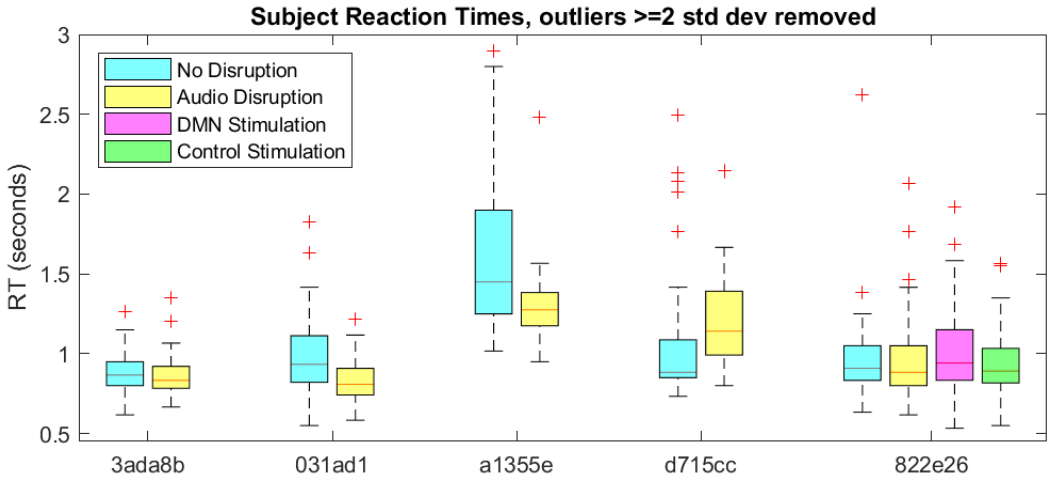

Figure 17. Reaction Time by disruption type. Subject reaction times for trials with different disruption conditions, excluding reaction times greater than or equal to two times the standard deviation of reaction time for the individual subject.

To quantify our observations, we conducted an ANOVA on a Fit Linear Mixed Effects Model fitting the effects of disruption type and ISI length on reaction time with subject set as a random effect variable,

as described in the methods (Equation 1). When running this test using the data from all subjects, we excluded stimulation trials to ensure the disruption types were consistent between all subjects. This ANOVA did not return any significant main effects for either disruption type ($F(1, 366) = 0.17279$, $p = 0.6788$) or ISI length ($F(2, 366) = 0.33905$, $p = 0.71267$).

To test the effect of all disruption types, including cortical stimulation, we also conducted an ANOVA on a Fit Linear Mixed Effects Model fit specifically to the effects of disruption type and ISI length on reaction time for subject 822e26 (Equation 2). With a standard alpha level of 0.05, we do not see a statistically significant main effect from disruption type ($F(3, 184) = 2.3993$, $p = 0.069397$) or ISI length ($F(2, 184) = 2.4701$, $p = 0.08737$).

6.4.3 Stimulation artifact removal

Prior to analyzing the ECoG data from our stimulation subject, we performed stimulation artifact removal using the artifact removal package developed by Caldwell et al. (2019). Through stimulation template subtraction, we were able to identify and remove the large artifacts introduced by cortical stimulation to both the DMN stimulation channel pair and to the control stimulation channel pair (Figure 18).

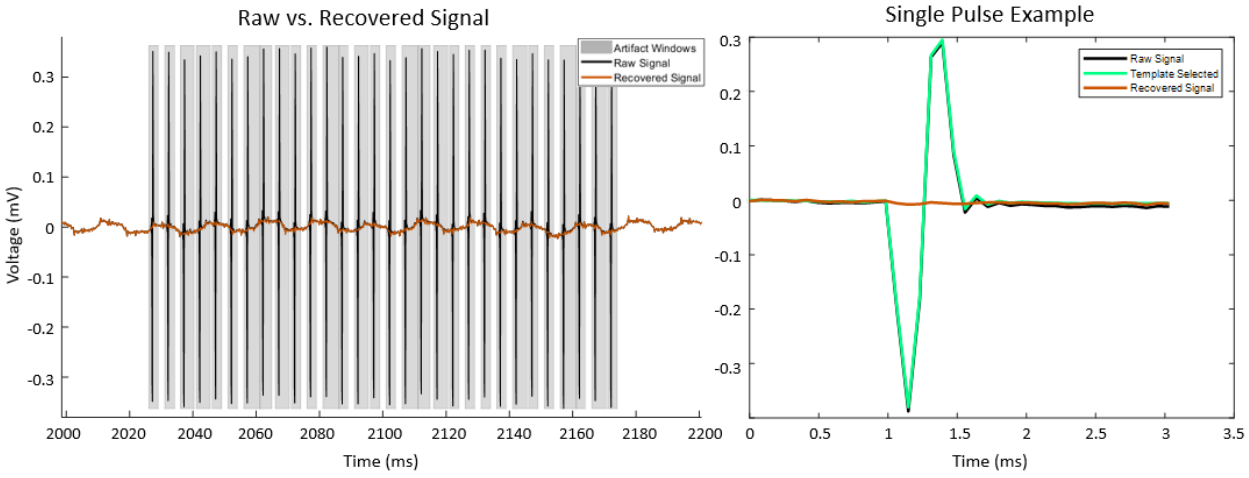

Figure 18. Stimulation template subtraction for artifact removal. (Left) Stimulation artifacts in the raw signal are much greater than the underlying ECoG and are present for the entire train duration of 150 ms. (Right) The template subtraction method allows individual pulses to be subtracted from the raw signal, resulting in the recovered signal which is on the scale of the raw signal without stimulation artifact.

Pre-removal, the artifact had large effects not only on the raw voltage, but also on broad-band spectral power, and for a longer duration than the 150 ms stimulation train delivered at t=0. Figure 19 reveals an example average time-frequency response from a single channel before and after stimulation artifact removal.

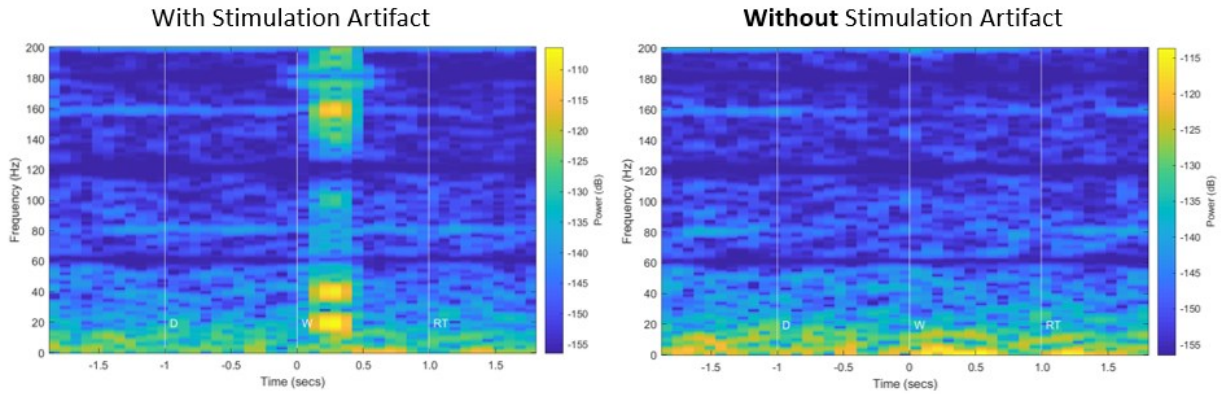

Figure 19. Spectral power across all bands of interest pre- and post-stimulation artifact removal. Stimulation delivered at t=0 leads to large, wide-band increases in power for approximately 500 ms. Dark horizontal bands around 60, 120, and 180 Hz reveal notch filtering effects of line noise and harmonics.

6.4.4 Verifying ECoG signal quality

While analyzing the ECoG data, we observed phenomena which are unrelated to our analysis but agree with previous findings in ECoG literature. Specifically, we observed suppression of beta power immediately preceding increase in high gamma power in some channels. Moreover, we observed an increase in high gamma power in some temporal channels at the time of the audio beep sounding.

6.4.4.1 Beta desynchronization and gamma synchronization with overt movement

In good agreement with the extent literature, we observed a decrease in beta power followed by an increase in gamma and high gamma power around the time of key press (Figure 20). The consistent decrease in beta power near reaction time for the various epochs (each epoch indicated by a different color in Figure 20) is indicative of beta desynchronization, also known as beta event-related desynchronization (ERD). Likewise, the consistent increase in gamma and high gamma power during reaction time is indicative of gamma event-related synchronization (ERS). This beta ERD followed by gamma ERS, measured through cortical electrodes in the motor area contralateral to the limb used for overt control, agrees with the ECoG literature regarding the dynamics of oscillatory activity in

canonical frequency bands during movement-based tasks (Babiloni et al., 2016; Pfurtscheller et al., 2003).

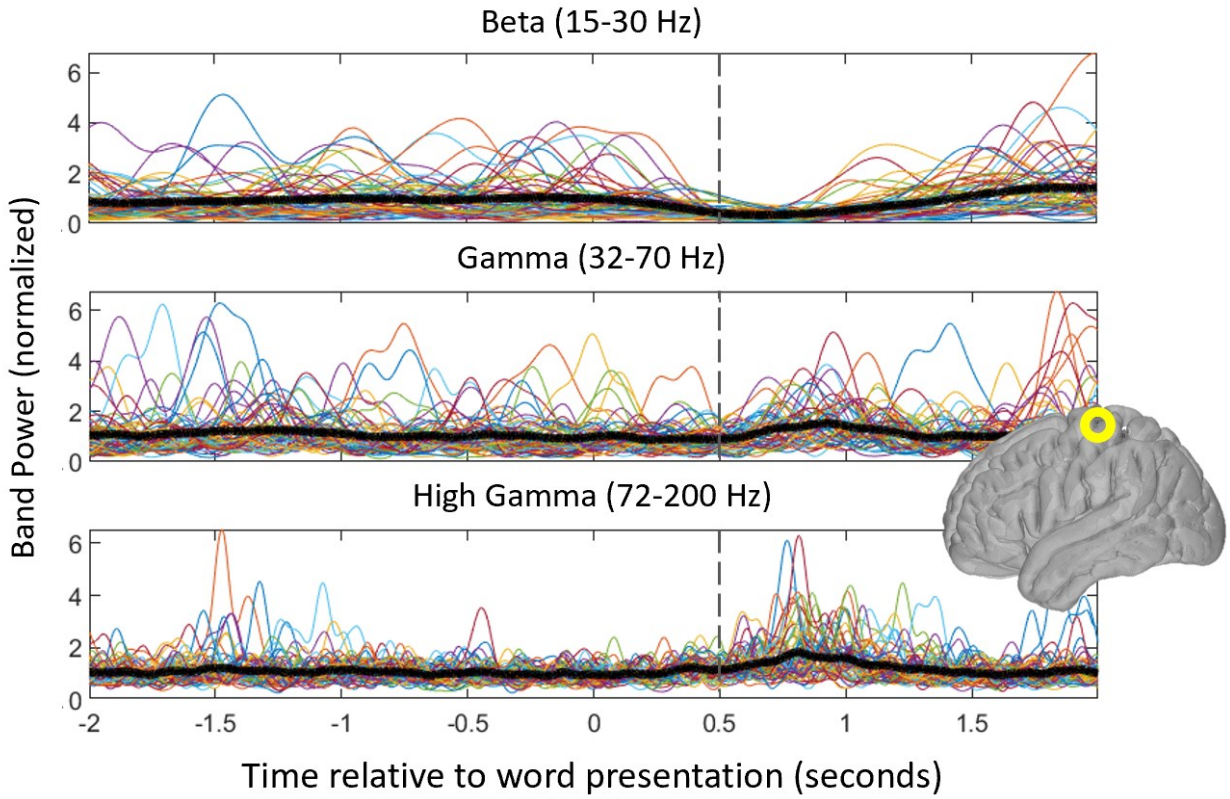

Figure 20. Observed motor cortex (highlighted yellow electrode) beta desynchronization and gamma synchronization clusters to reaction time (Subject 031ad1, channel 51). Each color waveform represents the band power of a single epoch centered around trial start (tied to word presentation). The thick black line represents average within band normalized power. The vertical dashed line indicates approximately where beta desynchronization and gamma synchronization begin.

The literature suggests this beta desynchronization is due to underlying sensorimotor information processing during action execution, including integrating visual observation of movement (Babiloni et al., 2016; Gastaut and Bert, 1954). Gamma synchronization, on the other hand, may represent an increase in local neuronal activity near the electrode (Babiloni et al., 2016). Given that the event in this case is the subject transitioning from rest to overtly pressing a key on the keyboard with their right hand, this beta desynchronization with gamma synchronization is not unexpected.

6.4.4.2 Recognition of audio

In multiple channels in or near the belt areas of auditory cortex, we observed a large increase in high gamma power at the time of audio beep presentation (t=-1) (Figure 21). Areas in or near the temporal

lobe, including but not limited to the superior-temporal gyrus and the inferior precentral gyrus, are known to show increased high gamma activity in response to auditory stimuli reflective of a role in auditory perception (Nakai et al., 2019). Figure 21 reveals a significant increase in high gamma power ($p = 4.3026e\text{-}17$) at the time of audio disruption (t=-1 to t=0 seconds) in trials preceded with an audio beep (red) for a single channel, located slightly superior to the superior-temporal gyrus. In the example for a single channel shown in Figure 21, the mean high gamma response at button press seems smaller than in no disruption trials but is not significantly smaller ($p = 0.2248$).

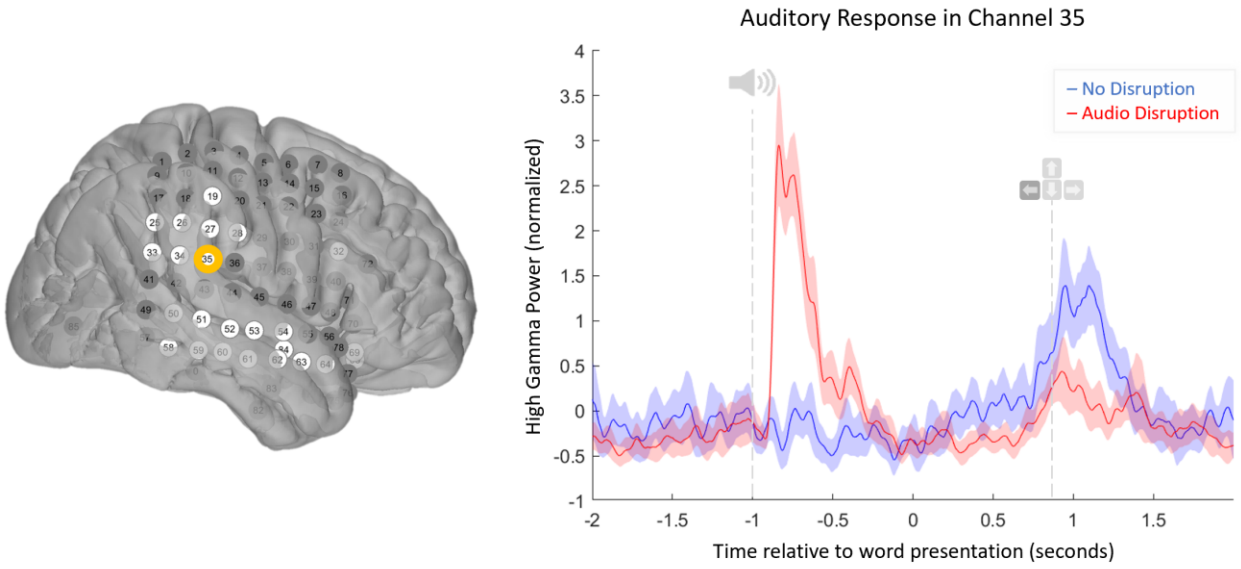

Figure 21. High gamma response to the audio beep presented at t=-1 in a single example electrode. High gamma power in channel 35 (highlighted) in subject 3ada8b exhibits the sharp increase in high gamma power that we expect from an area involved in auditory processing. The white channels displayed in the brain on the left were classified as DMN channels.

Because parts of the temporal lobe cortex owe membership within the Default Mode Network, we see high gamma increase in response to the audio beep in multiple DMN channels. In the following analyses, we avoid using spectral data from channels within auditory processing areas (BA21) during and immediately following the audio beep (t=-1 to t=0).

6.4.5 Effect of disruption on spectral power

Prior to running statistical analysis on the changes in spectral power due to DMN disruption, we visually inspected the spectrograms representing the spectral power over time for each disruption condition.

Example mean broad-band spectrogram responses for the four disruption conditions (no disruption, audio beep, DMN stimulation, control stimulation) are shown in Figure 22. Mean spectrograms were generated by creating spectrograms based on the mean response over all epochs within the given condition. In this single example from one channel from BA40, we observed increases in power in select higher frequency bands (approximately 80 and 160 Hz) in the control stimulation condition between word presentation (t=0) and reaction time (approximately t=1).

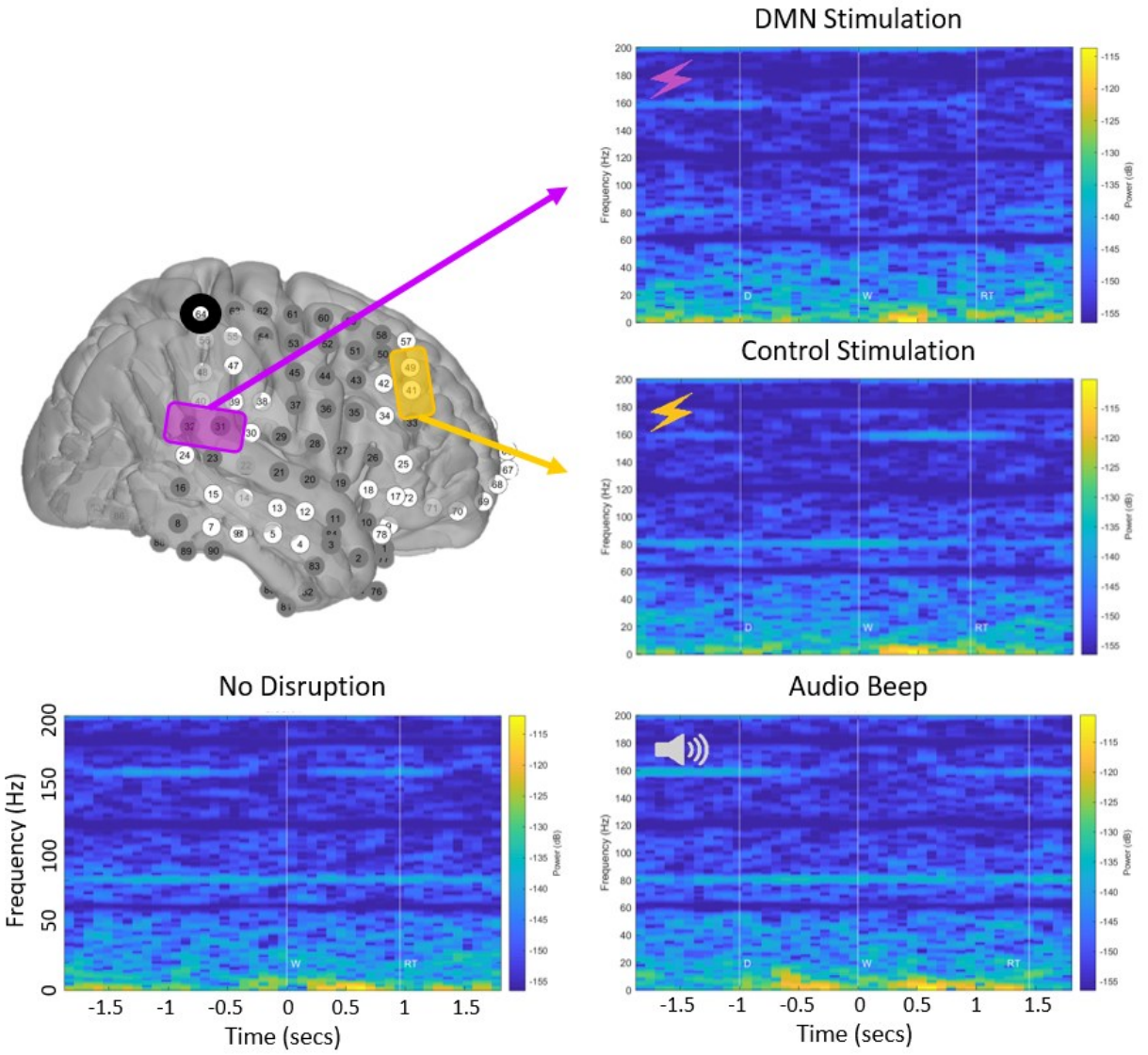

Figure 22. Mean response spectrograms for one channel in subject 822e26. Spectrograms for the different disruption conditions calculated for channel 64 (BA40, circled black in figure), including direct cortical stimulation to the Default Mode Network (purple) and to the control location (yellow). White electrodes indicate electrodes which were defined as within a DMN Brodmann Area through our MNI projection method. Vertical lines at t=-1, t=0, and after t=0 represent the time of initially planned disruption, the time of word presentation, and the mean reaction time for that condition, respectively. Note that although we initially planned to deliver cortical stimulation at t=-1, cortical stimulation was actually delivered at t=0.

Figure 22 suggests there may be a difference in low frequency power during and immediately following audio disruption (t=-1 to t=0 seconds) in channels outside of auditory processing areas, as compared to in no disruption trials. We examined if mean power across non-auditory DMN channels across all subjects was greater in audio beep trials than in no disruption trials for t=-1 to t=0 using unpaired two-sample t-tests for low frequency bands. We observed a significant increase in band power in the delta ($p = 0.0461$) and theta ($p = 6.2642e-10$) bands immediately following audio disruption in non-auditory DMN channels. However, we did not observe a statistically significant increase in alpha ($p = 0.0891$) or in beta ($p = 0.1642$) power following audio disruption.

To investigate whether audio disruption had an effect on mean power in the frequency bands of interest in DMN channels prior to RT, we initially fit a Linear Mixed Effects model fitting the effect of disruption type to the mean power within each band from t=0-500 ms in each epoch for all subjects together, with subject, frequency band, and channels set as random effect variables (Equation 3).

We then ran an ANOVA on this model and found disruption type (no disruption and audio disruption) to have a statistically significant main effect ($F(2, 47337) = 14.779$, $p = 3.8333e-07$) on mean power from t=0-500 ms across all channels. To better understand the specific effects, such as which frequency bands exhibited this effect, we conducted post hoc tests using unpaired t-tests.

We hypothesized that disruption from the audio beep would lower mean HG power across DMN channels. We ran a one-sided t-test testing if mean power following audio disruption was less than the mean power following no disruption (t=0-500 ms) for each frequency band using epochs from all DMN channels. We found that power in the alpha ($p = 0.0371$) and beta ($p = 4.2891e-04$) bands, but not in the gamma and high gamma bands, was statistically significantly greater for no disruption trials. If we instead tested if mean power following disruption was greater than mean power following no disruption, we saw a statistically significant difference in gamma ($p = 0.0261$) and in high gamma ($p = 7.9223e-06$).

To investigate whether cortical stimulation, as well as audio disruption, had an effect on mean power across DMN channels prior to button press, we fit a Linear Mixed Effects model to the effect of

disruption type on the mean power within each band from t=0-500 ms using all epochs for subject 822e26, who was the only subject to received cortical stimulation. Specific frequency bands and channels were treated as random effect variables in this model, as detailed in the methods (Equation 4).

We then ran an ANOVA on this model and found disruption type (no disruption, audio disruption, DMN stimulation, and control stimulation) to have a statistically significant main effect ($F(4,33475) = 32.47$, $p = 4.663e-27$) on mean power across DMN channels in subject 822e26 from t=0-500 ms. To better understand the specific effects, we conducted post hoc tests using unpaired t-tests.

We hypothesized that any form of disruption would lower mean HG power across DMN channels. We ran one-sided t-tests testing if mean power across DMN channels following a particular disruption type was less than the mean power across DMN channels following no disruption (t = 0-500 ms) for each frequency band.

When testing for audio disruption in subject 822e26, we found the mean power across DMN channels in trials with audio disruption to be statistically significantly less than the mean power across DMN channels in trials without disruption in the alpha band ($p = 0.0301$). However, no significant decrease was found in the higher frequency bands. When comparing DMN stimulation to no disruption, and when comparing control stimulation to no disruption, we did not observe any significant decrease in mean power across DMN channels from t=0-500 ms. However, if we instead tested if the mean power across DMN channels during disruption trials was greater than the mean power across DMN channels during trials without disruption, we found the following: mean power during audio disruption trials was statistically significantly greater than mean power during no disruption trials in the gamma ($p = 8.5113e-11$) and high gamma ($p = 3.1133e-19$) bands. For DMN stimulation compared to no disruption, we saw statistical significance in the alpha ($p = 0.0442$), beta ($p = 1.0766e-08$), gamma ($p = 6.4034e-10$), and high gamma ($p = 4.8937e-07$) bands. For control stimulation compared to no disruption, we see statistical significance in the gamma ($p = 9.3680e-07$) and high gamma ($p = 2.9160e-26$) bands.

6.4.6 Effect of ISI length on spectral power

Embedded within our experimental design, we varied ISI length from a typically short 1-2 second duration to a long 10 seconds, as an extended period to promote varied DMN activity related to mind wandering (Christoff et al., 2016). To investigate associations between ISI and pre-trial DMN activity, we ran a power analysis similar to our previous spectrogram approach on DMN disruption.

We then fit a Linear Mixed Effects model to the effect of ISI length on mean power within each band from the final second in the ISI preceding any possible disruption (t=-2000 ms to t=-1000 ms), across all DMN channels and subjects. Subject, frequency band, and channel were set as random effect variables in this model, as detailed in the methods (Equation 5).

We then ran an ANOVA on this model and found ISI length to have a statistically significant main effect ($F(2, 2.2724e05)=27.666$, $p = 9.6887e-13$) on power. To better understand the specific effects, such as in which frequency bands the effect was significant, we conducted post hoc tests using unpaired t-tests.

We hypothesized that mean HG power would be greater across DMN channels towards the end of longer ISIs. We ran one-sided t-tests testing if the mean power from one second of data (starting two seconds from the end of the ISI period) was greater in a longer ISI than a shorter ISI.

When comparing mean power in short ISIs to mean power in medium ISIs, we saw that the mean power across DMN channels was significantly greater in medium ISIs in the alpha ($p = 1.4154e-18$) and beta ($p = 4.9293e-09$) bands. When comparing mean power across DMN channels in short ISIs to mean power across DMN channels in long ISIs, we saw the mean power was significantly greater in long ISIs in only the alpha ($p = 1.8919e-20$) band. When comparing mean power in medium ISIs to the mean power in long ISIs, we also only observed statistical significance in the alpha ($p = 0.0315$) band.

6.4.7 Effect of disruption on connectivity

In addition to investigating the effects of disruption type on the local activity (through high gamma power) and on lower frequency band power in individual channels, we also explored the effects of disruption type on the connectivity of channels within the Default Mode Network.

6.4.7.1 Coherence

We estimated coherence as a measure of connectivity between electrodes across different Brodmann Areas within the DMN from t=0 to t=500 ms. One representative channel was selected for each DMN Brodmann Area, as described in the methods. Given the great change in coherence around 20 Hz for many trials across all subjects (Figure 23), we divided our coherence results into mean values below 20 Hz and mean values above 20 Hz.

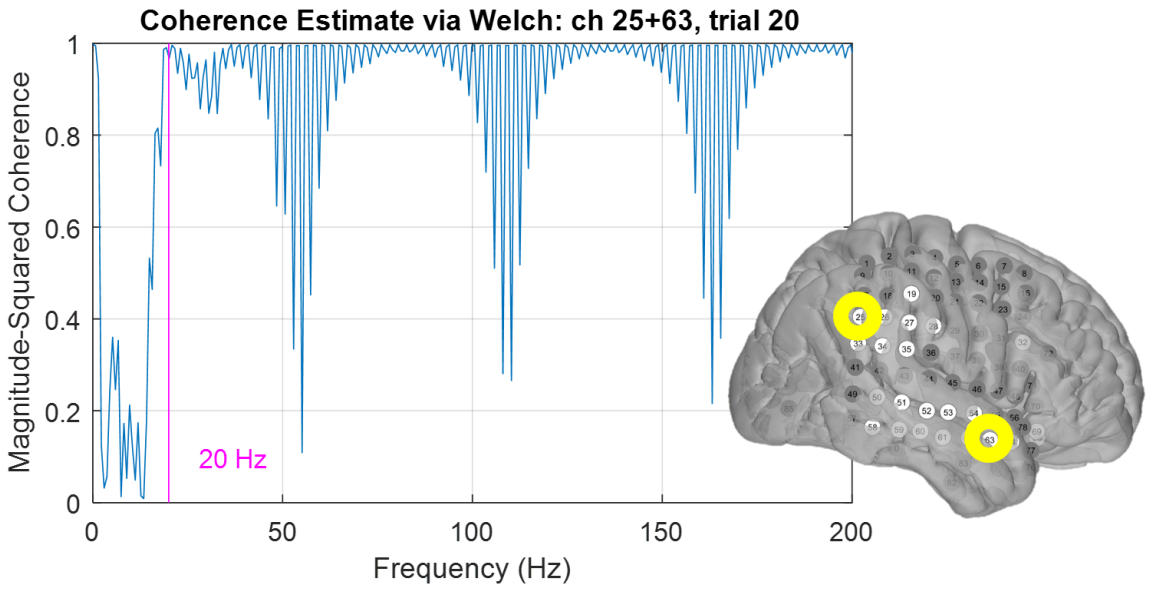

Figure 23. Example coherence between two DMN Brodmann Areas in a single trial. The coherence between Brodmann Areas within the Default Mode Network often changed greatly around 20 Hz. This individual example from subject 3ada8b, using channels 25 (BA40) and 63 (BA21) in a single trial, we see a large increase in coherence after approximately 20 Hz. This behavior holds for many trials between all our subjects.

When observing the effect of audio disruption on coherence for all subjects, we see that mean coherence (both above and below 20 Hz) between all Brodmann Area channel pairs in the DMN have statistically significantly lesser coherence in trials following audio disruption relative to trials without disruption (Figure 24). Figure 24 shows the mean difference in coherence values in text and the

significance of this difference in color, where significant differences have a non-white background color.

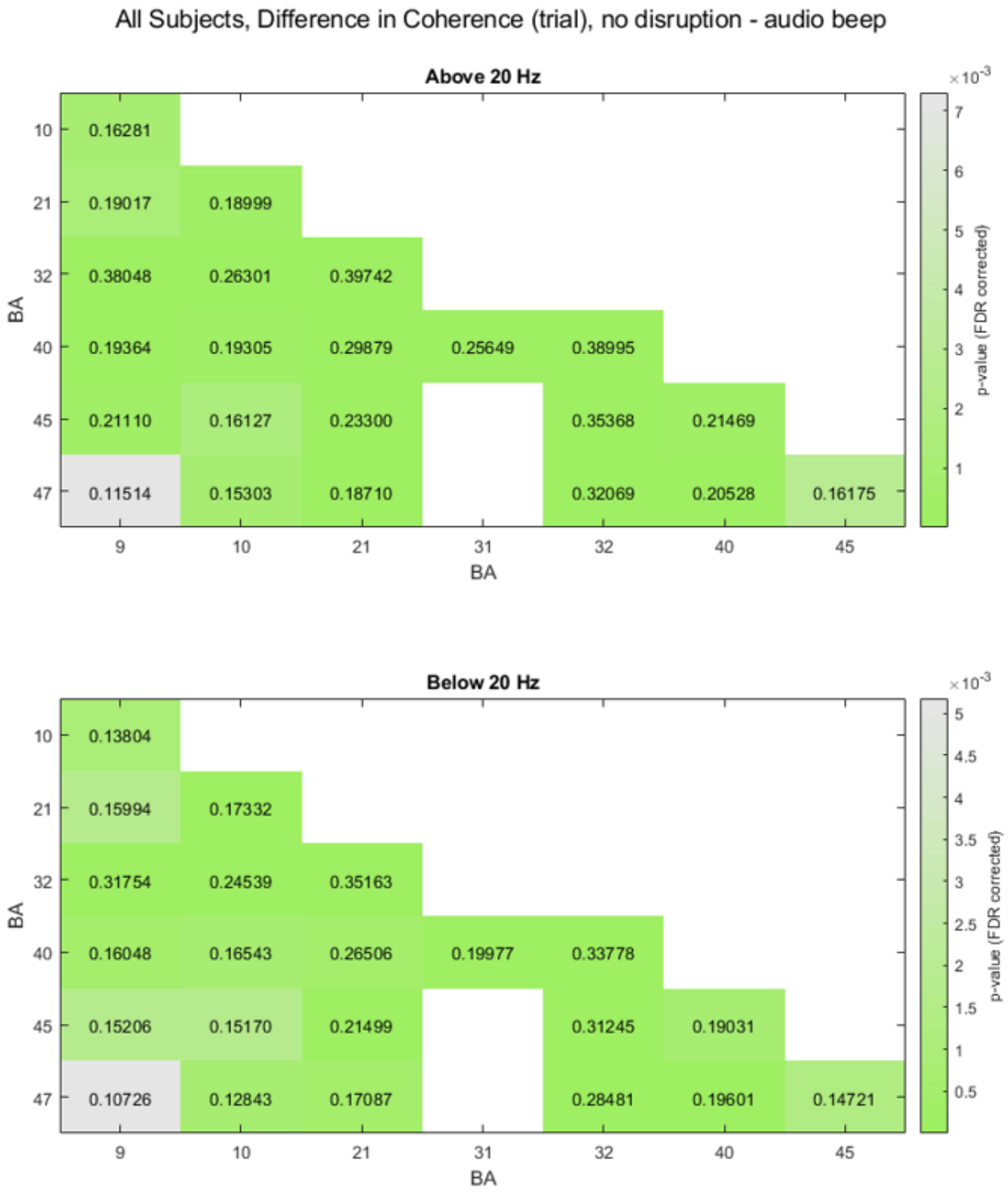

Figure 24. Difference in coherence between trials with no disruption and trials following audio disruption. Each difference value is printed in each cell, where each cell color corresponds to the significance of the difference as measured by the p-value (FDR corrected for multiple comparisons). Cells with white backgrounds indicate no statistical significance. Blank cells represent comparisons that were not performed either because there were no electrodes within a given Brodmann Area (BA) or the information would be redundant.

When observing the effect of cortical stimulation on coherence for subject 822e26, we see that mean coherence (both above and below 20 Hz) between all Brodmann Area channel pairs in the DMN have statistically significantly lesser coherence in trials with cortical stimulation than in trials without disruption (Figure 25).

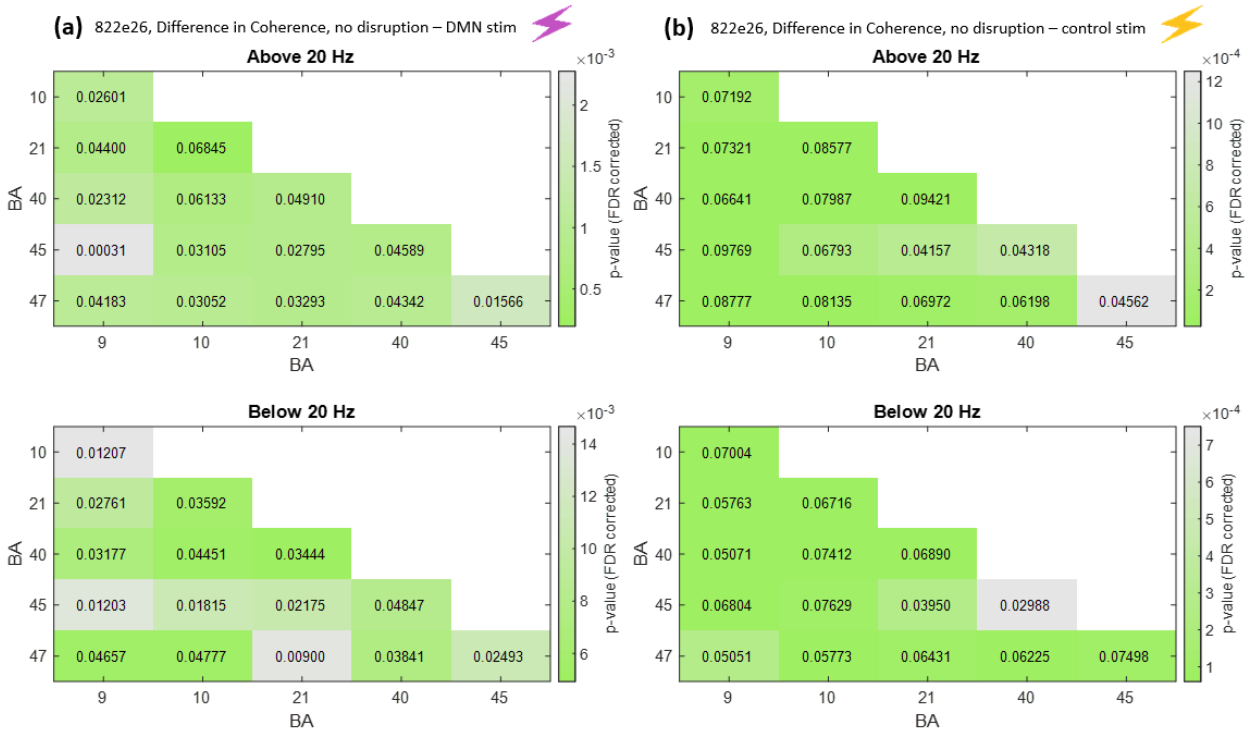

Figure 25. Change in coherence from cortical stimulation. (a) Difference in coherence between trials with no disruption and trials with DMN stimulation. (b) Difference in coherence between trials with no disruption and trials with stimulation to the control area. Each difference value is printed in each cell, where each cell color corresponds to the significance of the difference as measured by the p-value (FDR corrected for multiple comparisons). Cells with white backgrounds indicate no statistical significance. Blank cells represent comparisons that were not performed either because there were no electrodes within a given Brodmann Area (BA) or the information would be redundant.

6.4.7.2 Phase-Amplitude Coupling

In addition to coherence, we investigate Phase-Amplitude Coupling (PAC) as a measure of connectivity between the various Brodmann Areas in the DMN for the first 500 milliseconds in trials. PAC resolves the degree of amplitude modulation as a function of phase across two signals. We computed PAC within each channel representing each Brodmann Area. For each subject, we estimated the Modulation Index value (Tort et al., 2010) as a single value measure for the strength of Phase-Amplitude Coupling between alpha phase (7-12 Hz) and high gamma amplitude (70-200 Hz) or between beta phase (13-30

Hz) and high gamma amplitude, two band-limited indexes previously reported in extend DMN literature (Fox et al., 2018).

Alpha-HG coupling

We first investigate the change in PAC between alpha phase and high gamma amplitude due to the introduction of DMN disruption, either through audio beep, cortical stimulation to the DMN, or cortical stimulation to the control area. When comparing Modulation Index values from audio disruption trials to no disruption trials (from t=0 to t=500 ms), we only saw a significant decrease in PAC in the disruption trials for the following alpha phase high gamma amplitude pairs in subject 822e26 (unpaired two-sample t-tests, p-values FDR corrected for multiple comparisons): BA21 phase with BA21 amplitude ($p = 0.03555$), BA45 phase with BA10 amplitude ($p = 0.04762$), BA47 phase with BA21 amplitude ($p = 0.03764$), and BA47 phase with BA40 amplitude ($p = 0.03917$). The Modulation Index difference values for 822e26 are displayed in Figure 26, with the significant differences highlighted in green ($p < 0.05$, FDR corrected for multiple comparisons). No other subjects exhibited a significant decrease due to audio disruption.

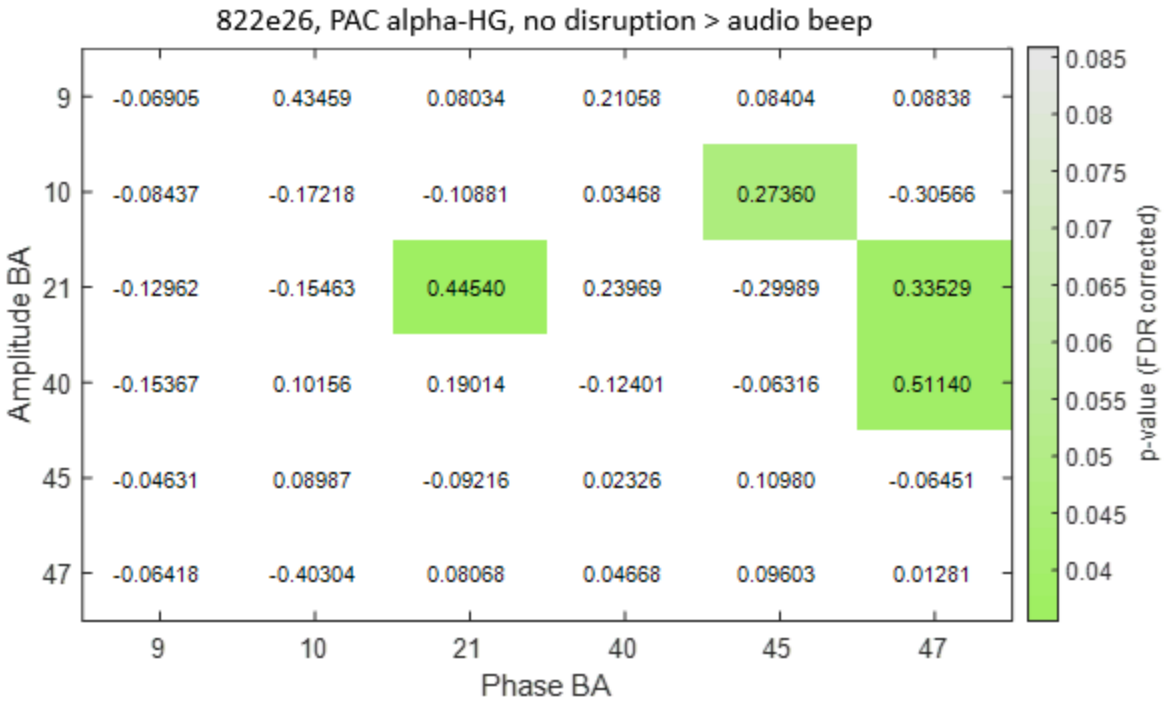

Figure 26. Difference in Modulation Index between no disruption and audio disruption in subject 822e26. Values displayed in each cell are the mean difference in Modulation Index. Cell color indicates p-value, where significant p-values are colored according to the color bar to the right. Insignificant differences are not highlighted.

For DMN disruption, we only saw a significant decrease in PAC in the BA40 alpha phase BA21 amplitude pair ($p = 0.03708$). For control stimulation, we did not see any significant decreases.

Beta-HG coupling

We then investigated the change in PAC between beta phase and high gamma amplitude due to the introduction of DMN disruption, either through audio beep, cortical stimulation to the DMN, or cortical stimulation to the control area. When comparing Modulation Index from audio disruption trials to no disruption trials (from t=0 to t=500 ms), we only saw a significant decrease in PAC in the disruption trials (unpaired two-sample t-tests, p-values FDR corrected for multiple comparisons) for the BA40 beta phase BA40 amplitude pair in subject 3ada8b ($p = 0.02375$). No other subjects exhibited a significant decrease due to audio disruption.

For DMN disruption, we saw a significant decrease in PAC between beta phase and high gamma amplitude from t=0 to t=500 ms in trial for subject 822e26 in the following Brodmann Area pairs: BA9 phase with BA10 amplitude ($p = 0.02949$), BA10 phase with BA40 amplitude ($p = 0.02531$), BA40 phase

with BA10 amplitude (p = 0.03094), BA40 phase with BA40 amplitude (p = 0.0452), BA40 phase with BA47 amplitude (p = 0.02539), BA47 phase with BA40 amplitude (p = 0.0258), and BA47 phase with BA47 amplitude (p = 0.01561) (Figure 27).

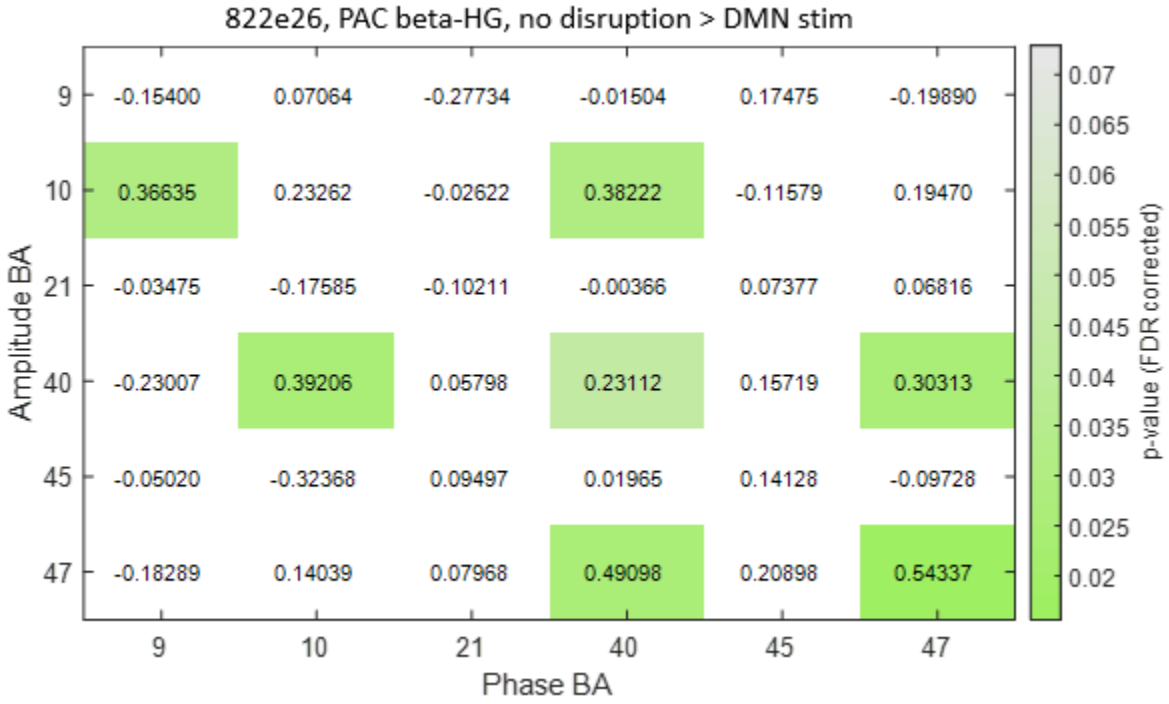

Figure 27. Difference in Modulation Index between no disruption and DMN disruption in subject 822e26. Values displayed in each cell are the mean difference in Modulation Index. Cell color indicates p-value, where significant p-values are colored according to the color bar to the right. Insignificant differences are not highlighted.

For control stimulation, we do not see any significant decreases.

6.5 Discussion

In this chapter, we have explored the effect of inter-stimulus interval length and Default Mode Network disruption on reaction time, and the effect of disruption on reaction time, on spectral power, and on connectivity. Here, we discuss our interpretations of these results and propose further investigations on the effects of subconscious and perceptible DMN disruption on connectivity between DMN areas.

6.5.1 Reaction time may be affected by disruption type and ISI length

While ISI length and disruption type did not generally have statistically significant effects on reaction time, we did observe some effects, particularly at the level of individual subjects. Our initial prediction was that reaction time would be shorter for trials following shorter ISI and for trials preceded by audio disruption. Consistent with this prediction, we noted significant effect for most subjects, an observation which is in agreement with the extent literature (Aiken and Lichtenstein, 1964). Apropos, disruption of the DMN through exogenous electrical stimulation somewhat unexpectedly increased reaction time in our single stimulation subject, given the well-established negative relationship between DMN activity and task performance (Ossandón et al., 2011). Stimulation to the control site did not seem to affect reaction time (Figure 17). This implies that disruption of the DMN through high-frequency cortical stimulation may have an effect on the subject's ability to process or execute the immediate demands of a goal-directed task.

It is likely, however, that such unexpected increase, as opposed to decrease, in reaction time may be due to the timing of the stimulation delivery. With the cortical stimulation delivered at t=0, it is possible that we were interfering with the inhibition of DMN areas which would normally occur when the trial begins. Had the cortical stimulation been delivered at t=-1 as initially intended, the stimulation may have instead interrupted ongoing DMN activity and lowered DMN activity leading up to the trial start and reaction time.

It is also possible that the stimulation current spread and impaired performance through inhibiting function of areas nearby the stimulation sites. For example, DMN stimulation was delivered to channels 31 and 32 in subject 822e26 (Figure 22). The DMN stimulation site neighbors channel 24, which is categorized as being in BA21, an area associated with processing of text and speech (Giraud et al., 2004; Vorobyev et al., 2004). Although this function is typically linked to BA21 of the left hemisphere, if interrupted via cortical stimulation at t=0 when the trial begins and the word is presented, it would not be unexpected for the subject to take longer to process the word before responding with a key press. It is conceivable that had this stimulation been delivered at t=-1, recovery of functional language processing may well have occurred by the time of trial start and not inhibited performance.

6.5.2 Audio disruption and cortical stimulation unexpectedly increase spectral power

Default Mode Network disruption, whether perceived through an audio beep or through sub-conscious cortical stimulation, seemed to increase spectral power for higher frequency bands in DMN channels 0-500 ms after trial start. We initially expected disruption to decrease spectral power in the high frequency bands, but found that this was instead true for the lower frequency bands (alpha and beta). Interestingly, power across DMN channels increased in the higher frequency bands with audio disruption from t=0-500 ms.

For the audio disruption trials, increased high gamma power in DMN channels during auditory processing may reflect perceptual processing of the audio stimulus. Although the auditory response from a single channel demonstrated in Figure 21 shows the transient increase in high gamma power ends by t=0, it is possible that the collective response across all DMN channels took longer to return to baseline.

For the DMN disruption during control stimulation trials, power in DMN channels near the stimulation sites may have had residual increases in power due to cortical stimulation even after direct cortical stimulation (DCS) termination and stimulation artifact removal. Although stimulation only lasted for 150 ms, we see in Figure 19 that stimulation may have impacted resulting band-limited power up to 400 ms after DCS offset and across a wide frequency range.

6.5.3 DMN disruption consistently lowers coherence between DMN areas

Although local activity – implied through high gamma power – increased across the DMN channels at the start of trials (t=0-500 ms) with disruption, the coherence between DMN Brodmann Areas decreased significantly with any form of disruption as expected. All possible Brodmann Area pairs in our subjects demonstrated this statistically significant decrease in coherence in frequencies below 20 Hz and in frequencies above 20 Hz. As a measure of functional connectivity, coherence quantifies how synchronous the phase and amplitude content is within a frequency band of interest across two sites (Bowyer, 2016). This significant decrease in coherence for all DMN BA combinations in disruption trials relative to no disruption trials implies that functional connectivity within the DMN is inhibited by both

perceived (audio beep) and sub-conscious (cortical stimulation to the DMN or to the control area) disruption. Conversely, this implies that functional connectivity between DMN areas was higher during no disruption trials, even though this time window (t=0-500 ms) occurred at the transition between rest and task engagement.

6.5.4 Phase-Amplitude Coupling lessens between some DMN areas with disruption

Unlike with coherence, we did not see a significant change in Phase-Amplitude Coupling between all Brodmann Area pairs with any form of DMN disruption. We observed significant change in the most BA pairs in beta phase high gamma amplitude coupling during DMN stimulation trials in subject 822e26. The significant decrease in BA9 beta phase and BA10 high gamma amplitude coupling due to cortical stimulation to the DMN may have transiently impaired the subject's ability to determine if the word presented at trial start was congruent or incongruent, given BA9's involvement in error processing (Fink et al., 1999) and BA10's involvement in conflict resolution (Rogers et al., 1999). Similarly, the decrease in coupling between BA10 phase and BA40 amplitude may have impaired the subject's ability to determine if the color of the presented word in the trial and the meaning of the word itself matched, given the right inferior parietal lobule's (BA40) involvement in same-different discrimination (Hirsch et al., 2001). The decrease in BA40 phase and BA10 amplitude coupling presumably would have the same negative effect on subject processing ability. The decrease in BA40 phase and BA47 amplitude coupling, and in BA47 phase and BA40 amplitude coupling, may have led to increased difficulty in inhibiting key press of the incorrect key, due to the right orbitofrontal cortex's (BA47) involvement in behavioral inhibition (Völlm et al., 2006). Interestingly, we also observe a significant decrease in PAC within BA40 and within BA47. Because each Brodmann Area was represented by a single channel, each within-Brodmann Area PAC change reflect the phase and amplitude coupling in an individual channel. While single channel changes in cross-frequency coupling through PAC have not been well studied, this phenomenon has been used in one study to classify sleep stages with high accuracy using a single EEG sensor (Dimitriadis et al., 2018), implying that single channel PAC can be informative but should be considered with a degree of caution (Jensen et al., 2017).

We do not observe any significant change in beta phase high gamma amplitude coupling due to the control stimulation. We, however, did note a significant change in one BA pair due to audio disruption in subject 3ada8b, the PAC within BA40. Like with the decrease due to DMN stimulation in 822e26, this decrease in PAC in BA40 may have led to difficulty in same-different discrimination for subject 3ada8b.

We observed the next highest number of significant pairs in alpha phase high gamma amplitude coupling during audio disruption in subject 822e26. Like with the BA40 beta phase BA47 high gamma amplitude coupling in the DMN stimulation condition, we see a significant decrease in BA40 alpha phase BA47 high gamma amplitude coupling in the audio disruption condition in subject 822e26. Notably, this change in PAC is significant with alpha phase only with audio disruption and is significant with beta phase only with DMN stimulation. No other significant pairs from beta PAC also resulted in significant alpha PAC. The decrease in BA45 alpha phase and BA10 high gamma amplitude coupling may have led to difficulty in processing text, as BA45 is associated with word processing (Gold et al., 2005; Vorobyev et al., 2004). However, it is important to note that this function of BA45 was observed from the left inferior prefrontal area and not from the right hemisphere, which is where we recorded from for subject 822e26. The decrease in BA47 phase and BA21 amplitude coupling may have also led to difficulty in verbal-linguistic processing, as BA21 is known to be involved in selective processing of text (Vorobyev et al., 2004). However, like with BA45, this effect for BA21 was observed in the left hemisphere in work by Vorobyev et al. (2004). Lastly, the alpha phase high gamma amplitude coupling within BA21 significantly decreased with audio disruption and likely led to difficulty in text processing.

Regarding cortical stimulation's effect on alpha phase high gamma amplitude coupling, we only observed a significant effect in one BA pair for DMN stimulation in subject 822e26. This decrease in BA40 alpha phase and BA21 high gamma amplitude coupling may have negatively impacted the subject's ability to perform same-different discrimination and to process the word presented.

Overall, we observed the greatest effect on Phase-Amplitude Coupling, specifically beta phase and high gamma amplitude coupling, with Default Mode Network stimulation.

6.5.5 ISI length on DMN activity

We next sought to determine whether increased inter-stimulus interval length (from the standard 1-2 second length up to 10 seconds) would encourage mind wandering and consequently increase Default Mode Network activation. It is well established that augmented DMN activity is associated with mind-wandering and errors in task-performance (Anticevic et al., 2012). We measured the difference in DMN HG activity for different ISI lengths (short, medium, and long) and found that DMN HG activity does not necessarily increase across the span of longer ISIs. However, power in both the alpha and beta bands were significantly higher in medium length ISIs as compared to in short length ISIs. When comparing spectral power from the medium length to long ISIs, we observed a significant increase in only the alpha band. We also observed a significant increase in alpha power in long ISIs as compared to short ISIs. This makes alpha the only band to exhibit a consistent increase in band power with increasing ISI length. Although not as direct a reflection of locally-specific activity as high gamma power, alpha power has been identified as related to the DMN activity (Bowman et al., 2017; Rusiniak et al., 2018). However, as elucidated by Bowman et al. (2017), the relationship between alpha power and DMN activity varies by subpopulations within classic DMN nodes on the scale of overlapping voxels in fMRI. Because contemporary high-resolution fMRI provides a finer spatial resolution than ECoG, we are uncertain if we would be able to reliably identify and separate these subpopulations in our analysis. As a result, we cannot definitively state that DMN activity increases with longer ISI length in this study.

6.5.6 Future work

Through this work, we have demonstrated that disruption of Default Mode Network activity has statistically significant effects on spectral power, coherence, and Phase-Amplitude Coupling in DMN channels. However, the delivery of cortical stimulation at trial start (t=0) limits confidence in our stimulation results aimed at impairing DMN function during sustained, task-directed focus. We suggest future work to modify the task such that cortical stimulation is delivered at t=-1 and analyze the effect on reaction time, spectral power, and connectivity. We believe this would allow for greater confidence in the interpretation of the results. In addition, further analysis could be performed to investigate the effect of DMN disruption during reaction time and immediately after.

6.6 Conclusion

In this chapter, we discussed the effects of attention and disruption of the Default Mode Network on reaction time in a Stroop Task performed by individuals implanted with subdural electrodes. While we observed that reaction time was generally faster for short ISI for most subjects, longer ISI duration did not consistently lead to a statistically significantly slower reaction time. Similarly, we observed that reaction time for trials following audio disruption of the DMN tended to be faster for most subjects than for trials with no disruption, but did not see a statistically significant effect. In investigating the cortical signals, we found local activity (measured through high gamma power) increased in DMN channels in trials preceded by audio disruption and in trials with either DMN or cortical stimulation. We also found that audio disruption and disruption through cortical stimulation significantly decrease coherence between all DMN Brodmann Area pairs available. Although not as widespread as the change in coherence, audio disruption and DMN stimulation led to significant reductions in Phase-Amplitude Coupling within and between a few Brodmann Areas. Stimulation to the control area, however, did not have any significant effect on Phase-Amplitude Coupling.

From this work, we gained a better understanding of effect of attention and cognition – implied through Default Mode Network activity – and how we may affect subject performance through DMN disruption. This leads us into the next chapter, which uses both error-related potentials (as explored in the previous chapter) and attention to create a co-adaptive Brain-Computer Interface.

7. Combining error potentials and DMN activity to create a co-adaptive BCI system

7.1 Motivation

BCI co-adaptation is typically restricted to settings where we have all the metadata necessary to manually make changes to the system, such as actuator kinematics and explicit task performance measures. However, obtaining metadata through additional sensors or manual human behavior monitoring is impractical for BCI use in at-home, or even clinical, settings. Through the use of neural performance monitoring signals already being collected during BCI use, we developed a BCI that automatically adapts to the user without the need for specific task information or a researcher. The adaptive BCI presented in this chapter uses both error-related potentials and attention via Default Mode Network activity to selectively adapt to the user based on their estimated performance. This is the first demonstration of a motor imagery based co-adaptive BCI which relies on a combination of error and attention for performance estimation.

Studying error-related potentials and the Default Mode Network at the cortical level allowed us to gain a better understanding of performance related signal involvement in task performance. However, while we could develop a co-adaptive system using these performance related signals in minimally-invasive electrocorticography (ECoG), we believe developing and demonstrating such a system for non-invasive EEG will allow for greater impact. In addition, the non-invasive nature of EEG allows us to iterate through the BCI design and testing process much quicker.

7.2 Introduction

Brain-Computer Interfaces (BCI) are systems that enable users to control devices such as computer cursors (Bacher et al., 2015; Simeral et al., 2011; Spuler, 2015), keyboards (Bacher et al., 2015; Guy et al., 2018; Spuler, 2015), and robotic arms (Gao et al., 2017; Hochberg et al., 2012; Kim et al., 2015; Schiatti et al., 2017) through their own neural signals. These systems have the potential to improve the

quality of life for individuals with sensorimotor disabilities due to neurological conditions such as spinal cord injury and stroke. All BCIs consist of three main components: (1) the neural signals of the user, (2) the signal decoder which is responsible for processing the signals to output control instructions for the end effector, and (3) the end effector which can take many forms including but not limited to virtual controls on a computer or a robotic limb. Brain signals may be recorded either invasively or non-invasively for BCI use (Chaudhary et al., 2016), however, regardless of the recording method most BCI exhibit difficulty in maintaining performance over long term use (Shenoy et al., 2006; Simeral et al., 2011). To combat this, researchers have begun to investigate multiple methods to enable decoder adaptation, with each method typically falling under one of the following broad categories: (1) adaptation relying on external sensor data, kinematics, or task behavioral data (Margaux et al., 2012; Mattout et al., 2015; Mondini et al., 2016; Rozado et al., 2015), (2) adaptation based on the neural signal without context (Faller et al., 2014; Vidaurre and Blankertz, 2010; Vidaurre et al., 2006), and (3) adaptation based on performance-related neural signals (Cruz et al., 2018; Iturrate et al., 2015; Myrden and Chau, 2016; Spüler et al., 2012a, 2012b). Decoder adaptation is of particular interest among researchers due to the non-stationarity of the signals being recorded (Shenoy et al., 2006). Brain signals recorded during one session for a particular task may differ enough in another session such that the decoder has difficulty correctly translating the signals into the proper output.

Of the three major categories of decoder adaptation, we believe adaptation based on performance related neural signals is the most useful choice going forward. Future BCI will ideally function reliably for users in multiple contexts, whether they are using the BCI to type at the computer or to prepare a meal. When working in multiple contexts, it is difficult to keep track of BCI performance through things often used in controlled experimental settings, such as behavioral data. While using behavioral data is not impossible in the at-home setting, it may feel very cumbersome and invasive with the introduction of multiple sensors, such as cameras to monitor actions continuously. Fortunately, we have our own performance monitoring system integrated into our brain function. By measuring error-related potentials and attention, we can estimate subject performance using the signals we are already recording with the BCI without introducing the need for any additional sensors.

In this chapter, we discuss the development and testing of a co-adaptive BCI which uses error-related potentials and attention as performance related neural signals to adapt to the user over time.

7.3 Determining the EEG system

Prior to starting the study, we explored different EEG systems to determine which would work best for our needs, and which may most closely emulate future BCI systems used in at-home settings. Of particular interest were the Wearable Sensing DSI-7 and the Neuroelectrics Enobio due to their quick setup time, reported signal quality, and availability of dry electrode sensors.

In deciding which system to use, we took into account four factors: (1) signal quality, (2) ease of setup, use, and maintenance, (3) electrode coverage, and (4) comfort. Both systems exhibited comparable signal quality when electrodes were in good contact with the scalp. While both systems were fairly easy to setup and maintain, we found the Enobio to be a bit more versatile and easier to interface reliably. The DSI-7 electrode positions are fixed in the headset and cannot be moved to other locations, whereas the Enobio is in the form of a standard EEG cap with electrodes which may be moved to various standard 10-20 system locations. In terms of comfort, both systems were comparable.

Additionally, the Enobio works with not only dry electrodes, but also with traditional gel electrodes and new solid gel electrodes. We test recorded with all three available electrode types with the Enobio and found the dry electrodes to have the most reliable and consistent contact with the scalp.

Ultimately, we decided to use the Neuroelectrics Enobio due to the ability to move the electrodes around to create custom montages, and also due to less difficult interfacing through Python. Although the Enobio was the better solution for this study, we believe the DSI-7 has great potential. It is possible that BCI users would prefer to don EEG headsets like the DSI-7 instead of donning an EEG cap like the Enobio.

7.4 Methods

7.4.1 Subjects

Healthy participants (n = 25, 12 male, mean age 23 years old) consented and volunteered to participate in this EEG study in accordance with the University of Washington Institutional Review Board (see Table 9 for demographics). Three subjects have previous history of a neurological disorder. Subjects were compensated $50 total for completing all three sessions or were compensated $15 per session if they did not complete all three.

Data were collected through two consecutive studies. The recording methods and task were the same for both Study 1 and Study 2, however, we discovered a bug in the BCI code which was present for all subjects in Study 1. We fixed the issue and subsequently collected data from new subjects for Study 2. Therefore, we simulated the performance for all subjects from Study 1, as described in the section below titled “Simulated Adaptation”.

Data were recorded using a Neuroelectrics Enobio EEG recording device (Ruffini et al., 2006) with 8 dry contact electrodes. Subjects were fitted with either a medium or large size cap, as indicated in Table 9. We recorded from the following eight channels at 500 Hz for all subjects: F3, Fz, F4, either FC1 for the medium cap or FCz for the large cap, C3, Cz, C4, Pz. We used FC1 instead of FCz in the medium cap because the medium cap did not have FCz as an available location to place an electrode.

Data from subject 97e442 were excluded from analyses because the subject was falling asleep consistently throughout all three of their sessions.

Subject ID	Study #	Group #	Age	Sex	Handedness	Cap Size	BCI Experience	History of Neurological Disorders	Session 1	Session 2	Session 3
b12a46	1	1	21	M	R	M	None	No	0	8	15
41d8ff	1	1	21	F	R	M	None	No	0	5	12
1e8b34	1	1	29	M	R	L	None	No	0	3	14
ad11cf	1	1	20	F	R	M	None	Yes	0	7	12
af9af3	1	1	23	M	R	M	None	No	0	4	17
c795d2	1	1	26	F	R	M	None	No	0	1	20
97e442	1	1	20	F	R	L[+]	None	No	0	4	10
5ea9e5	1	1	21	F	R	M	None	No	0	12	25
e2cbc4*	1	1	21	M	R	M	None	No	0	7	14
b7ff16	1	2	20	F	R	M	None	No	0	19	21
42feb7*	1	2	21	F	R	L	None	No	0	3	7
9d4921	1	2	20	M	L	L	None	No	0	14	16
05ecbc	1	2	19	F	R	M	None	No	0	7	22
912433	1	2	19	F	R	M	None	No	0	5	6
6f6b76	1	2	19	M	R	L	None	No	0	1	2
dcdb48	1	2	25	M	R	M	None	No	0	1	2
d4aee6	1	2	33	F	R	L	Tried once at an event but no training	Yes	0	1	2
994dba	1	2	21	M	R	M	None	No	0	3	5
303d01*	1	2	38	M	L	M	None	No	0	1	13
a1e6c0	2	1	32	M	R	M	None	No	0	3	7
851238	2	1	18	M	L	M	None	No	0	3	4
c37099	2	1	20	F	R	M	None	No	0	2	3
972a6f	2	2	18	F	R	M	None	No	0	15	18
520f16	2	2	18	F	R	M	None	No	0	1	2
bd9e40	2	2	21	M	R	M	None	Yes	0	1	4

Table 9. EEG Study Demographics Table. Study number represented whether subjects had data collected through Study 1 or Study 2. Group number represents whether the subjects were using an adaptive decoder (Group 2) or a static one (Group 1). The numbers in the Session columns represent the number of days since the respective subject's first session. Subjects with a * on their ID performed an alternate motor screening task (described in the section title Motor Screening). [+]Subject 97e442 completed session 1 with a medium sized cap but switched over to a large cap for the remaining two sessions for comfort.

7.4.2 Experimental design

Subjects attempted to learn to control a 1-D BCI over three separate sessions, each lasting about one hour with no more than one session on any given day. Within each session, subjects performed both a motor screening task, to train the motor imagery decoder to classify imagined left vs imagined right hand movement, and then multiple runs of a BCI control task. In the first session, subjects also performed an error screening task to elicit error-related potentials (ErrPs), which are used in BCI decoder adaptation. We selected motor imagery as the control scheme to provide subjects with a chance to improve performance within or across sessions. Signals with typically above chance performance without any training, such as Steady-State Visually Evoked Potentials (SSVEP), may not allow for demonstration of learning.

In each session, subjects perform five runs of the BCI task with or without decoder adaptation between runs. Subjects were randomly placed into Group 1 (no adaptation between runs) or Group 2 (decoder adaptation between runs) prior to their first session.

All tasks were created in Python using a combination of the PsychoPy (Peirce et al., 2019), Arcade, and Lab Streaming Layer libraries.

7.4.2.1 Error screening

In the first session, subjects performed an overt control 1-D center-out task for approximately 10 minutes. In this task, subjects attempted to reach a target placed either to the left or to the right of the center start position by pressing the left or right arrow key on the keyboard. In order to move the cursor one step, the subject must press the directional key of choice three times in a row. For each step taken, there is a 20% chance that the cursor will move in the direction opposite of what is pressed. Subjects had 7 seconds to move the cursor into the target to trigger the end of the trial. If they did not reach the target within the time limit, the trial automatically ended. Each trial was followed by a rest period where a fixation cross was displayed in the center of the screen for 1-2 seconds.

The purpose of this task is to elicit error-related potentials (ErrPs) in an environment like that of the BCI task. These potentials elicited immediately after witnessing the cursor move in an unexpected direction are used to create an ErrP classifier, which is used in the creation of confidence scores for BCI decoder adaptation (see the section “Confidence Score Generation”).

7.4.2.2 Motor screening

At the start of each session, subjects were presented with a stimulus presentation task where they were required to perform motor imagery (MI) of their hands. When presented with a left-pointing arrow, subjects imagined moving their left hand, and when presented with a right-pointing arrow, subjects imagined moving their right hand. Subjects were instructed to keep their hands separate and relaxed in a comfortable position as they employed one motor imagery strategy (e.g., imagined visualizing their hand moving, imagined the sensation of the finger tips hitting the palm, imagined

wiggling their fingers, etc.). Each arrow was displayed on the screen for 4 seconds, followed by a 1-2 second rest period where a fixation cross was displayed at the center of the screen. The motor screening task consisted of 100 trials, evenly split between left MI and right MI trials.

Three subjects (indicated by the * in Table 9) were shown a box moving to the left or right in discrete steps instead of a static arrow pointing left or right. These subjects were instructed to imagine they were moving the cursor left with their left hand or imagine moving the cursor right with their right hand.

The purpose of this task was to collect data to train the MI classifier used to control the cursor movement in the BCI task. This MI classifier, which we will refer to as the BCI decoder, is a Multi-layer Perceptron (MLP) shallow artificial neural network with a constant learning rate, and additional model parameters determined through a cross-validation grid search (more detail in Model Validation). The model input is in the form of a 4 x m array where each example consists of 4 features – the alpha (8-12 Hz) and beta (13-30 Hz) spectral density in channels C3 and C4 – and where m represents the number of examples used as input into the model. These features were extracted by first, bandpass filtering the data from 7-31 Hz, and then taking the sum of the spectral density of frequencies falling within each respective range via the SciPy Welch method (Welch, 1967) of estimating power spectral density. The examples are shuffled prior to training and are scaled to have zero mean and unit variance.

Model validation

To prevent over- or under-fitting, model parameters were determined using the Sci-kit Learn grid search cross validation with 5 K-fold splits on the shuffled examples. For the Multi-layer Perceptron, the grid search was performed over activation functions, alphas, and solvers (Table 10).

Parameter	Value Space
Activation Function	‘relu’, ‘tanh’
Alpha	[1e-6, 1e-5, 1e-4, 1e-3, 1e-2, 1e-1, 1e0, 1e+1, 1e+2, 1e+3] (np.logspace(-6,3,10))
Solver	‘lbfgs’, ’sgd’

Table 10. Multi-layer Perceptron Model Parameters and Values.

After the grid search determined the optimal parameters for generalizing to the data, we split the examples into 70% training and 30% testing and generated Receiver-Operating Characteristic (ROC) curves and learning curves (Figure 28). These plots were used to check performance of this model trained on motor screening data.

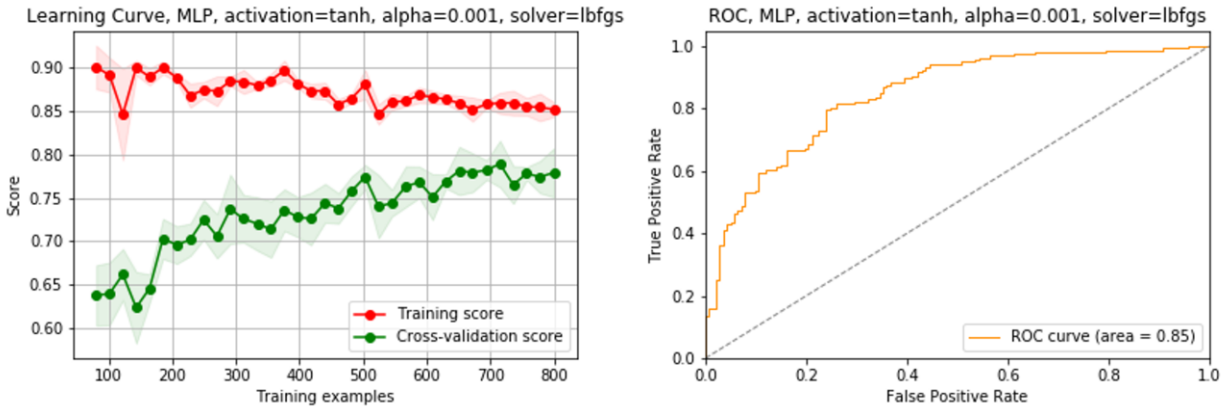

Figure 28. Model Validation Example. Initial model performance was evaluated by observing the learning curve (left) and the Receiver-Operating Characteristic curve (right). These example plots are for the motor imagery classifier for subject 1e8b34, session 3.

The same model was then re-fit to include all the motor screening examples (training and testing data combined) and saved for use in the following BCI run.

7.4.2.3 The BCI task

Similar to the error screening task, subjects attempted to move a cursor into a target placed either to the left or to the right of the center starting position in each trial. To move the cursor, subjects performed motor imagery of their left hand to move the cursor left, or of their right hand to move the cursor right. Every 2 seconds, the cursor would move one step either to the left or to the right based on 1750 ms of EEG data collected starting 2 seconds prior. The 1750 ms of data was processed into alpha (8-12 Hz) and beta (13-30 Hz) spectral density in channels C3 and C4 as described in the Motor

Screening description above, yielding four features that are fed into the MI classifier built from the Motor Screening task. These four features were scaled by subtracting by the mean of and dividing by the standard deviation of the pre-scaled training examples which were used to train the decoder.

In all 12 trials, subjects have 20 seconds to reach the target. If the cursor reached the target before 20 seconds had passed, the trial would end early. Once the trial ends, a fixation cross was displayed on the screen for a rest period of 2 seconds (with jitter). The trials were evenly split between having the target placed on the left or on the right.

This BCI task was then repeated 4 more times for a total of 5 runs per session. Subjects in Group 1 used the same decoder throughout all 5 runs, whereas subjects in Group 2 had the decoder adapted between each BCI run (Figure 29).

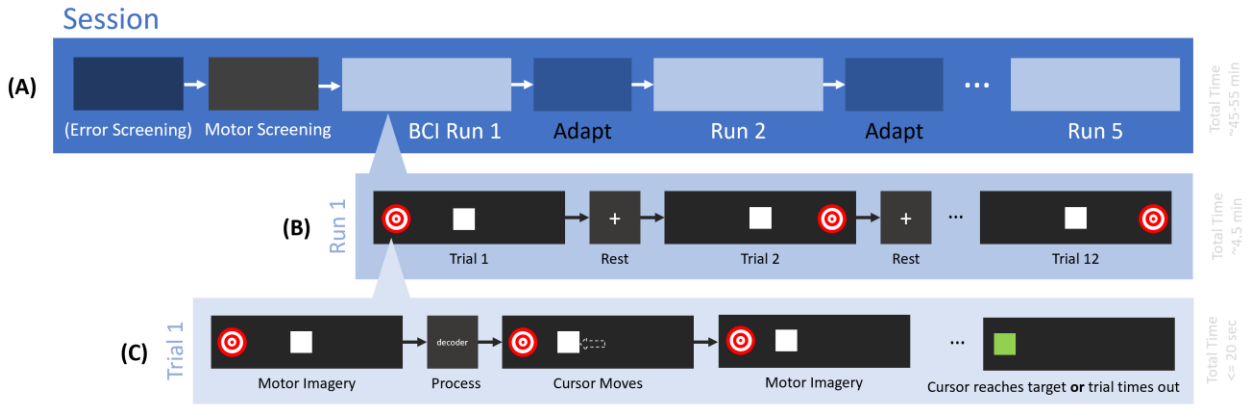

Figure 29. Experimental Paradigm. (A) The 1-D BCI task is run multiple times within each session, with decoder adaptation being applied between runs for subjects in Group 2 (adaptation). **(B)** Each run contains multiple trials that are separated by short rest periods lasting 1-2 seconds. For each trial, the subject attempts to move the cursor to collide with a target randomly placed on the left or the right. The trial will end once the cursor hits the target or once 20 seconds have passed, whichever comes first. **(C)** In each trial, the subject imagines moving their left or right hand to move the cursor one step closer to the target. The cursor moves one step every 2 seconds. Cursor movement direction is determined through a decoder which uses the data collected during motor imagery.

7.4.3 Decoder adaptation

In this investigation, we were interested in investigating the effects of BCI co-adaptation on BCI learning. For all subjects, the decoder (MI classifier) used in BCI run 1 was created using the data from the motor screening task from that session. Subjects in Group 1 performed the BCI task without any decoder adaptation within sessions. Subjects in Group 2, however, used an adaptive BCI decoder which would update between runs. We would adapt this decoder by loading the most recent MI classifier and

retrain it using epochs of data from the most recent BCI run with high “confidence scores”, in addition to all the previous data used to train prior versions of the decoder in the session. These epochs were periods of MI control during the most recent BCI run, lasting 1750 ms each (Figure 30). An epoch would have a high confidence score if we did not detect an error potential following visual feedback of the resultant cursor movement from the MI and if the subject was focused (more detail below).

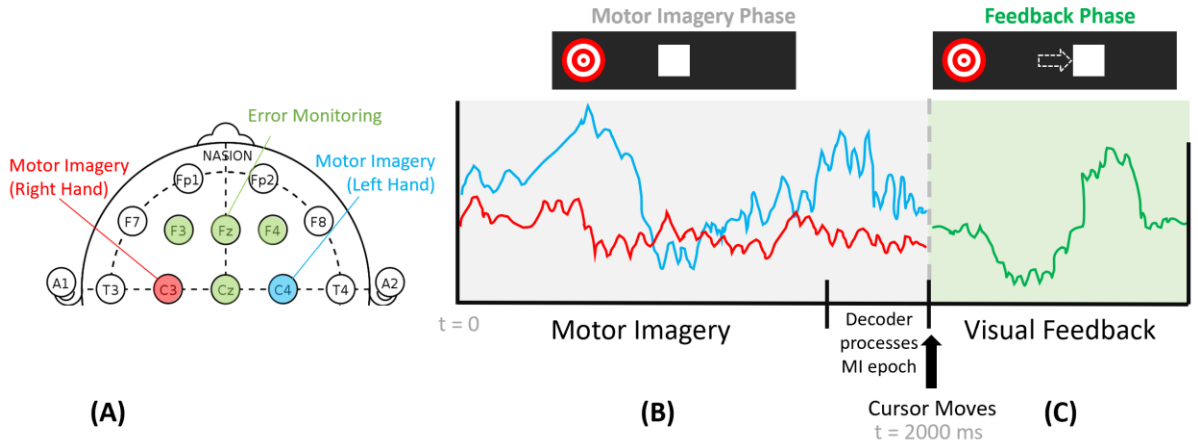

Figure 30. BCI Control and Performance Feedback in a Single Movement. The cursor moves one step left or right every 2 seconds. Cursor movements continue until the cursor hits the target or the trial times out (see **Figure 29**). Note, the waveforms in this figure were drawn as examples and do not represent actual data. **(A)** The colors of the channels correspond with the example waveforms in (B) and in (C). **(B)** Data from channels C3 and C4 are used to measure motor imagery and are fed into the decoder to determine cursor movement direction. The cursor moves in the determined direction 2000 ms after the motor imagery phase begun. **(C)** Data from all frontal channels available and Cz are used to capture any error-related potentials that may rise when the cursor moves in the direction away from the target position. Data from this feedback phase are not used in live control of the BCI, but are used in decoder adaptation between runs.

7.4.3.1 Confidence Score generation

Confidence scores (CS) were generated using measures of error and attention. Error was estimated by determining if an error-related potential (ErrP) was present during visual feedback immediately following the movement of the MI-controlled box. Attention was estimated by observing beta band power during motor imagery control in the central parietal channel, Pz, a corollary for Default Mode Network activity (Jann et al., 2010). More detail on confidence score calculation is provided below.

Error-related potentials

Error-related potentials (ErrPs) were detected using one of two methods. Both methods used data from all available channels recorded during the Error Screening task.

Method 1: Time domain template projection

To detect ErrPs in the time domain, we performed a template projection technique inspired by Miller et al. (2015). We first organized EEG voltage signals (bandpass filtered 1-40 Hz) into 600 ms epochs normalized to the data 700 to 100 ms prior to the start of the epoch, where t=0 is when the box moved one step in the Error Screening task. We then generated error potential templates by averaging all epochs where the box moved in the direction away from the target in the trial, and generated correct performance templates by averaging all epochs where the box moved in the direction towards the target in the trial (Figure 31).

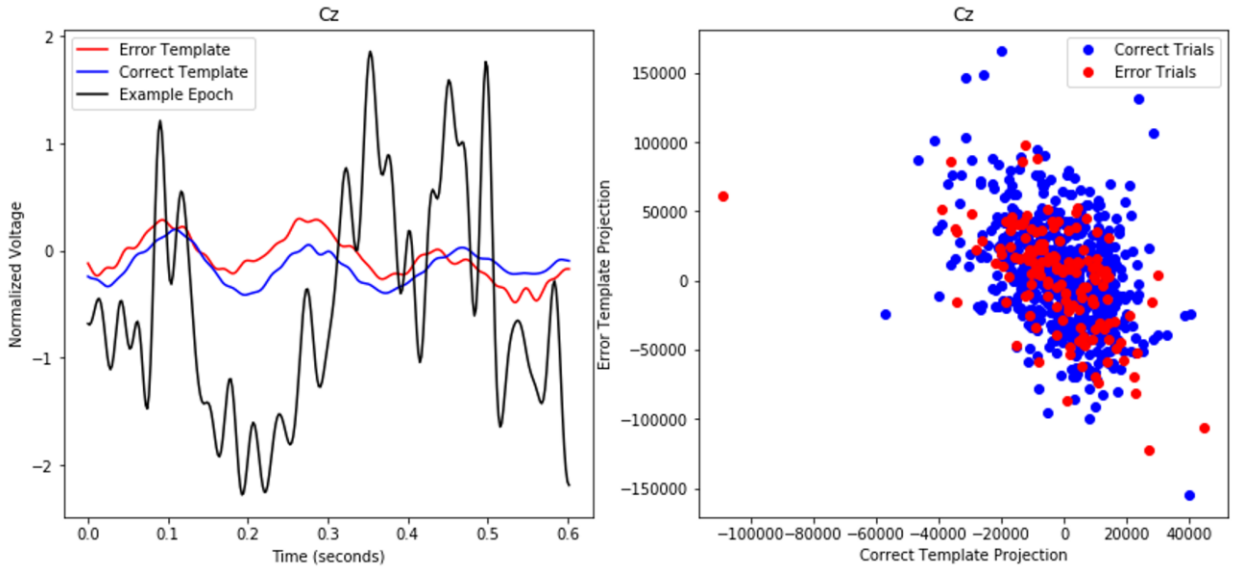

Figure 31. ErrP Template Projection in a Single Channel. (Left) Individual 600 ms epochs were compared against the templates generated for the error and correct conditions. For each epoch in every channel, we calculated how similar the waveform was to the error template and to the correct template. Example data pairs for channel Cz are shown to the (right). Note that data from all frontal channels and Cz were used as features in the error classifier.

We then generated features based on how similar each epoch was to the error template and to the correct template. Similarity between epochs and templates were estimated by convolving the epochs with each respective template and summing the results to return a single scalar value representing similarity for each template. Because templates were created by averaging all epochs of the given condition together, the overall amplitude of the templates was generally smaller than that of an individual epoch. Both templates were scaled to match the normalized voltage range of each epoch by subtracting the mean of the error template and dividing by the standard deviation of the error

template. We scale both templates using the mean and standard deviation of the error template, instead of to their own mean and standard deviation values respectively, as to preserve any magnitude difference between the error and correct templates.

The similarity values to the correct and error templates for each channel were used as input features in a shallow artificial neural network, with the same architecture as the model used for motor imagery classification. The model parameters were also determined using the same methods as described for the BCI decoder (MI classifier). Individual example epochs were labeled as not having error (y=0) if the epoch was associated with box movement in the correct direction towards the target. Epochs were labeled as having error (y=1) if the associated box movement went in the direction away from the target.

After the model and templates were created using the Error Screening task, we estimated the presence of ErrPs during each BCI run by organizing the BCI epochs, creating features based on the pre-loaded templates, and feeding the new projections into the model.

Method 2: Frequency domain power

To detect ErrPs in the frequency domain, we observed spectral density in both the delta (<4 Hz) and theta (4-7 Hz) bands in the 600 ms of data (bandpass filtered 1-40 Hz) immediately following the movement of the box in the Error Screening task. Like with Method 1, the 600 ms epochs were normalized to the data 700 to 100 ms prior to the start of the movement onset (t=0). Spectral density for both bands were calculated using the Welch method as described in the Motor Screening methods.

The spectral density in both the delta and theta bands for all channels were used as input features in a shallow artificial neural network, as described in Method 1: Time Domain Template Projection.

Performance of the error classification model using Method 1 and Method 2 was comparable. We decided to use Method 2 (frequency domain) for the study due to its marginally better performance on an initial test dataset.

Attention

Attention was estimated using a measure of beta band (13-30 Hz) spectral density in our parietal channel, Pz, which is believed to coincide with Default Mode Network (DMN) activity (Jann et al., 2010). High beta band activity may be indicative of high DMN activity, suggesting lower attention on the task at hand. Epochs were marked as occurring during low attention if the beta value in Pz was above a threshold set by using data collected during rest periods (Figure 32). Specifically, the threshold was created by subtracting two standard deviations from the mean of the beta density in Pz during all inter-trial intervals within an individual run.

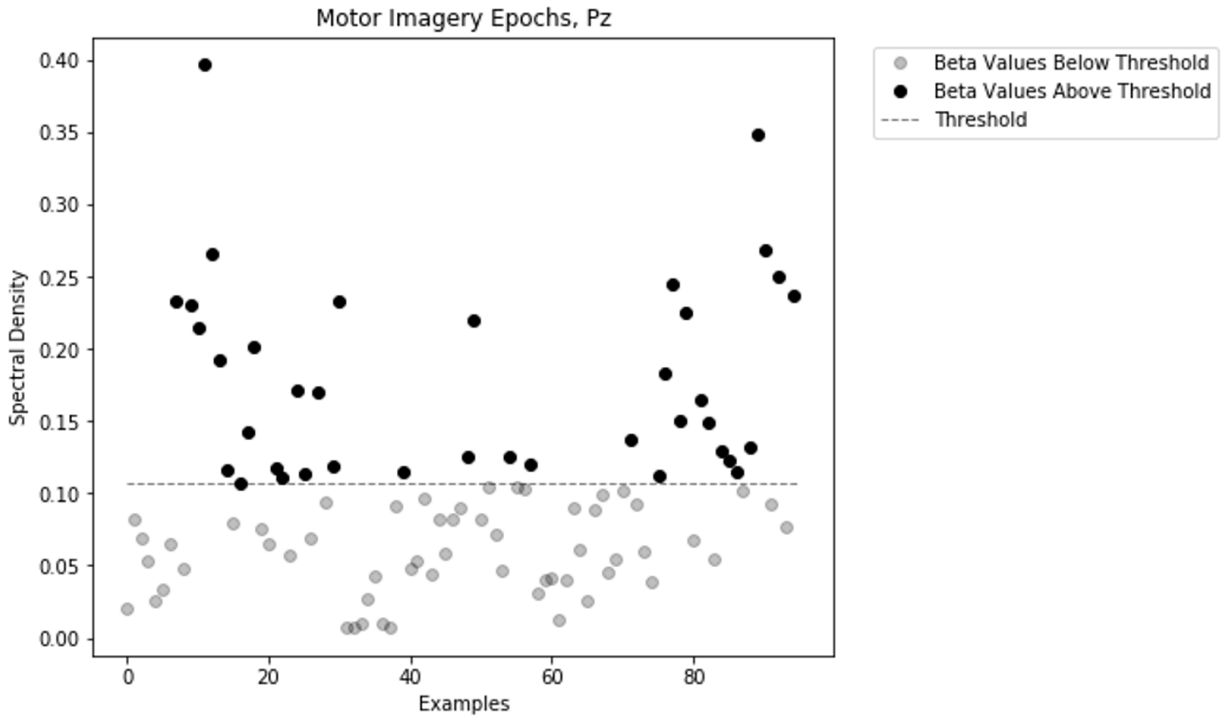

Figure 32. Example of Parietal Beta in a BCI Run. Spectral density in the beta band in Pz was calculated for all motor imagery epochs used to execute movement in the BCI task. Epochs are represented by single dots in this plot. Epochs with beta spectral density above the threshold indicate likely high Default Mode Network activity and low attention. The threshold is two standard deviations below the mean of the beta spectral density during the rest periods in the run.

The scoring formula

To generate "confidence scores", representing how confident we are on epochs being associated with correct BCI performance, we combined the output of the error classification model with our above or below threshold Pz beta value. We combined the values using the following formula:

$$CS = \frac{(P(E') - P(E) + 1) - w_a d_{threshold}}{2} \quad (6)$$

Where CS = Confidence Score, CS_{scaled} = Confidence Score (scaled), P(E) = Probability of an ErrP being present for this example based on the error classifier output, P(E') = Probability of an ErrP **not** being present for this example based on the error classifier output, w_a = weight for attention (a value from 0 to 1), and $d_{threshold}$ = normalized distance of the example's Pz beta value from the beta value threshold.

Depending on the distance values and the assigned weight, the values could go slightly above 1 and slightly below 0. We scale the confidence scores (pre-normalized) such that the minimum is 0 and the maximum is 1 by subtracting by the minimum and dividing by the range using the following formula:

$$CS_{scaled} = \frac{CS - min(CS)}{max(CS) - min(CS)} \quad (7)$$

Where the range of values for CS_{scaled} is [0, 1]. Confidence Scores using just error potential information, using both error and attention (pre-scaled), and using both error and attention (scaled) are presented in Figure 33.

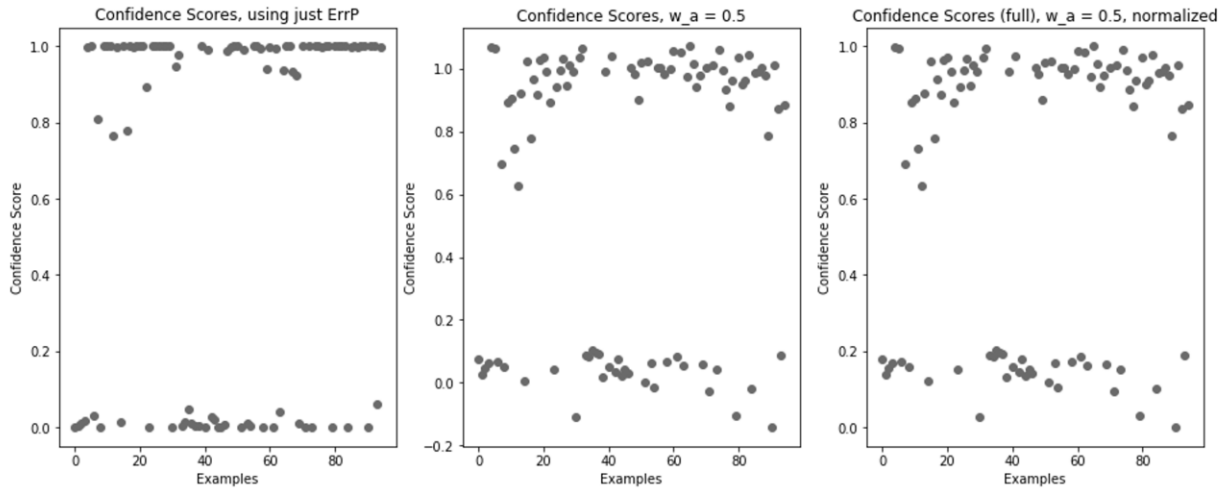

Figure 33. Confidence Score Normalization. (Left) Using just error classifier output, and no attention information, the confidence score values tend to be either very close to 0 or to 1. **(Middle)** If we add in attention information, the confidence scores spread further but may go below 0 or above 1. **(Right)** By scaling the confidence scores using both error and attention, we are able to create confidence scores ranging from 0 to 1, where 1 indicates higher confidence in epoch being associated with correct behavior.

During decoder adaptation, models would be retrained using the data previously used to train the model in addition to the most recent BCI run epochs with confidence scores above a set threshold (default threshold set to 0.7). Epochs below the threshold were excluded in classifier re-fitting.

7.4.4 Simulated adaptation

Because roughly half of the subjects experienced BCI decoder co-adaptation during their sessions and the other half did not, we also simulated how subject performance may have been had they been placed in the group with the other adaptation type.

For subjects in Group 1 (no adaptation), performance was simulated by performing offline adaptation of the motor imagery classifier (BCI decoder) between each BCI run, and then running the BCI task using their pre-recorded EEG data and the newly adapted model for each run. Because this method uses pre-recorded EEG, it is important to clarify that this results in a simulated one-way adaptation of the decoder, and not in co-adaptation between the decoder and the subject.

For subjects in Group 2 (co-adaptation), performance was simulated by running each BCI task using their pre-recorded EEG data with only the initial motor imagery classifier, which was created using the motor screening data from that session.

We also simulate true label adaptation for all subjects, regardless of if they were in Group 1 or in Group 2. The true label adaptation is identical to the confidence score-based adaptation, except that instead of using confidence scores generated on estimates of error and attention, we use task behavioral data. Epochs that were associated with movement towards the target were assigned confidence score values of 1 and epochs that moved away from the target were assigned confidence score values of 0.

7.4.4.1 Simulating Study 1 subject performance

For subjects in Study 1, their performance may have been hampered by a bug in the BCI code. Specifically, the order of features fed into the BCI decoder did not match the order of features used in creating and adapting the decoder for subjects in Study 1. To salvage the data, we simulated how well the subjects may have done had the order of features in the BCI matched the order used in decoder creation and adaptation. Analysis including subjects from Study 1 use the simulated performance data instead of the original performance data resultant of this bug.

7.4.5 Statistical analysis

In order to test the effects of adaptation scheme (no adaptation, co-adaptation, or simulated true label adaptation) on subject performance and learning, we fit the performance data to a few different linear models. We then followed each model fitting with an ANOVA. For any statistically significant main effect results from the ANOVAs, we ran post hoc unpaired t-tests to better understand the effect.

To test the overall effect of adaptation scheme (no adaptation, co-adaptation, or simulated true label adaptation) on subject performance, we fit a Linear Mixed Effects model using the following equation.

$$Score \sim AdaptationScheme + (SessionNumber * RunNumber) + (1|Subject) \quad (8)$$

To test the effect of adaptation scheme on learning within sessions, we fit a Linear Mixed Effects model using the following equation:

$$Score \sim AdaptationScheme + RunNumber + (AdaptationScheme * RunNumber) + (1|SessionNumber) + (1|Subject) \quad (9)$$

To test the effect of adaptation scheme on learning between sessions, we fit a Linear Mixed Effects model using the following equation:

$$Score \sim AdaptationScheme + SessionNumber + (AdaptationScheme * SessionNumber) + (1|RunNumber) + (1|Subject) \quad (10)$$

7.5 Results

In this section, we confirm the presence of informative EEG signals and present our findings regarding the effect of adaptation scheme on subject performance and learning.

7.5.1 Verifying the classifiers

7.5.1.1 Motor imagery classification

For each subject, motor imagery (MI) was classified using four signal features: alpha (8-12 Hz) power in C3, beta (13-30 Hz) power in C3, alpha power in C4, and beta power in C4. As seen earlier in Figure 28, our MI classifiers (BCI decoders) were able to accurately predict the direction of intended cursor

movement near 80% in the motor screening data. We selected these specific features because Event-related Desynchronization (ERD) is known to occur in the mu band (8-13 Hz) during overt movements and motor imagery in trained individuals (Pfurtscheller and Lopes da Silva, 1999). However, the exact frequency range varies from subject to subject and often extends to upper beta, hence the inclusion of both alpha and beta (Blankertz et al., 2010). C3 and C4 are commonly used to measure primary motor cortex activity due to right limb and left limb movement in EEG, respectively (Blankertz et al., 2010; Pfurtscheller and Lopes da Silva, 1999; Wolpaw and McFarland, 2004).

Figure 34 shows an example of ERD for right hand MI in channel C3 and for left hand MI in channel C4, where we see a decrease in spectral density during MI relative to rest in high beta ranges (highlighted gray).

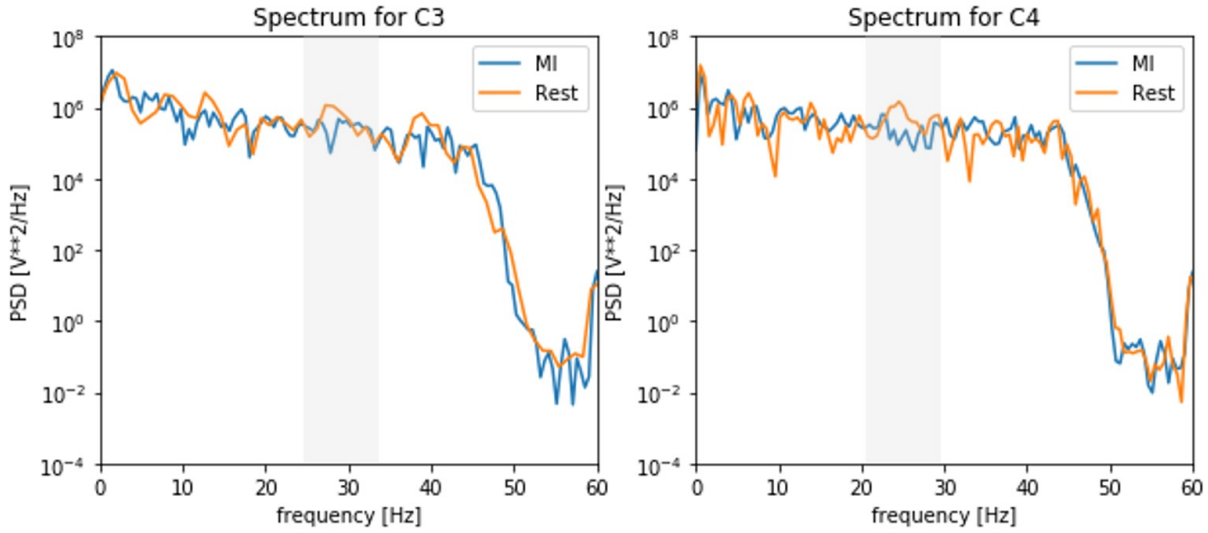

Figure 34. Event-related Desynchronization with motor imagery. In one subject, spectral density around the upper limits of the beta band (13-30 Hz) decreases during motor imagery (MI) as compared to during rest. The left shows this change in power due to Event-related Desynchronization (ERD) in channel C3 during right hand MI, and the right shows this change in power due to ERD in channel C4 during left hand MI.

7.5.1.2 Error-related potential classification

For subjects who performed the BCI task with adaptation between runs, we created an error classifier using either (1) delta and theta power or (2) measures of how well an individual epoch fit a grand-average error template or a grand-average correct template (Figure 31) as features. This error classifier was used in the generation of confidence scores, as described previously in the methods.

From visual inspection of the EEG spectrum, it can be difficult to identify if an individual epoch, extracted during visual feedback, was associated with correct behavior or with error (Figure 35). The EEG error literature states that power in the delta and theta band in centro-midline channels should increase in the presence of error (Spüler and Niethammer, 2015).

Because we do not see this robustly, we use data from all frontal channels and Cz, and not just from a single channel, to create features for our error classifier.

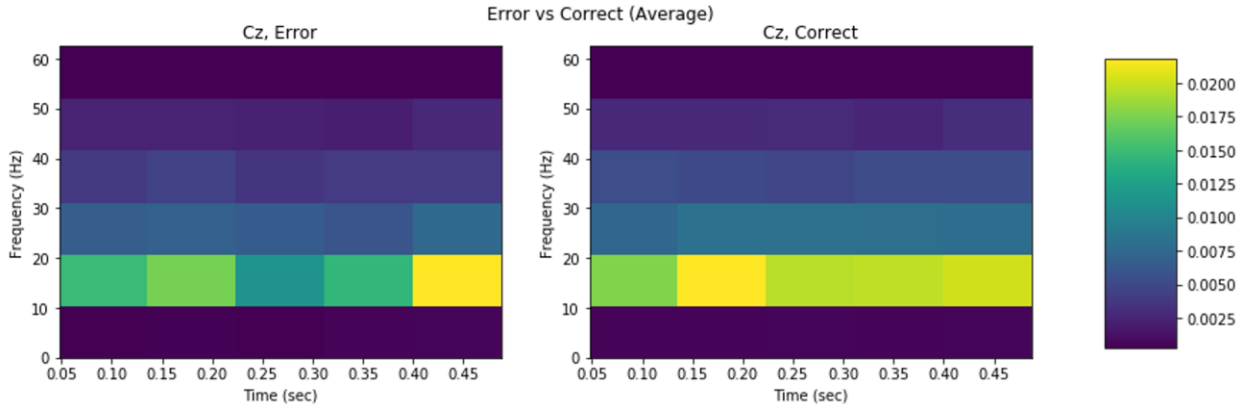

Figure 35. Average Spectral Response to Error and Correct in One Subject. From the motor screening task, we create features based on either delta and theta spectral power, or on how well individual epochs match error and correct templates. The average response in a single channel (Cz) is shown here, with limited frequency resolution for plotting.

7.5.1.3 Confidence Score accuracy

To evaluate how well we were able to predict subject performance using error-related potentials and attention, we compared our confidence scores (CS) to the true labels (TL) obtained through task behavioral data. As a reminder, confidence scores are used to determine which epochs of in-task motor imagery are included in decoder adaptation between runs.

We generated a confidence score for each cursor movement resultant of motor imagery, in each run. Our confidence scores ranged in value from 0 to 1, where 1 indicates high confidence that the box controlled by the subject moved correctly towards the target. These same movements were assigned TL values of either 0 or 1 depending on if they moved away from or towards the target, respectively.

As seen in Figure 36, our confidence scores (thresholded such that values greater than or equal to 0.7 were rounded up to 1, and values below 0.7 were rounded down to zero) matched the true labels

approximately 62% of the time for erroneous movements away from the target, and matched the true labels approximately 38% of the time for correct movements towards the target. Our confidence score calculations were more likely to assign lower values to movements, leading to less epochs exceeding the CS threshold, leading to less epochs being included in retraining of the BCI decoder between runs.

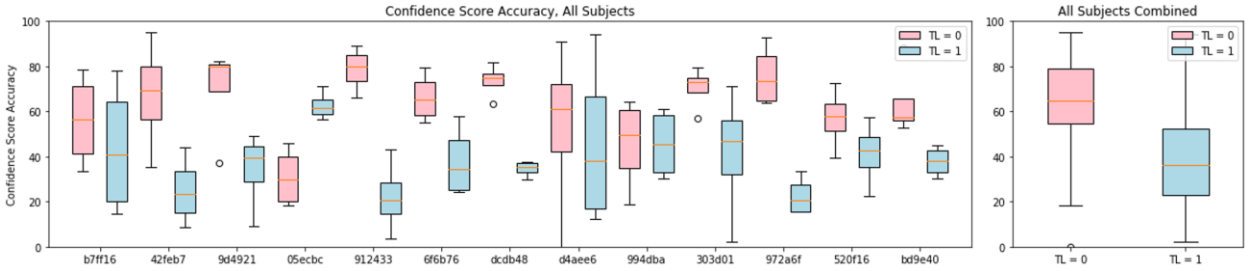

Figure 36. Confidence Score Accuracy. How well Confidence Scores (CS) matched the True Labels (TL) for each Group 2 (co-adaptation) subject (left). Pink boxes represent what percentage of CS during TL = 0 movements fall below the threshold and are excluded from decoder adaptation. Blue boxes represent what percentage of CS during TL = 1 movements meet or exceed the threshold and are included in decoder adaptation. The box plots to the right show the mean accuracy across all Group 2 subjects.

7.5.2 Subject performance

Although all subjects participated in three sessions with five BCI runs per session, no subjects achieved performance above 70% for any run. Table 11 shows each subject's overall performance per session, averaged across all five funs within each session. As a reminder, subject performance was measured by dividing the number of correct movements towards the target by the total number of movements.

			Performance (%)			
Subject ID	Study #	Group #	Session 1	Session 2	Session 3	Overall
b12a46	1	1	54.00	55.05	41.60	50.22
41d8ff	1	1	44.23	53.23	48.69	48.72
1e8b34	1	1	44.81	49.82	43.36	46.00
ad11cf	1	1	45.23	57.45	51.56	51.41
af9af3	1	1	47.05	46.83	41.43	45.10
c795d2	1	1	48.73	49.23	44.73	47.56
97e442	1	1	-	-	-	-
5ea9e5	1	1	56.21	54.18	43.32	51.24
e2cbc4*	1	1	48.01	47.65	44.57	46.74
b7ff16	1	2	50.52	53.95	48.25	50.91
42feb7*	1	2	48.60	49.59	50.99	49.73
9d4921	1	2	49.59	47.13	50.77	49.16
05ecbc	1	2	47.82	51.60	47.63	49.02
912433	1	2	49.15	54.14	53.24	52.17
6f6b76	1	2	50.82	54.70	48.99	51.50
dcdb48	1	2	53.42	49.79	50.12	51.11
d4aee6	1	2	47.07	48.48	51.59	49.05
994dba	1	2	55.75	46.86	54.80	52.47
303d01*	1	2	49.73	50.24	43.14	47.71
a1e6c0	2	1	45.49	45.86	49.22	46.86

851238	2	1	43.72	44.96	48.35	45.68
c37099	2	1	43.04	50.00	46.51	46.52
972a6f	2	2	50.09	49.09	41.82	47.00
520f16	2	2	48.01	55.70	49.14	50.95
bd9e40	2	2	50.51	51.53	47.04	49.70
Average	-	-	**48.82**	**50.72**	**47.54**	**49.02**

Table 11. Average performance for each subject. Note, we excluded subject 97e442 from the analysis. All subjects with asterisks (*) performed the motor screening task by observing the moving box instead of seeing an arrow pointing left or right.

7.5.2.1 Qualitative observations

Observing mean performance per run for all subjects, we see that the overall performance for subjects in Group 2 (co-adaptation) tends to be higher than that for subjects in Group 1 (no adaptation) within most runs in all sessions, with the largest impact in Session 1 (Figure 37). For almost all runs, simulated true label adaptation seems to lead to greater performance than through no adaptation or co-adaptation. From Figure 37, it seems there may be learning within Session 1 for both subject groups.

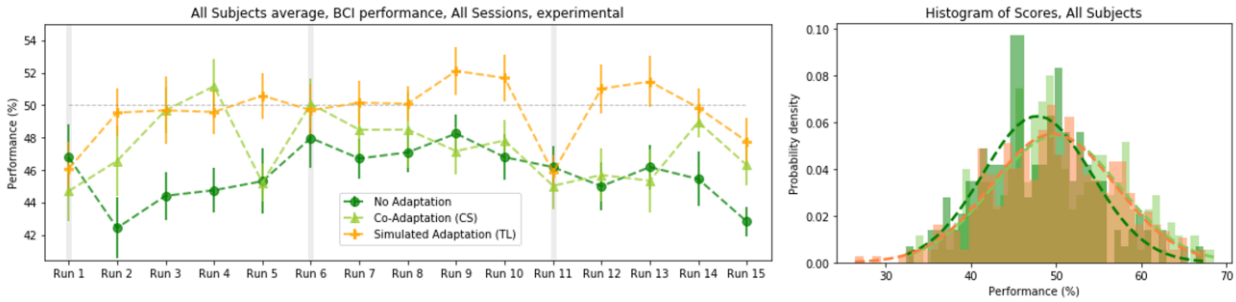

Figure 37. Average subject performance across all sessions. Overall, the average performance across subjects tended to be higher during simulated true label adaptation. Vertical lines at each point show the standard error of the mean. Gray vertical lines represent the first run within each of the three sessions.

Although not clearly present for all subjects, we do observe continuous improvement within a single session for subject 6f6b76 (Group 2, co-adaptation) (Figure 38). In Session 2, we see that the subject's performance continuously increases starting from the 2nd run in the session.

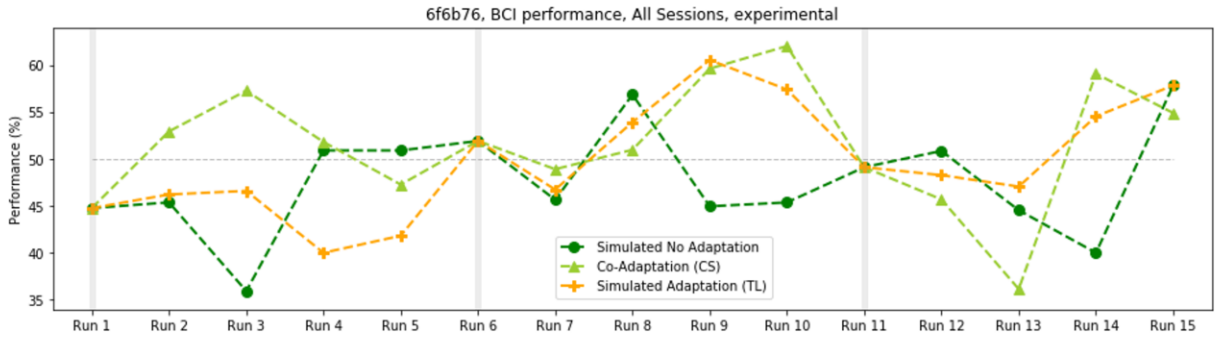

Figure 38. Recorded and simulated performance of 6f6b76 (Group 2). Recorded performance is displayed in light green, representing the performance resultant of co-adaptation. The dark green and orange lines show simulated performance for if the subject had been placed in Group 1 instead, and for true label adaptation, respectively.

7.5.3 Learning within sessions

To test if subjects were improving their BCI control over runs within sessions (learning within sessions), we fit the linear model described in Equation 9 to the data.

Running an ANOVA on this model, we do not see a statistically significant main effect from adaptation scheme ($F(2, 714) = 0.4076$, $p = 0.6654$), from run number ($F(1, 714) = 0.0967$, $p = 0.7559$), or from the interaction between adaptation scheme and run number ($F(2, 714) = 1.1904$, $p = 0.3047$).

7.5.4 Learning between sessions

To test if subjects were improving their BCI control between sessions (learning across sessions), we fit the linear model described in Equation 10 to the data.

Running an ANOVA on this model, we do not see a statistically significant main effect from adaptation scheme ($F(2, 714) = 0.6250$, $p = 0.5355$), from session number ($F(1, 714) = 1.3959$, $p = 0.2378$), or from the interaction between adaptation scheme and session number ($F(2, 714) = 0.6311$, $p = 0.5323$).

7.5.5 The overall effect of adaptation scheme on performance

To test if subject performance overall was affected by adaptation scheme, we fit the linear model described in Equation 8 to the data.

Through running an ANOVA on this data, we did see a statistically significant main effect from adaptation scheme ($F(2, 714) = 5.1720$, $p = 0.0059$). To further investigate how adaptation scheme affected performance, we conducted post hoc unpaired two-sample t-tests comparing the performance between the adaptation schemes. From these tests, we saw that the scores from both co-adaptation ($p = 0.0013$) and from simulated true label adaptation ($p = 0.0025$) were statistically significantly greater than the scores from no adaptation. Performance from simulated true label adaptation, however, was not statistically significantly greater than performance from co-adaptation ($p = 0.7095$).

From the ANOVA, we did not see a statistically significant main effect from session number ($F(1, 714) = 9.4374e\text{-}04$, $p = 0.9755$), from run number ($F(1, 714) = 1.1929$, $p = 0.2751$), or from the interaction between session number and run number ($F(1, 714) = 0.1606$, $p = 0.6887$).

7.6 Discussion

In this chapter, we have explored the implementation of a co-adaptive BCI based on performance monitoring signals using EEG. Here, we discuss the results of the statistical analyses, explore why subject performance was lower than desired, evaluate our adaptation scheme, and present future work which may lead to improved performance.

7.6.1 The effect of adaptation on overall performance

Although adaptation scheme does not seem to affect learning within or between sessions, it does have a statistically significant effect on overall performance. Co-adaptation using our generated Confidence Scores (CS) led to significantly higher performance overall for subjects in Group 2 (co-adaptation) as compared to subjects without any adaptation in Group 1. As expected, the scores from simulated true label (TL) adaptation were also significantly higher than those from runs without any adaptation (Group 1). This is encouraging as it suggests co-adaptation using performance monitoring signals, namely error-

related potentials and attention via Default Mode Network activity, can improve BCI performance without relying on kinematic or task-specific behavioral data.

7.6.2 The effect of adaptation on BCI Learning

Overall, the adaptation scheme did not have a statistically significant effect on how subjects learned to perform the BCI task within or across sessions. Regardless of whether subjects had or did not have decoder adaptation between runs, the rate at which their performance changed did not differ significantly. Although this suggests the adaptive decoders do not improve the rate of learning, we are hesitant to make this claim given how low subject performance was across the board.

Motor imagery (MI) based BCIs are known to be difficult to control and often require extensive training periods (Mondini et al., 2016; Vidaurre and Blankertz, 2010). For example, in seminal work by Wolpaw and McFarland (2004), subjects trained for 22-68 daily sessions, each session lasting approximately half an hour. In a more recent study by Mondini et al. (2016), subjects trained through six sessions, with two per day. Because the initial decoder for each session was trained just using the motor screening data from the session (100 trials, 50 for left MI and 50 for right MI) and not including data from any previous sessions, it is likely that subjects did not have ample time to train.

Other factors which may have led to low performance include but are not limited to (1) changes in signal or signal quality between runs, (2) waning motivation, and (3) possible “BCI illiteracy” for some portion of the subjects (Myrden and Chau, 2015; Vidaurre and Blankertz, 2010). Subjects were instructed to stay as still and relaxed as possible while performing the motor screening task and the BCI runs. However, they could stretch and adjust their seating position between runs. We would always wait until the impedance measures from the Neuroelectrics software would turn green for all channels before starting the next run, but it is possible that the dry electrodes may have shifted slightly between runs. It is also possible that subjects would evaluate their performance between runs and try to adopt new strategies, although we advised against it. Regardless of if subjects were consciously adopting new strategies or not, subconscious changes in neural populations responsible for the EEG signal output may have occurred continuously throughout and between runs (Green and Kalaska, 2011;

Mizuguchi and Kanosue, 2017). In addition, because subjects were experiencing difficulty controlling the box movement in the BCI, subjects may have been discouraged and would have decreased motivation as their performance continued to not improve. A few subjects verbally expressed their discouragement during their sessions. Although work by Myrden and Chau (2015) suggests that increased frustration can lead to better performance, most likely due to increased attention, earlier work by D'Mello and Graesser (2012) suggests high frustration can conversely increase boredom, reduce attention, and lead to poorer performance. Some subjects also expressed being slightly fatigued by performing the BCI multiple times, which may have affected performance negatively (Talukdar et al., 2019). Lastly, motor imagery as a control signal might not be conducive to BCI control for some portion of the subjects. As explored in work by Myrden and Chau (2015), other mental strategies may work better for some individuals, including music imagery and word generation.

7.6.3 Efficacy of co-adaptive systems

Like other adaptive BCI, our confidence score based co-adaptive system may help improve BCI performance (Faller et al., 2014; Iturrate et al., 2015; Margaux et al., 2012; Myrden and Chau, 2016; Rozado et al., 2015; Spüler et al., 2012b; Vidaurre and Blankertz, 2010; Vidaurre et al., 2006). However, unlike in most other systems, our co-adaptation is based on non-control EEG signal, and not on task behavioral or kinematic data. Reliance on task-specific cues or on behavioral data would drastically limit the capabilities of future BCI which may allow control for various tasks and function in various contexts. If we instead use performance monitoring signals already present in the brain signals being recorded, we can provide feedback to the decoder using the BCI user's own subconscious evaluations of performance.

Previous work by other investigators on adaptive systems using just error-related potentials or just estimates of performance using mental state (i.e., measure of attention, frustration, and fatigue) agree with our finding. An error-related potential-based adaptive decoder used in a code-modulated visual evoked potential (c-VEP) BCI by Spüler et al. (2012a) increased control accuracy across subjects, with an improvement of up to 4% in a single subject. In a maze navigation BCI, adaptation based on

performance estimation using mental state increased performance overall for most subjects and led to an improvement of 2.4% in one subject (Myrden and Chau, 2016).

In their mental state-based adaptation study, Myrden and Chau (2016) report difficulty in accurately estimating performance using just their measures of mental state, with a balanced accuracy measure of about 54%. Using both error-related potentials and our estimation of user attention through parietal beta power, our confidence scores were overall 50% accurate, with 62% accuracy for predicting erroneous behavior and 38% accuracy for predicting correct performance (Figure 36). Although this overall performance may seem low, it results in a greater amount of false negatives, meaning that less data is added to the training set for each decoder adaptation. In an error-based adaptive EEG BCI, it was found that error detection did not need to perform particularly well in order to positively affect performance through adaptation (Iturrate et al., 2015). In their system, Iturrate et al. (2015) found it was sufficient for their error-related potential decoder just to perform better than chance. In our study, we see that confidence score-based adaptation can improve BCI performance even with a performance estimation accuracy of approximately 50% overall.

7.6.4 Future work

Although we were able to demonstrate an improvement in overall BCI performance using our confidence score-based co-adaptation, future work may be done to better allow subjects to gain proficient control of the BCI. In future iterations of this experiment, we would hope for subjects to consistently achieve at least 70% performance to demonstrate that they have learned to control the BCI. Changes that may be made to the system to possibly improve control include but are not limited to (1) increasing training time, (2) using data from previous sessions in training the decoder, (3) changing the amount of time allowed for motor imagery, (4) allowing for different mental strategies for control, (5) adjusting the frequency band(s) of control per individual subject, and (6) using spatial filters on the EEG data before feature extraction for the BCI decoder.

As mentioned earlier in this discussion, it is common for subjects to spend a significant amount of time training motor imagery before controlling a motor imagery-based BCI (Mondini et al., 2016; Vidaurre

and Blankertz, 2010; Wolpaw and McFarland, 2004). In this experiment, subjects trained for approximately 10 minutes via the motor screening task before their first attempt at controlling the BCI. If we increase the training period in the first session and carry over data from previous sessions into all sessions after session 1, we may see better motor imagery classification from the BCI decoder. Another way to possibly keep the training period to a minimum is to introduce feedback during training. Feedback could be provided visually or through auditory cues based on the strength of event-related desynchronization in the alpha or beta band.

Interestingly, the amount of time allowed for motor imagery can change the strength of event-related desynchronization (ERD) and event-related synchronization (ERS) (Jeon et al., 2011). In work by Jeon et al. (2011), it was found that brief motor imagery led to greater pre-movement ERD than continuous motor imagery, and continuous motor imagery led to greater post-movement ERS. In our task, subjects performed motor imagery continuously for 2 seconds (1.75 seconds of which were used for classification) before movement would occur. However, in the motor screening task, subjects would continuously perform motor imagery for 4 seconds as they observed an arrow pointing to the direction of the hand they should perform motor imagery for, or as they observed a box moving left or right for four seconds for three subjects. The EEG from these 4 second motor screening trials were divided using a sliding window of 1.75 second length. These 1.75 second windows from the motor screening task were used to train the motor imagery classifier (BCI decoder). If 4 seconds of motor imagery is considered continuous, the strength of ERD/ERS may have changed between the 1.75 second windows extracted from the 4 second trials. This possible inconsistency in ERD/ERS between training examples may have hampered decoder performance. To address this, future iterations of this experiment should ensure the length of EEG for decoder training examples and online classification epochs match.

In addition to changing training time and timing of training epochs, changing the control strategy may benefit many subjects. In an EEG BCI study by Myrden and Chau (2016), subjects were able to choose the mental strategy they wanted to use to control the BCI. All subjects in their study trained using motor imagery, mental arithmetic, music imagery, and word generation to control the BCI prior to selecting which strategy they would use in the test sessions. Of all eleven subjects, only two selected

motor imagery as their control strategy for the test sessions. If we trained our subjects with multiple mental strategies, it is likely that the majority would select a strategy other than motor imagery, which may allow for greater performance and possible task mastery.

Our BCI decoder used change in spectral density in both the alpha and beta bands for all subjects to classify motor imagery, however, the optimal features for classification may vary per subject. As reviewed in Malan and Sharma (2019), EEG signals for BCI control often undergo spatial filtering or wrapper methods to select which features to use for control. A common spatial filtering technique applied to EEG data is the Common Spatial Pattern (CSP) algorithm, which results in greater signal-to-noise ratio and allows for more robust ERD/ERS detection (Blankertz et al., 2008b; Fukunaga, 1990). Note that we decided to use the same four features across all four subjects to allow for further investigation on the generalizability of our system, as described in the following chapter.

7.7 Conclusion

In this chapter, we discussed our novel co-adaptive BCI which selectively retrains the decoder using performance estimates via error-related potentials and attention. Although subject performance over multiple sessions did not reflect learning or mastery of the BCI, our adaptation did help increase overall subject performance. In the next chapter, we discuss the possibility of transfer learning and creating a general model to work with this BCI such that new users may achieve greater than chance performance on their first attempt of control without any training.

8. Transfer learning for first time BCI users

8.1 Motivation

First-time users of Brain-Computer Interfaces often undergo extensive training periods before they are able to operate the BCI. These repeated, and often-times lengthy, training sessions can exhaust the subjects before they even attempt to use the BCI. In addition, long training periods may discourage individuals who would benefit from BCI technology from deciding to obtain a BCI. Building upon the work from Chapter 7, in this chapter we investigate if it is possible to allow BCI-naïve users to control a BCI without any training at a performance level comparable to what we would expect with training.

8.2 Introduction

Advancements in various fields have recently rekindled interest in deep learning and advanced machine learning applications to Brain-Computer Interfaces (Dai et al., 2019; Majidov and Whangbo, 2019; Schirrmeister et al., 2017; Tabar and Halici, 2017). One principle that has revolutionized deep learning is the concept of transfer learning. Transfer learning can broadly be defined as the use of data from one domain or group in training a model that ultimately is used on a different dataset (Pan and Yang, 2010). In the case of BCI, transfer learning can be thought of as (1) using data from previous BCI users to train a general model for a particular task or (2) using data from previous sessions recorded from the individual of interest. Within the last year, researchers have begun to explore the methods and applications of transfer learning in EEG BCI (Dai et al., 2018; Fahimi et al., 2019; Hossain et al., 2018; Zanini et al., 2018). By creating a general model, we may allow first time BCI users to operate the BCI without any extensive training. Our investigation is the first to attempt transfer learning with simple features based on spectral density within central motor EEG channels.

In the work presented in this chapter, we created a general model trained on features from the highest performance BCI run of all subjects (excluding the respective subjects of interest) and simulated each subjects of interest's first BCI session performance.

8.3 Methods

8.3.1 Data acquisition

The data used for this transfer learning experiment were collected as part of an EEG BCI experiment focusing on testing the effects of adaptation scheme on BCI performance, as described in Chapter 7. Instead of collecting data from new subjects to test transfer learning, we instead opted to simulate the transfer learning for each subject in this dataset.

8.3.2 Subjects

The dataset contained EEG, motor imagery classifiers, error classifiers, and performance data for healthy subjects (n = 25, 12 male, mean age 23 years old). EEG data were collected through a Neuroelectrics Enobio 8-channel dry electrode EEG system. For more detail, please refer to Chapter 7 methods.

8.3.3 Experimental design

Subjects performed a one-dimensional center-out BCI task where they would attempt to control the direction of movement for a virtual box through motor imagery to reach a target. Subjects would attend three separate sessions, each consisting of a motor screening task and five runs of the BCI. The motor screening task data were used to create the initial motor imagery classifier (BCI decoder) for each session. All subjects also performed an error screening task in Session 1 to create an error classifier.

Half of the subjects were placed in Group 1, where they would use the decoder created from the motor screening data throughout their entire session. The other half, who were placed in Group 2, had their BCI decoder adapted between runs using data from the previous BCI run.

For more detail, please refer to Chapter 7.

8.3.4 General Model creation

Prior to simulating transfer learning for a given subject, we created a general BCI decoder trained on data from the best run of each subject, excluding the subject of interest. Specifically, the data were the scaled training examples used to fit the loaded models. The best run was defined as the run with the highest percentage of movements in the correct direction towards the target, per subject. Each training example was a 4x1 array containing the alpha and beta spectral density for channels C3 and C4. The model parameters were determined by performing a five-fold cross validation grid search over activation function, alpha, and solver in a manner identical to the model validation method as described in Chapter 7.

8.3.5 Simulating transfer learning

To simulate transfer learning, we simulated the Session 1 performance of all subjects in Group 1 in Study 2 (n = 3), who originally did not have any adaptation of the decoder between runs. Instead of using the decoder created using the data from the motor screening task of that session, we simulated the five BCI runs in Session 1 using the general model on the original EEG data for each run. We excluded Group 1 subjects from Study 1 because their behavior was simulated due to a bug present during data collection (more detail in Chapter 7).

8.3.6 Statistical analysis

We compared actual subject performance in the first session to their simulated first session performance using the general BCI decoder, created using the data of multiple other individuals. To test the effect of model type (individual or general) on learning within the first session, we fit the data to the following linear model.

$$Score \sim ModelType + RunNumber + (ModelType * RunNumber) + (1|Subject) \quad (11)$$

To test the effect of model type on the overall performance within the first session, we fit the data to the following linear model.

$$Score \sim ModelType + (1|Subject) \quad (12)$$

After fitting each model, we ran an ANOVA on the model to see if there were any statistically significant main effects. For any significant findings from the ANOVA, we would follow with post hoc unpaired, two-sample t-tests to further examine the effect.

8.4 Results

In this section, we explore general model performance and the effect of transfer learning on initial subject performance.

8.4.1 General Model training

For each subject, we trained a general model by using the data from the best run of all subjects excluding the subject of interest. General model training was evaluated by observing the learning curves and the Receiver-Operating Characteristic (ROC) curve for each model. In Figure 39, we see the learning and ROC curves for the general model created for subject a1e6c0. For this subject, the learning curve scores converge fairly low at around 56%, and the ROC curve has an area of 0.58. The performance for the other subjects' general models is similarly low (Table 12).

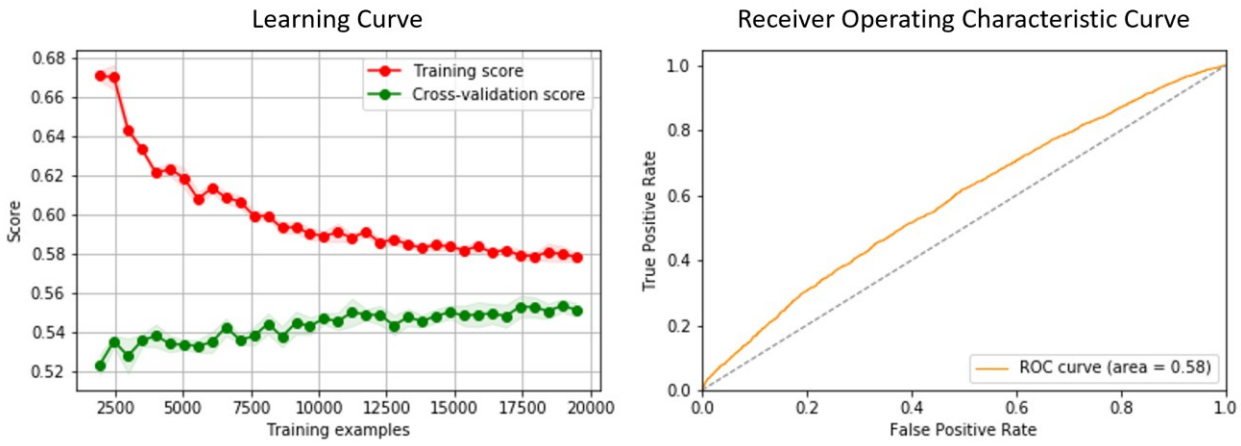

Figure 39. Model Validation Example. General model training was evaluated by observing the learning curve (left) and the Receiver-Operating Characteristic curve (right). These example plots were created from the training of the general model for subject a1e6c0.

		Model Parameters		
Subject	ROC curve area	Activation Function	Alpha	Solver
a1e6c0	0.58	relu	0.001	lbfgs
851238	0.58	relu	1e-06	lbfgs
c37099	0.58	relu	1e-05	lbfgs

Table 12. Receiver Operating Characteristic curve area and model parameters for the general models created for each subject.

8.4.2 Simulated transfer learning

Through simulating the Session 1 performance for the Study 2 Group 1 subjects, we qualitatively observe an increase in overall BCI performance when using the general models in place of the original models trained on each individual's motor screening data (Figure 40). For one subject, we see the performance within each run in Session 1 is greater with the general model than with the original model (Figure 40, left). Across all three subjects, the mean performance over all Session 1 runs was greater with the general models (Figure 40, right).

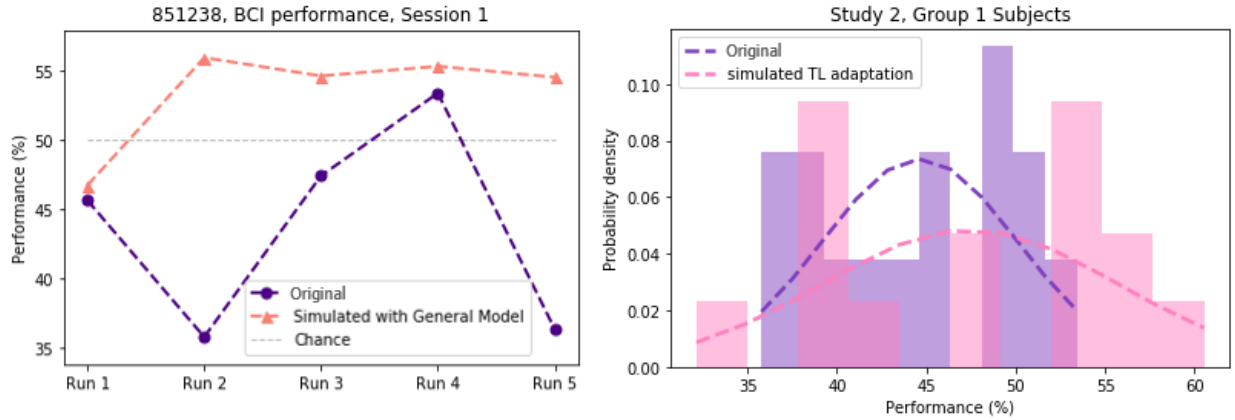

Figure 40. Original subject performance compared to performance with general model. (Left) In subject 851238, the performance with the general model (trained on the best run data from all subjects excluding their own data) results in better performance for each run than the original model. (Right) Histogram of original and simulated general model performance for all three Study 2 Group 1 subjects.

Between all five runs in the first session, the maximum performance achieved with the general model surpassed that achieved with the original model for all three subjects (Table 13).

	Original Model Score (%)		General Model Score (%)	
Subject	Mean Score	Max Score	Mean Score	Max Score
a1e6c0	45.85	49.56	43.53	52.38
851238	45.01	53.40	53.45	55.96
c37099	43.04	50.88	45.37	60.53

Table 13. Original and simulated transfer learning performance. Subject performance in Session 1 with the original model trained on the motor screening data and with the general model train on other subject data.

To test if the model type (original model trained on the individual's motor screening data or general model created using the BCI data from all other subjects' best runs) had an effect on learning within the first session, we fit the linear model described in Equation 11 to the data.

Running an ANOVA on this model, we do not see a statistically significant main effect from model type ($F(1, 26) = 0.3153$, $p = 0.5793$), run number ($F(1, 26) = 0.0091$, $p = 0.9249$), or from the interaction between model type and run number ($F(1, 26) = 1.3633$, $p = 0.2536$).

To test if the model type had an effect on the overall performance within the first session, we fit the linear model described in Equation 12 to the data.

Running an ANOVA on this model, we do not see a statistically significant main effect from model type ($F(1, 28) = 1.2212$, $p = 0.2785$).

8.5 Discussion

In this chapter, we have explored the concept of transfer learning and its application to motor imagery BCI control using the EEG data described in and collected for Chapter 7. Here, we discuss the general models, the results of the simulated general model performance, and future work which may lead to more significant outcomes.

8.5.1 Low training and validation scores for the general models

Ideally, we would see the training and validation scores converge to a higher score further away from chance on the learning curve, and we would see a higher area under the ROC. The low convergence scores indicate that the models had difficulty finding a consistent pattern in the features associated with the two classes: left motor imagery and right motor imagery. Because these general models were trained using data from all subjects, excluding the subject of interest, it is possible that the change in feature values for the two classes varied enough between subjects to prevent the model from learning one reliable rule to discriminate left and right motor imagery.

As discussed in Jeon et al. (2011), how motor imagery presents itself may vary from person to person. Here, it is likely that some subjects exhibited event-related desynchronization (ERD) in the alpha band while others exhibited ERD in the beta band. Individual models trained on data for just one subject may learn to recognize alpha ERD for motor imagery by classifying examples with low alpha spectral density in C3 for right hand motor imagery and examples with low alpha spectral density in C4 for left hand motor imagery. Likewise, an individual model trained on one subject with beta ERD may learn to classify motor imagery based on the beta spectral density in C3 and C4. However, if you train a new model using the data from these two subjects, it becomes less clear what difference in features is associated with each class.

To address inconsistent feature changes, we could create multiple general models for any subject of interest, where each general model is trained on only one presentation type of motor imagery. For example, one general model would be trained on data from all subjects who exhibited alpha ERD and another model would be trained on data from all subjects who exhibited beta ERD. Because there would be more than one general model available for the test subject, we would need to determine which model to use as the BCI decoder prior to BCI use. This calibration phase should only take a minute or two to run, where we collect motor imagery and perhaps some motor observation data from the subject and use the data to predict which model might work best for them. Although this prevents the user from immediately starting to attempt BCI control, this short calibration phase would possibly allow for greater performance while still allowing subjects to attempt control without an extensive training period.

8.5.2 The effect of transfer learning on initial BCI performance

Although we did not find the general models to significantly improve performance for any of the test subjects, we did observe better mean performance for two out of three subjects and better maximum performance in all three subjects (Table 13). For subject 851238, performance with the general model is better than with the original model for all five simulated runs (Figure 40). It is encouraging that the model allowed for higher performance, allowing the subject to achieve above chance performance for four out of five runs, as opposed to for one run with the original model in Session 1. The performance

with the general model for subject a1e6c0 was very similar to the performance with the original model (Figure 41). However, in subject c37099, we see a great increase in performance with the general model towards the end of the session. Interestingly, this seems to coincide with the increase in performance with the original model in runs 4 and 5 (Figure 41).

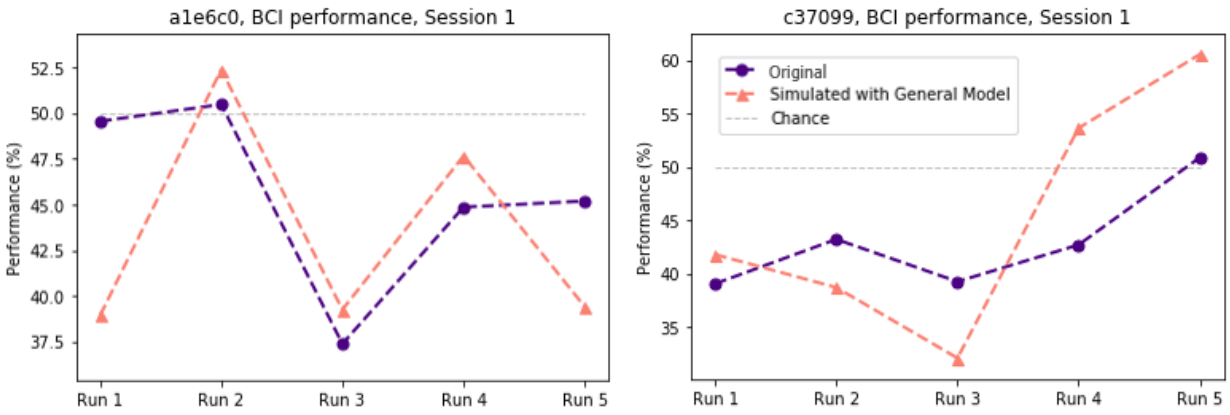

Figure 41. Original and simulated general model performance for subjects a1e6c0 and c37099. Both plots share the same key but have different y-axis scales.

Despite the general model validation scores and ROC areas being relatively low, they still seem to allow for comparable or even slightly better performance for subjects without requiring training.

8.5.3 Applications of transfer learning in BCI

As demonstrated in our simulation, general models trained on the data from multiple subjects may be used to allow first-time users to control a Brain-Computer Interface with approximately the same or better accuracy than they might have performed had they trained a personalized decoder. While work may be done to improve the efficacy of the original individuals' models trained in the BCI study described in Chapter 7, it is also worth pursuing building upon the work in this chapter and improving the efficacy of general models.

General models can allow subjects to achieve above chance performance without any prior training, which lowers a large barrier for BCI development and BCI use. If we develop multiple general models to fit different overarching types of motor imagery data (e.g., models trained on subjects whose motor imagery presented as beta ERD), we may select the optimal general model for new subjects and allow for even greater first session performance. Even if the initial performance with the general model is

lower than expected, data from the new subject can be fed into the general model between runs to better fit the model to the individual.

By removing the need for extensive training prior to BCI use, investigators can design their experiments to explore questions of interest in greater depth or more thoroughly without risking as much subject fatigue due to long training periods. With the premise that general models may function better with a larger amount of training data, researchers may be more motivated to share or upload their data to large cloud repositories to allow for general model training. Outside of the research context, better first time performance without extensive training might increase interest in BCIs for medical or therapeutic use, especially considering the cost of time and services individuals from these populations often have to consider.

8.5.4 Future work

This initial investigation into transfer learning for motor imagery BCI demonstrates that general models have the potential to impact how BCI are developed and used. However, significant improvements need to be made before these general models replace training periods for non-novel BCI paradigms. As discussed earlier, one change which may lead to greater performance is the creation of multiple general models based on motor imagery presentation in the subjects in the training data. Another step which may be taken to improve performance is to provide more data by using features not only from the single best run per subject, but from multiple high performance runs per subject.

In addition to creating general models based on data from multiple subjects, further work should be performed to simulate or test how well subjects would perform when the decoder is trained on data from the current session and from previous sessions from the given subject. Does transfer learning across sessions within individual subjects improve performance?

Lastly, it would be interesting to attempt to create a general model for error detection. If we were able to create a general model for classifying error-related potentials, then we would be able to create confidence scores for BCI data and allow for co-adaptation without spending time training an error

classifier. Having both an effective motor imagery general model and an error general model could allow new users to fully utilize a co-adaptive motor imagery BCI without any training whatsoever.

8.6 Conclusion

In this chapter, we explored transfer learning as applied to the dataset collected and described in Chapter 7. Although not statistically significant, we found our general models (trained on all subjects excluding the subjects of interest) allowed for BCI performance on-par or slightly better than the performance using personalized models trained on individual subject motor screening data. This suggests that general models may be used to lower a barrier to BCI use and can be used in conjunction with the performance monitoring based co-adaptive BCI detailed in the previous chapter, which utilizes both error-related potentials and attention via Default Mode Network activity.

9. Conclusion

Brain-Computer Interface (BCI) use is largely restricted to research settings due to various factors, including but not limited to the need for researcher expertise in ensuring the system will continue to operate well over time. If not constrained to research settings, these systems could positively impact the quality of life for many people with sensorimotor disabilities due to neurological conditions. With the ultimate goal of increasing the viability of future BCIs in at-home settings, the work presented in this dissertation focused on promoting individualized, automatic co-adaptation between the BCI user and the BCI decoder.

To enable and demonstrate this co-adaptation, we built a BCI that would adapt using performance-related neural signals without the need for explicit task performance information. This reliance on performance-related neural signals should theoretically allow the BCI to adapt in various task contexts, closer representing how BCIs may be used in at-home settings. In order to build this co-adaptive BCI, we first investigated two performance-related neural signals which would be used to provide feedback to the BCI decoder. These two signals were error-related potentials and attention via Default Mode Network activity, as explored in-depth in Chapters 5 and 6, respectively.

Through our investigations, we found that error-related potentials in a continuous control one-dimensional center-out BCI task were observed in the somatosensory, motor, premotor, and parietal areas, matching with previous literature investigating error in an overt movement task. We also found that perceived disruption of the Default Mode Network (through the form of an auditory beep) tended to improve subject reaction time in a modified Stroop Task. Interestingly, we also observed decreases in connectivity between Default Mode Network regions following both conscious and sub-conscious disruption through audio beep and cortical stimulation, respectively.

Using error-related potentials and attention, we created a novel estimate of subject BCI performance called “confidence scores” which were used to selectively adapt the BCI decoder over multiple runs of a simple one-dimensional center-out task. With our novel “confidence score” based co-adaptation, we

were able to demonstrate improved overall BCI performance as compared to for subjects without decoder adaptation.

Although further work is required for increasing the viability of BCI for at-home use, the work presented in this dissertation contributes to the field by demonstrating that automatic, individualized co-adaptation using performance-related neural signals can indeed improve BCI performance. In addition, this work includes novel investigations on error-related potentials at the cortical level in the context of a continuous-control BCI and on the effects of conscious and sub-conscious disruption of the Default Mode Network on task performance and functional connectivity between Default Mode Network regions.

10. References

Adleman, N.E., Menon, V., Blasey, C.M., White, C.D., Warsofsky, I.S., Glover, G.H., and Reiss, A.L. (2002). A developmental fMRI study of the Stroop color-word task. NeuroImage *16*, 61–75.

Aiken, L.R. Jr., and Lichtenstein, M. (1964). Interstimulus and inter-response time variables in reaction times to regularly recurring visual stimuli. Percept. Mot. Skills *19*, 339–342.

Ang, K.K., Chin, Z.Y., Zhang, H., and Guan, C. (2008). Filter Bank Common Spatial Pattern (FBCSP) in Brain-Computer Interface. In 2008 IEEE International Joint Conference on Neural Networks (IEEE World Congress on Computational Intelligence), pp. 2390–2397.

Anticevic, A., Cole, M.W., Murray, J.D., Corlett, P.R., Wang, X.-J., and Krystal, J.H. (2012). The role of default network deactivation in cognition and disease. Trends Cogn. Sci. *16*, 584–592.

Aoki, Y., Ishii, R., Pascual-Marqui, R.D., Canuet, L., Ikeda, S., Hata, M., Imajo, K., Matsuzaki, H., Musha, T., Asada, T., et al. (2015). Detection of EEG-resting state independent networks by eLORETA-ICA method. Front. Hum. Neurosci. *9*.

Atchley, R., Klee, D., and Oken, B. (2017). EEG frequency changes prior to making errors in an easy Stroop task. Front. Hum. Neurosci. *11*.

Babiloni, C., Del Percio, C., Vecchio, F., Sebastiano, F., Di Gennaro, G., Quarato, P.P., Morace, R., Pavone, L., Soricelli, A., Noce, G., et al. (2016). Alpha, beta and gamma electrocorticographic rhythms in somatosensory, motor, premotor and prefrontal cortical areas differ in movement execution and observation in humans. Clin. Neurophysiol. *127*, 641–654.

Bacher, D., Jarosiewicz, B., Masse, N.Y., Stavisky, S.D., Simeral, J.D., Newell, K., Oakley, E.M., Cash, S.S., Friehs, G., and Hochberg, L.R. (2015). Neural point-and-click communication by a person with incomplete locked-in syndrome. Neurorehabil. Neural Repair *29*, 462–471.

Badre, D., and Wagner, A.D. (2007). Left ventrolateral prefrontal cortex and the cognitive control of memory. Neuropsychologia *45*, 2883–2901.

Bechtereva, N.P., Shemyakina, N.V., Starchenko, M.G., Danko, S.G., and Medvedev, S.V. (2005). Error detection mechanisms of the brain: Background and prospects. Int. J. Psychophysiol. *58*, 227–234.

Blankertz, B., Dornhege, G., Krauledat, M., Müller, K.-R., and Curio, G. (2007). The non-invasive Berlin Brain–Computer Interface: Fast acquisition of effective performance in untrained subjects. NeuroImage *37*, 539–550.

Blankertz, B., Losch, F., Krauledat, M., Dornhege, G., Curio, G., and Müller, K.-R. (2008). The Berlin Brain–Computer Interface: Accurate performance from first-session in BCI-naive subjects. IEEE Trans. Biomed. Eng. *55*, 2452–2462.

Blankertz, B., Tomioka, R., Lemm, S., Kawanabe, M., and Müller, K.-R. (2008b). Optimizing spatial filters for robust EEG single-trial analysis. IEEE Signal Process. Mag. *25*, 41–56.

Blankertz, B., Sannelli, C., Halder, S., Hammer, E.M., Kübler, A., Müller, K.-R., Curio, G., and Dickhaus, T. (2010). Neurophysiological predictor of SMR-based BCI performance. NeuroImage *51*, 1303–1309.

Bowman, A.D., Griffis, J.C., Visscher, K.M., Dobbins, A.C., Gawne, T.J., DiFrancesco, M.W., and Szaflarski, J.P. (2017). Relationship between alpha rhythm and the Default Mode Network: An EEG-fMRI study. J. Clin. Neurophysiol. Off. Publ. Am. Electroencephalogr. Soc. *34*, 527–533.

Bowyer, S.M. (2016). Coherence a measure of the brain networks: past and present. Neuropsychiatr. Electrophysiol. *2*, 1.

Brainard, D.H. (1997). The Psychophysics Toolbox. Spat. Vis. *10*, 433–436.

Buzsáki, G., Anastassiou, C.A., and Koch, C. (2012). The origin of extracellular fields and currents — EEG, ECoG, LFP and spikes. Nat. Rev. Neurosci. *13*, 407–420.

Caldwell, D. (2019). Code and data for ECoG artifact rejection with pulse trains. Github: davidjuliancaldwell/artifactRejection.

Calhoun, V.D., Adali, T., Pearlson, G.D., and Kiehl, K.A. (2006). Neuronal chronometry of target detection: Fusion of hemodynamic and event-related potential data. NeuroImage *30*, 544–553.

Canolty, R.T., and Knight, R.T. (2010). The functional role of cross-frequency coupling. Trends Cogn. Sci. *14*, 506–515.

Canolty, R.T., Edwards, E., Dalal, S.S., Soltani, M., Nagarajan, S.S., Kirsch, H.E., Berger, M.S., Barbaro, N.M., and Knight, R.T. (2006). High gamma power is phase-locked to theta oscillations in human neocortex. Science *313*, 1626–1628.

Casey, B.J., Trainor, R., Giedd, J., Vauss, Y., Vaituzis, C.K., Hamburger, S., Kozuch, P., and Rapoport, J.L. (1997). The role of the anterior cingulate in automatic and controlled processes: a developmental neuroanatomical study. Dev. Psychobiol. *30*, 61–69.

Casimo, K., Darvas, F., Wander, J., Ko, A., Grabowski, T.J., Novotny, E., Poliakov, A., Ojemann, J.G., and Weaver, K.E. (2016). Regional patterns of cortical phase synchrony in the resting state. Brain Connect. *6*, 470–481.

Cavanagh, J.F., and Frank, M.J. (2014). Frontal theta as a mechanism for cognitive control. Trends Cogn. Sci. *18*, 414–421.

Chaudhary, U., Birbaumer, N., and Ramos-Murguialday, A. (2016). Brain–computer interfaces for communication and rehabilitation. Nat. Rev. Neurol. *12*, 513–525.

Chavarriaga, R., and Millan, J.D.R. (2010). Learning from EEG error-related potentials in noninvasive brain-computer interfaces. IEEE Trans. Neural Syst. Rehabil. Eng. Publ. IEEE Eng. Med. Biol. Soc. *18*, 381–388.

Chen, A.C.N., Feng, W., Zhao, H., Yin, Y., and Wang, P. (2008). EEG default mode network in the human brain: Spectral regional field powers. NeuroImage *41*, 561–574.

Christoff, K., Irving, Z.C., Fox, K.C.R., Spreng, R.N., and Andrews-Hanna, J.R. (2016). Mind-wandering as spontaneous thought: a dynamic framework. Nat. Rev. Neurosci. *17*, 718–731.

Collins, K.L., Guterstam, A., Cronin, J., Olson, J.D., Ehrsson, H.H., and Ojemann, J.G. (2017). Ownership of an artificial limb induced by electrical brain stimulation. Proc. Natl. Acad. Sci. *114*, 166–171.

Cronin, J.A., Wu, J., Collins, K.L., Sarma, D., Rao, R.P.N., Ojemann, J.G., and Olson, J.D. (2016). Task-Specific Somatosensory Feedback via Cortical Stimulation in Humans. IEEE Trans. Haptics *9*, 515–522.

Cruz, A., Pires, G., and Nunes, U.J. (2018). Double ErrP detection for automatic error correction in an ERP-based BCI speller. IEEE Trans. Neural Syst. Rehabil. Eng. Publ. IEEE Eng. Med. Biol. Soc. *26*, 26–36.

Dai, M., Zheng, D., Liu, S., and Zhang, P. (2018). Transfer kernel Common Spatial Patterns for motor imagery Brain-Computer Interface classification. Comput. Math. Methods Med. *2018*, 9871603.

Dai, M., Zheng, D., Na, R., Wang, S., and Zhang, S. (2019). EEG classification of motor imagery using a novel Deep Learning framework. Sensors *19*.

Dastjerdi, M., Foster, B.L., Nasrullah, S., Rauschecker, A.M., Dougherty, R.F., Townsend, J.D., Chang, C., Greicius, M.D., Menon, V., Kennedy, D.P., et al. (2011). Differential electrophysiological response during rest, self-referential, and non–self-referential tasks in human posteromedial cortex. Proc. Natl. Acad. Sci. *108*, 3023–3028.

Diez, P.F., Correa, A.G., Orosco, L., Laciar, E., and Mut, V. (2015). Attention-level transitory response: a novel hybrid BCI approach. J. Neural Eng. *12*, 056007.

DiGiovanna, J., Mahmoudi, B., Fortes, J., Principe, J.C., and Sanchez, J.C. (2009). Coadaptive brain-machine interface via reinforcement learning. IEEE Trans. Biomed. Eng. *56*, 54–64.

Dimitriadis, S.I., Salis, C., and Linden, D. (2018). A novel, fast and efficient single-sensor automatic sleep-stage classification based on complementary cross-frequency coupling estimates. Clin. Neurophysiol. Off. J. Int. Fed. Clin. Neurophysiol. *129*, 815–828.

D'Mello, S., and Graesser, A. (2012). Dynamics of affective states during complex learning. Learn. Instr. *22*, 145–157.

Donchin, E., Spencer, K.M., and Wijesinghe, R. (2000). The mental prosthesis: assessing the speed of a P300-based brain-computer interface. IEEE Trans. Rehabil. Eng. *8*, 174–179.

Evans, A.C., Collins, D.L., Mills, S.R., Brown, E.D., Kelly, R.L., and Peters, T.M. (1993). 3D statistical neuroanatomical models from 305 MRI volumes. In 1993 IEEE Conference Record Nuclear Science Symposium and Medical Imaging Conference, pp. 1813–1817 vol.3.

Fahimi, F., Zhang, Z., Goh, W.B., Lee, T.-S., Ang, K.K., and Guan, C. (2019). Inter-subject transfer learning with an end-to-end deep convolutional neural network for EEG-based BCI. J. Neural Eng. *16*, 026007.

Falkenstein, M., Hohnsbein, J., Hoormann, J., and Blanke, L. (1991). Effects of crossmodal divided attention on late ERP components. II. Error processing in choice reaction tasks. Electroencephalogr. Clin. Neurophysiol. *78*, 447–455.

Falkenstein, M., Hoormann, J., Christ, S., and Hohnsbein, J. (2000). ERP components on reaction errors and their functional significance: a tutorial. Biol. Psychol. *51*, 87–107.

Faller, J., Scherer, R., Costa, U., Opisso, E., Medina, J., and Müller-Putz, G.R. (2014). A Co-Adaptive Brain-Computer Interface for End Users with Severe Motor Impairment. PLoS ONE *9*.

Farwell, L.A., and Donchin, E. (1988). Talking off the top of your head: toward a mental prosthesis utilizing event-related brain potentials. Electroencephalogr. Clin. Neurophysiol. *70*, 510–523.

Ferrez, P.W., and Millan, J.D.R. (2008). Error-related EEG potentials generated during simulated brain-computer interaction. IEEE Trans. Biomed. Eng. *55*, 923–929.

Fetz, E.E. (1969). Operant conditioning of cortical unit activity. Science *163*, 955–958.

Fiddick, L., Spampinato, M.V., and Grafman, J. (2005). Social contracts and precautions activate different neurological systems: an fMRI investigation of deontic reasoning. NeuroImage *28*, 778–786.

Fink, G.R., Marshall, J.C., Halligan, P.W., Frith, C.D., Driver, J., Frackowiak, R.S.J., and Dolan, R.J. (1999). The neural consequences of conflict between intention and the senses. Brain *122*, 497–512.

Fischl, B. (2012). FreeSurfer. NeuroImage *62*, 774–781.

Florin, E., and Baillet, S. (2015). The brain's resting-state activity is shaped by synchronized cross-frequency coupling of neural oscillations. NeuroImage *111*, 26–35.

Formaggio, E., Storti, S.F., Tramontano, V., Casarin, A., Bertoldo, A., Fiaschi, A., Talacchi, A., Sala, F., Toffolo, G.M., and Manganotti, P. (2013). Frequency and time-frequency analysis of intraoperative ECoG during awake brain stimulation. Front. Neuroengineering *6*.

Foster, B.L., and Parvizi, J. (2017). Direct cortical stimulation of human posteromedial cortex. Neurology *88*, 685–691.

Fox, K.C.R., Foster, B.L., Kucyi, A., Daitch, A.L., and Parvizi, J. (2018). Intracranial electrophysiology of the human Default Network. Trends Cogn. Sci. *22*, 307–324.

Frank, M.J., Woroch, B.S., and Curran, T. (2005). Error-Related Negativity predicts Reinforcement Learning and conflict biases. Neuron *47*, 495–501.

Fukunaga, K. (1990). Introduction to Statistical Pattern Recognition (Elsevier).

Gao, Q., Dou, L., Belkacem, A.N., and Chen, C. (2017). Noninvasive electroencephalogram based control of a robotic arm for writing task using hybrid BCI system. BioMed Res. Int. *2017*, 8316485.

Gastaut, H.J., and Bert, J. (1954). EEG changes during cinematographic presentation (Moving picture activation of the EEG). Electroencephalogr. Clin. Neurophysiol. *6*, 433–444.

Gehring, W.J., Goss, B., Coles, M.G.H., Meyer, D.E., and Donchin, E. (1993). A neural system for error detection and compensation. Psychol. Sci. *4*, 385–390.

Gerson, A.D., Parra, L.C., and Sajda, P. (2005). Cortical origins of response time variability during rapid discrimination of visual objects. NeuroImage *28*, 342–353.

Gias, C. (2011). Phase randomization - File Exchange - MATLAB Central.

Giraud, A.L., Kell, C., Thierfelder, C., Sterzer, P., Russ, M.O., Preibisch, C., and Kleinschmidt, A. (2004). Contributions of sensory input, auditory search and verbal comprehension to cortical activity during speech processing. Cereb. Cortex N. Y. N 1991 *14*, 247–255.

Glazer, J.E., Kelley, N.J., Pornpattananangkul, N., Mittal, V.A., and Nusslock, R. (2018). Beyond the FRN: Broadening the time-course of EEG and ERP components implicated in reward processing. Int. J. Psychophysiol. *132*, 184–202.

Goel, V., Gold, B., Kapur, S., and Houle, S. (1998). Neuroanatomical correlates of human reasoning. J. Cogn. Neurosci. *10*, 293–302.

Gold, B.T., Balota, D.A., Kirchhoff, B.A., and Buckner, R.L. (2005). Common and dissociable activation patterns associated with controlled semantic and phonological processing: evidence from FMRI adaptation. Cereb. Cortex N. Y. N 1991 *15*, 1438–1450.

Green, A.M., and Kalaska, J.F. (2011). Learning to move machines with the mind. Trends Neurosci. *34*, 61–75.

Guy, V., Soriani, M.-H., Bruno, M., Papadopoulo, T., Desnuelle, C., and Clerc, M. (2018). Brain computer interface with the P300 speller: Usability for disabled people with amyotrophic lateral sclerosis. Ann. Phys. Rehabil. Med. *61*, 5–11.

Haglund, M.M., Berger, M.S., Shamseldin, M., Lettich, E., and Ojemann, G.A. (1994). Cortical localization of temporal lobe language sites in patients with gliomas. Neurosurgery *34*, 567–576; discussion 576.

Hirsch, J., Moreno, D.R., and Kim, K.H. (2001). Interconnected large-scale systems for three fundamental cognitive tasks revealed by functional MRI. J. Cogn. Neurosci. *13*, 389–405.

Hochberg, L.R., Bacher, D., Jarosiewicz, B., Masse, N.Y., Simeral, J.D., Vogel, J., Haddadin, S., Liu, J., Cash, S.S., van der Smagt, P., et al. (2012). Reach and grasp by people with tetraplegia using a neurally controlled robotic arm. Nature *485*, 372–375.

Holroyd, C.B., and Coles, M.G.H. (2002). The neural basis of human error processing: reinforcement learning, dopamine, and the error-related negativity. Psychol. Rev. *109*, 679–709.

Hossain, I., Khosravi, A., Hettiarachchi, I., and Nahavandi, S. (2018). Multiclass informative instance Transfer Learning framework for motor imagery-based Brain-Computer Interface. Comput. Intell. Neurosci. *2018*, 6323414.

Huggins-Daines, D., Kumar, M., Chan, A., Black, A.W., Ravishankar, M., and Rudnicky, A.I. (2006). Pocketsphinx: A free, real-time continuous speech recognition system for hand-held devices. In 2006 IEEE International Conference on Acoustics Speech and Signal Processing Proceedings, pp. I–I.

Iannaccone, R., Hauser, T.U., Staempfli, P., Walitza, S., Brandeis, D., and Brem, S. (2015). Conflict monitoring and error processing: New insights from simultaneous EEG–fMRI. NeuroImage *105*, 395–407.

Imperatori, C., Della Marca, G., Brunetti, R., Carbone, G.A., Massullo, C., Valenti, E.M., Amoroso, N., Maestoso, G., Contardi, A., and Farina, B. (2016). Default Mode Network alterations in alexithymia: an EEG power spectra and connectivity study. Sci. Rep. *6*, 36653.

Iturrate, I., Montesano, L., and Minguez, J. (2013). Task-dependent signal variations in EEG error-related potentials for brain-computer interfaces. J. Neural Eng. *10*, 026024.

Iturrate, I., Chavarriaga, R., Montesano, L., Minguez, J., and Millán, J.D.R. (2015). Teaching brain-machine interfaces as an alternative paradigm to neuroprosthetics control. Sci. Rep. *5*, 13893.

Jann, K., Kottlow, M., Dierks, T., Boesch, C., and Koenig, T. (2010). Topographic electrophysiological signatures of FMRI Resting State Networks. PloS One *5*, e12945.

Jatoi, M.A., Kamel, N., Malik, A.S., Faye, I., and Begum, T. (2014). A survey of methods used for source localization using EEG signals. Biomed. Signal Process. Control *11*, 42–52.

Jensen, O., and Colgin, L.L. (2007). Cross-frequency coupling between neuronal oscillations. Trends Cogn. Sci. *11*, 267–269.

Jensen, O., Spaak, E., and Park, H. (2017). Discriminating valid from spurious indices of Phase-Amplitude Coupling. ENeuro *3*.

Jeon, Y., Nam, C.S., Kim, Y.-J., and Whang, M.C. (2011). Event-related (De)synchronization (ERD/ERS) during motor imagery tasks: Implications for brain–computer interfaces. Int. J. Ind. Ergon. *41*, 428–436.

Keles, G.E., Lundin, D.A., Lamborn, K.R., Chang, E.F., Ojemann, G., and Berger, M.S. (2004). Intraoperative subcortical stimulation mapping for hemispherical perirolandic gliomas located within or adjacent to the descending motor pathways: evaluation of morbidity and assessment of functional outcome in 294 patients. J. Neurosurg. *100*, 369–375.

Kim, S.K., and Kirchner, E.A. (2013). Classifier transferability in the detection of error related potentials from observation to interaction. In 2013 IEEE International Conference on Systems, Man, and Cybernetics, pp. 3360–3365.

Kim, Y.J., Park, S.W., Yeom, H.G., Bang, M.S., Kim, J.S., Chung, C.K., and Kim, S. (2015). A study on a robot arm driven by three-dimensional trajectories predicted from non-invasive neural signals. Biomed. Eng. Online *14*, 81.

Kleiner, M., Brainard, D., Pelli, D., Ingling, A., Murray, R., and Broussard, C. (2007). What's new in psychtoolbox-3. Perception *36*, 1–16.

Knyazev, G.G., Slobodskoj-Plusnin, J.Y., Bocharov, A.V., and Pylkova, L.V. (2011). The default mode network and EEG α oscillations: an independent component analysis. Brain Res. *1402*, 67–79.

Kreilinger, A., Hiebel, H., and Müller-Putz, G.R. (2016). Single Versus Multiple Events Error Potential Detection in a BCI-Controlled Car Game With Continuous and Discrete Feedback. IEEE Trans. Biomed. Eng. *63*, 519–529.

Krigolson, O.E., and Holroyd, C.B. (2007). Hierarchical error processing: different errors, different systems. Brain Res. *1155*, 70–80.

Krigolson, O.E., Holroyd, C.B., Van Gyn, G., and Heath, M. (2008). Electroencephalographic correlates of target and outcome errors. Exp. Brain Res. *190*, 401–411.

Krizhevsky, A., Sutskever, I., and Hinton, G.E. (2012). ImageNet classification with Deep Convolutional Neural Networks. In Advances in Neural Information Processing Systems 25, F. Pereira, C.J.C. Burges, L. Bottou, and K.Q. Weinberger, eds. (Curran Associates, Inc.), pp. 1097–1105.

Kuś, R., Duszyk, A., Milanowski, P., Łabęcki, M., Bierzyńska, M., Radzikowska, Z., Michalska, M., Żygierewicz, J., Suffczyński, P., and Durka, P.J. (2013). On the quantification of SSVEP frequency responses in human EEG in realistic BCI conditions. PLOS ONE *8*, e77536.

Ladouceur, C.D., Dahl, R.E., and Carter, C.S. (2007). Development of action monitoring through adolescence into adulthood: ERP and source localization. Dev. Sci. *10*, 874–891.

Lakey, C.E., Berry, D.R., and Sellers, E.W. (2011). Manipulating attention via mindfulness induction improves P300-based Brain-Computer Interface performance. J. Neural Eng. *8*, 025019.

Lopes da Silva, F. (2013). EEG and MEG: Relevance to neuroscience. Neuron *80*, 1112–1128.

Lotte, F., Congedo, M., Lécuyer, A., Lamarche, F., and Arnaldi, B. (2007). A review of classification algorithms for EEG-based brain-computer interfaces. J. Neural Eng. *4*, R1–R13.

Lotte, F., Bougrain, L., Cichocki, A., Clerc, M., Congedo, M., Rakotomamonjy, A., and Yger, F. (2018). A review of classification algorithms for EEG-based brain-computer interfaces: a 10 year update. J. Neural Eng. *15*, 031005.

MacLean, S.J., Hassall, C.D., Ishigami, Y., Krigolson, O.E., and Eskes, G.A. (2015). Using brain potentials to understand prism adaptation: the error-related negativity and the P300. Front. Hum. Neurosci. *9*, 335.

Majidov, I., and Whangbo, T. (2019). Efficient classification of motor imagery electroencephalography signals using Deep Learning methods. Sensors *19*.

Malan, N.S., and Sharma, S. (2019). Feature selection using regularized neighbourhood component analysis to enhance the classification performance of motor imagery signals. Comput. Biol. Med. *107*, 118–126.

Manning, J.R., Jacobs, J., Fried, I., and Kahana, M.J. (2009). Broadband shifts in local field potential power spectra are correlated with single-neuron spiking in humans. J. Neurosci. Off. J. Soc. Neurosci. *29*, 13613–13620.

Margaux, P., Emmanuel, M., Sébastien, D., Olivier, B., and Jérémie, M. (2012). Objective and subjective evaluation of online error correction during P300-based spelling. Adv Hum-Comp Int *2012*, 4:4–4:4.

Mattout, J., Perrin, M., Bertrand, O., and Maby, E. (2015). Improving BCI performance through co-adaptation: Applications to the P300-speller. Ann. Phys. Rehabil. Med. *58*, 23–28.

Merel, J., Pianto, D.M., Cunningham, J.P., and Paninski, L. (2015). Encoder-decoder optimization for Brain-Computer Interfaces. PLOS Comput. Biol. *11*, e1004288.

Miall, R.C., and Wolpert, D.M. (1996). Forward models for physiological motor control. Neural Netw. *9*, 1265–1279.

Milekovic, T., Ball, T., Schulze-Bonhage, A., Aertsen, A., and Mehring, C. (2012). Error-related electrocorticographic activity in humans during continuous movements. J. Neural Eng. *9*, 026007.

Milekovic, T., Ball, T., Schulze-Bonhage, A., Aertsen, A., and Mehring, C. (2013). Detection of error related neuronal responses recorded by electrocorticography in humans during continuous movements. PloS One *8*, e55235.

Miller, K.J., Den Nijs, M., Shenoy, P., Miller, J.W., Rao, R.P.N., and Ojemann, J.G. (2007a). Real-time functional brain mapping using electrocorticography. NeuroImage *37*, 504–507.

Miller, K.J., Leuthardt, E.C., Schalk, G., Rao, R.P.N., Anderson, N.R., Moran, D.W., Miller, J.W., and Ojemann, J.G. (2007b). Spectral changes in cortical surface potentials during motor movement. J. Neurosci. *27*, 2424–2432.

Miller, K.J., Sorensen, L.B., Ojemann, J.G., and Den Nijs, M. (2009a). Power-law scaling in the brain surface electric potential. PLOS Comput Biol *5*, e1000609.

Miller, K.J., Weaver, K.E., and Ojemann, J.G. (2009b). Direct electrophysiological measurement of human default network areas. Proc. Natl. Acad. Sci. U. S. A. *106*, 12174–12177.

Miller, K.J., Schalk, G., Fetz, E.E., Den Nijs, M., Ojemann, J.G., and Rao, R.P.N. (2010). Cortical activity during motor execution, motor imagery, and imagery-based online feedback. Proc. Natl. Acad. Sci. *107*, 4430–4435.

Miller, K.J., Hermes, D., Witthoft, N., Rao, R.P.N., and Ojemann, J.G. (2015). The physiology of perception in human temporal lobe is specialized for contextual novelty. J. Neurophysiol. *114*, 256–263.

Mittner, M., Boekel, W., Tucker, A.M., Turner, B.M., Heathcote, A., and Forstmann, B.U. (2014). When the brain takes a break: a model-based analysis of mind wandering. J. Neurosci. Off. J. Soc. Neurosci. *34*, 16286–16295.

Mizuguchi, N., and Kanosue, K. (2017). Changes in brain activity during action observation and motor imagery: Their relationship with motor learning. Prog. Brain Res. *234*, 189–204.

Mondini, V., Mangia, A.L., and Cappello, A. (2016). EEG-based BCI system using adaptive features extraction and classification procedures. Comput. Intell. Neurosci. *2016*.

Myrden, A., and Chau, T. (2015). Effects of user mental state on EEG-BCI performance. Front. Hum. Neurosci. *9*.

Myrden, A., and Chau, T. (2016). Towards psychologically adaptive brain-computer interfaces. J. Neural Eng. *13*, 066022.

Nakai, Y., Sugiura, A., Brown, E.C., Sonoda, M., Jeong, J.-W., Rothermel, R., Luat, A.F., Sood, S., and Asano, E. (2019). Four-dimensional functional cortical maps of visual and auditory language: Intracranial recording. Epilepsia *60*, 255–267.

Navarro-Cebrian, A., Knight, R.T., and Kayser, A.S. (2016). Frontal monitoring and parietal evidence: Mechanisms of error correction. J. Cogn. Neurosci. *28*, 1166–1177.

Newell, K.M. (1991). Motor skill acquisition. Annu. Rev. Psychol. *42*, 213–237.

Nieuwenhuis, S., Ridderinkhof, K.R., Blom, J., Band, G.P.H., and Kok, A. (2001). Error-related brain potentials are differentially related to awareness of response errors: Evidence from an antisaccade task. Psychophysiology *38*, 752–760.

Nieuwenhuis, S., Holroyd, C.B., Mol, N., and Coles, M.G.H. (2004). Reinforcement-related brain potentials from medial frontal cortex: origins and functional significance. Neurosci. Biobehav. Rev. *28*, 441–448.

Normann, R.A., and Fernandez, E. (2016). Clinical applications of penetrating neural interfaces and Utah Electrode Array technologies. J. Neural Eng. *13*, 061003.

Nourski, K.V. (2017). Auditory processing in the human cortex: An intracranial electrophysiology perspective. Laryngoscope Investig. Otolaryngol. *2*, 147–156.

O'Connell, R.G., Dockree, P.M., Bellgrove, M.A., Kelly, S.P., Hester, R., Garavan, H., Robertson, I.H., and Foxe, J.J. (2007). The role of cingulate cortex in the detection of errors with and without awareness: a high-density electrical mapping study. Eur. J. Neurosci. *25*, 2571–2579.

Olson, J.D., Wander, J.D., Johnson, L., Sarma, D., Weaver, K., Novotny, E.J., Ojemann, J.G., and Darvas, F. (2016). Comparison of subdural and subgaleal recordings of cortical high-gamma activity in humans. Clin. Neurophysiol. Off. J. Int. Fed. Clin. Neurophysiol. *127*, 277–284.

Ordikhani-Seyedlar, M., Sorensen, H.B.D., Kjaer, T.W., Siebner, H.R., and Puthusserypady, S. (2014). SSVEP-modulation by covert and overt attention: Novel features for BCI in attention neuro-rehabilitation. In 2014 36th Annual International Conference of the IEEE Engineering in Medicine and Biology Society, pp. 5462–5465.

Orsborn, A.L., Moorman, H.G., Overduin, S.A., Shanechi, M.M., Dimitrov, D.F., and Carmena, J.M. (2014). Closed-loop decoder adaptation shapes neural plasticity for skillful neuroprosthetic control. Neuron *82*, 1380–1393.

Ossandón, T., Jerbi, K., Vidal, J.R., Bayle, D.J., Henaff, M.-A., Jung, J., Minotti, L., Bertrand, O., Kahane, P., and Lachaux, J.-P. (2011). Transient suppression of broadband gamma power in the default-mode network is correlated with task complexity and subject performance. J. Neurosci. Off. J. Soc. Neurosci. *31*, 14521–14530.

Pan, S.J., and Yang, Q. (2010). A survey on Transfer Learning. IEEE Trans. Knowl. Data Eng. *22*, 1345–1359.

Papademetris, X., Jackowski, M.P., Rajeevan, N., DiStasio, M., Okuda, H., Constable, R.T., and Staib, L.H. (2006). BioImage Suite: An integrated medical image analysis suite: An update. Insight J. *2006*, 209.

Parvizi, J., and Kastner, S. (2018). Promises and limitations of human intracranial electroencephalography. Nat. Neurosci. *21*, 474–483.

Pascual-Leone, A., Bartres-Faz, D., and Keenan, J.P. (1999). Transcranial magnetic stimulation: studying the brain-behaviour relationship by induction of "virtual lesions". Philos. Trans. R. Soc. B Biol. Sci. *354*, 1229–1238.

Pascual-Leone, A., Walsh, V., and Rothwell, J. (2000). Transcranial magnetic stimulation in cognitive neuroscience – virtual lesion, chronometry, and functional connectivity. Curr. Opin. Neurobiol. *10*, 232–237.

Peirce, J., Gray, J.R., Simpson, S., MacAskill, M., Höchenberger, R., Sogo, H., Kastman, E., and Lindeløv, J.K. (2019). PsychoPy2: Experiments in behavior made easy. Behav. Res. Methods *51*, 195–203.

Pezzetta, R., Nicolardi, V., Tidoni, E., and Aglioti, S.M. (2018). Error, rather than its probability, elicits specific electrocortical signatures: a combined EEG-immersive virtual reality study of action observation. J. Neurophysiol. *120*, 1107–1118.

Pfurtscheller, G., and Lopes da Silva, F.H. (1999). Event-related EEG/MEG synchronization and desynchronization: basic principles. Clin. Neurophysiol. *110*, 1842–1857.

Pfurtscheller, G., Graimann, B., Huggins, J.E., Levine, S.P., and Schuh, L.A. (2003). Spatiotemporal patterns of beta desynchronization and gamma synchronization in corticographic data during self-paced movement. Clin. Neurophysiol. *114*, 1226–1236.

Phillips, H.N., Blenkmann, A., Hughes, L.E., Kochen, S., Bekinschtein, T.A., Cam-Can, null, and Rowe, J.B. (2016). Convergent evidence for hierarchical prediction networks from human electrocorticography and magnetoencephalography. Cortex J. Devoted Study Nerv. Syst. Behav. *82*, 192–205.

Pohlmeyer, E.A., Mahmoudi, B., Geng, S., Prins, N.W., and Sanchez, J.C. (2014). Using Reinforcement Learning to provide stable Brain-Machine Interface control despite neural input reorganization. PLoS ONE *9*, e87253.

Prichard, D., and Theiler, J. (1994). Generating surrogate data for time series with several simultaneously measured variables. Phys. Rev. Lett. *73*, 951–954.

Raichle, M.E. (2015). The brain's Default Mode Network. Annu. Rev. Neurosci. *38*, 433–447.

Raichle, M.E., MacLeod, A.M., Snyder, A.Z., Powers, W.J., Gusnard, D.A., and Shulman, G.L. (2001). A default mode of brain function. Proc. Natl. Acad. Sci. U. S. A. *98*, 676–682.

Ramoser, H., Muller-Gerking, J., and Pfurtscheller, G. (2000). Optimal spatial filtering of single trial EEG during imagined hand movement. IEEE Trans. Rehabil. Eng. *8*, 441–446.

Ramot, M., Fisch, L., Harel, M., Kipervasser, S., Andelman, F., Neufeld, M.Y., Kramer, U., Fried, I., and Malach, R. (2012). A widely distributed spectral signature of task-negative electrocorticography responses revealed during a visuomotor task in the human cortex. J. Neurosci. *32*, 10458–10469.

Ray, S., Crone, N.E., Niebur, E., Franaszczuk, P.J., and Hsiao, S.S. (2008). Neural correlates of high-gamma oscillations (60–200 Hz) in macaque local field potentials and their potential implications in electrocorticography. J. Neurosci. Off. J. Soc. Neurosci. *28*, 11526–11536.

Rogers, R.D., Owen, A.M., Middleton, H.C., Williams, E.J., Pickard, J.D., Sahakian, B.J., and Robbins, T.W. (1999). Choosing between small, likely rewards and large, unlikely rewards activates inferior and orbital prefrontal cortex. J. Neurosci. Off. J. Soc. Neurosci. *19*, 9029–9038.

Rozado, D., Duenser, A., and Howell, B. (2015). Improving the performance of an EEG-based motor imagery Brain Computer Interface using task evoked changes in pupil diameter. PLOS ONE *10*, e0121262.

Ruffini, G., Dunne, S., Farres, E., Watts, P.C.P., Mendoza, E., Silva, S.R.P., Grau, C., Marco-Pallares, J., Fuentemilla, L., and Vandecasteele, B. (2006). ENOBIO - First tests of a dry electrophysiology electrode using carbon nanotubes. In 2006 International Conference of the IEEE Engineering in Medicine and Biology Society, pp. 1826–1829.

Rusiniak, M., Wróbel, A., Cieśla, K., Pluta, A., Lewandowska, M., Wójcik, J., Skarżyński, P.H., and Wolak, T. (2018). The relationship between alpha burst activity and the default mode network. Acta Neurobiol. Exp. (Warsz.) *78*, 92–113.

Schalk, G., McFarland, D.J., Hinterberger, T., Birbaumer, N., and Wolpaw, J.R. (2004). BCI2000: a general-purpose brain-computer interface (BCI) system. IEEE Trans. Biomed. Eng. *51*, 1034–1043.

Scheibner, H.J., Bogler, C., Gleich, T., Haynes, J.-D., and Bermpohl, F. (2017). Internal and external attention and the default mode network. NeuroImage *148*, 381–389.

Schiatti, L., Tessadori, J., Barresi, G., Mattos, L.S., and Ajoudani, A. (2017). Soft brain-machine interfaces for assistive robotics: A novel control approach. IEEE Int. Conf. Rehabil. Robot. Proc. *2017*, 863–869.

Schirrmeister, R.T., Springenberg, J.T., Fiederer, L.D.J., Glasstetter, M., Eggensperger, K., Tangermann, M., Hutter, F., Burgard, W., and Ball, T. (2017). Deep learning with convolutional neural networks for EEG decoding and visualization. Hum. Brain Mapp. *38*, 5391–5420.

Shenoy, P., Krauledat, M., Blankertz, B., Rao, R.P.N., and Müller, K.-R. (2006). Towards adaptive classification for BCI. J. Neural Eng. *3*, R13–R23.

Shulman, G.L., Fiez, J.A., Corbetta, M., Buckner, R.L., Miezin, F.M., Raichle, M.E., and Petersen, S.E. (1997). Common blood flow changes across visual tasks: II. Decreases in cerebral cortex. J. Cogn. Neurosci. *9*, 648–663.

Siebner, H.R., Hartwigsen, G., Kassuba, T., and Rothwell, J. (2009). How does transcranial magnetic stimulation modify neuronal activity in the brain? - Implications for studies of cognition. Cortex J. Devoted Study Nerv. Syst. Behav. *45*, 1035–1042.

Simeral, J.D., Kim, S.-P., Black, M.J., Donoghue, J.P., and Hochberg, L.R. (2011). Neural control of cursor trajectory and click by a human with tetraplegia 1000 days after implant of an intracortical microelectrode array. J. Neural Eng. *8*, 025027.

Sliwinska, M.W., Vitello, S., and Devlin, J.T. (2014). Transcranial magnetic stimulation for investigating causal brain-behavioral relationships and their time course. J. Vis. Exp. JoVE.

Spuler, M. (2015). A Brain-Computer Interface (BCI) system to use arbitrary Windows applications by directly controlling mouse and keyboard. Conf. Proc. Annu. Int. Conf. IEEE Eng. Med. Biol. Soc. IEEE Eng. Med. Biol. Soc. Annu. Conf. *2015*, 1087–1090.

Spüler, M., and Niethammer, C. (2015). Error-related potentials during continuous feedback: using EEG to detect errors of different type and severity. Front. Hum. Neurosci. *9*.

Spüler, M., Rosenstiel, W., and Bogdan, M. (2012a). Online adaptation of a c-VEP Brain-Computer Interface (BCI) based on error-related potentials and unsupervised learning. PLOS ONE *7*, e51077.

Spüler, M., Bensch, M., Kleih, S., Rosenstiel, W., Bogdan, M., and Kübler, A. (2012b). Online use of error-related potentials in healthy users and people with severe motor impairment increases performance of a P300-BCI. Clin. Neurophysiol. *123*, 1328–1337.

Stevens, M.C., Kiehl, K.A., Pearlson, G.D., and Calhoun, V.D. (2009). Brain network dynamics during error commission. Hum. Brain Mapp. *30*, 24–37.

Tabar, Y.R., and Halici, U. (2017). A novel deep learning approach for classification of EEG motor imagery signals. J. Neural Eng. *14*, 016003.

Talairach, J., and Tournoux, T. (1988). Co-planar stereotaxic atlas of the human brain: 3-Dimensional proportional system - an approach to cerebral imaging (Thieme Medical Publishers).

Talukdar, U., Hazarika, S.M., and Gan, J.Q. (2019). Motor imagery and mental fatigue: inter-relationship and EEG based estimation. J. Comput. Neurosci. *46*, 55–76.

Tort, A.B.L., Komorowski, R., Eichenbaum, H., and Kopell, N. (2010). Measuring Phase-Amplitude Coupling between neuronal oscillations of different frequencies. J. Neurophysiol. *104*, 1195–1210.

Trujillo, L.T., and Allen, J.J.B. (2007). Theta EEG dynamics of the error-related negativity. Clin. Neurophysiol. *118*, 645–668.

Ullsperger, M., and von Cramon, D.Y. (2006). How does error correction differ from error signaling? An event-related potential study. Brain Res. *1105*, 102–109.

Ullsperger, M., Danielmeier, C., and Jocham, G. (2014). Neurophysiology of performance monitoring and adaptive behavior. Physiol. Rev. *94*, 35–79.

Van Veen, V., and Carter, C.S. (2002). The timing of action-monitoring processes in the anterior cingulate cortex. J. Cogn. Neurosci. *14*, 593–602.

Vidaurre, C., and Blankertz, B. (2010). Towards a cure for BCI illiteracy. Brain Topogr. *23*, 194–198.

Vidaurre, C., Schlogl, A., Cabeza, R., Scherer, R., and Pfurtscheller, G. (2006). A fully on-line adaptive BCI. IEEE Trans. Biomed. Eng. *53*, 1214–1219.

Völker, M., Fiederer, L.D.J., Berberich, S., Hammer, J., Behncke, J., Kršek, P., Tomášek, M., Marusič, P., Reinacher, P.C., Coenen, V.A., et al. (2018). The dynamics of error processing in the human brain as reflected by high-gamma activity in noninvasive and intracranial EEG. NeuroImage *173*, 564–579.

Völlm, B., Richardson, P., McKie, S., Elliott, R., Deakin, J.F.W., and Anderson, I.M. (2006). Serotonergic modulation of neuronal responses to behavioural inhibition and reinforcing stimuli: an fMRI study in healthy volunteers. Eur. J. Neurosci. *23*, 552–560.

Volz, K.G., Schubotz, R.I., and von Cramon, D.Y. (2005). Variants of uncertainty in decision-making and their neural correlates. Brain Res. Bull. *67*, 403–412.

Vorobyev, V.A., Alho, K., Medvedev, S.V., Pakhomov, S.V., Roudas, M.S., Rutkovskaya, J.M., Tervaniemi, M., Van Zuijen, T.L., and Näätänen, R. (2004). Linguistic processing in visual and modality-nonspecific brain areas: PET recordings during selective attention. Brain Res. Cogn. Brain Res. *20*, 309–322.

Wander, J. (2015). Neural correlates of learning and intent during human brain-computer interface use. Thesis.

Wang, N.X.R., Olson, J.D., Ojemann, J.G., Rao, R.P.N., and Brunton, B.W. (2016). Unsupervised decoding of long-term, naturalistic human neural recordings with automated video and audio annotations. Front. Hum. Neurosci. *10*.

Welch, P. (1967). The use of fast Fourier transform for the estimation of power spectra: A method based on time averaging over short, modified periodograms. IEEE Trans. Audio Electroacoustics *15*, 70–73.

Wessel, J.R. (2012). Error awareness and the error-related negativity: evaluating the first decade of evidence. Front. Hum. Neurosci. *6*, 88.

West, R., and Travers, S. (2008). Tracking the temporal dynamics of updating cognitive control: an examination of error processing. Cereb. Cortex N. Y. N 1991 *18*, 1112–1124.

Wilson, N., Wang, X.R., Shean, R., Ojemann, J., Rao, R., and Brunton, B. (2017). The “Oops” Detector: Spontaneous vs in-task error-related potentials in long-term humanelectrocorticography. In 2017 Society for Neuroscience Conference, Washington, D.C.

Wilson, N., Weaver, K., Ojemann, J., and Rao, R. (2018). The effect of Default Mode Network disruption on reaction-timing and cortical activity in a modified Stroop task. In 2018 Society for Neuroscience Conference, San Diego, CA.

Wilson, N., Sarma, D., Wander, J., Weaver, K., Ojemann, J., and Rao, R. (2019). Cortical topography of error-related high-frequency potentials during erroneous control in a continuous control Brain-Computer Interface. Front. Neurosci. Sect. Neuroprosthetics. *(Accepted)*

Wolpaw, J.R., and McFarland, D.J. (2004). Control of a two-dimensional movement signal by a noninvasive brain-computer interface in humans. Proc. Natl. Acad. Sci. *101*, 17849–17854.

Wolpert, D.M., Miall, R.C., and Kawato, M. (1998). Internal models in the cerebellum. Trends Cogn. Sci. *2*, 338–347.

Xygonakis, I., Athanasiou, A., Pandria, N., Kugiumtzis, D., and Bamidis, P.D. (2018). Decoding motor imagery through Common Spatial Pattern Filters at the EEG source space. Comput. Intell. Neurosci. *2018*.

Zander, T.O., Krol, L.R., Birbaumer, N.P., and Gramann, K. (2016). Neuroadaptive technology enables implicit cursor control based on medial prefrontal cortex activity. Proc. Natl. Acad. Sci. U. S. A. *113*, 14898–14903.

Zanini, P., Congedo, M., Jutten, C., Said, S., and Berthoumieu, Y. (2018). Transfer Learning: A Riemannian geometry framework with applications to Brain-Computer Interfaces. IEEE Trans. Biomed. Eng. *65*, 1107–1116.

Zhang, H., Chavarriaga, R., Khaliliardali, Z., Gheorghe, L., Iturrate, I., and Millán, J. d R. (2015). EEG-based decoding of error-related brain activity in a real-world driving task. J. Neural Eng. *12*, 066028.